Experimental Characterization of Thermoelectric Module-Variable Conductance Heat Pipe Assemblies for Reduced Power Precision Temperature Control

Submitted by
David A. Brooks

IN PARTIAL FULFILLMENT OF THE REQUIREMENTS FOR THE DEGREE OF
MASTER OF SCIENCE IN MECHANICAL ENGINEERING

School of Engineering
Tufts University
Medford, Massachusetts

February 2012

Author:
David A. Brooks
Department of Mechanical Engineering
Tufts University

Certified By:
Associate Professor Marc Hodes
Department of Mechanical Engineering
Tufts University

Committee:
Vincent P. Manno
Adjunct Professor of Mechanical Engineering
Tufts University

Committee:
Martin Cleary
Postdoctoral Associate
Massachusetts Institute of Technology

ABSTRACT

Experimental Characterization of Thermoelectric Module-Variable Conductance Heat Pipe Assemblies for Reduced Power Precision Temperature Control

by

David A. Brooks

Chair: Marc Hodes

Thermoelectric modules (TEMs) are used to precisely maintain the specified operating temperature of photonics components which generate variable heat loads while being subjected to a wide range of ambient temperatures. This setpoint temperature of a photonics component is maintained by mounting it onto the controlled side of a TEM. Normally, a conventional heat sink (CHS), of fixed thermal resistance, is mounted to the uncontrolled side of a TEM. To minimize TEM power consumption, a CHS is replaced by a variable conductance heat pipe (VCHP) which offers the ability to passively decrease its thermal resistance as ambient temperature and/or heat load increase and vice versa.

This thesis presents detailed fabrication techniques for an as-built TEM-VCHP assembly, which covers heat pipe wick construction, cleaning, leak testing and charging. Furthermore, a means of interfacing a TEM to a heat pipe through an evaporator stackup is provided. Next, specific details are provided for an experimental apparatus setup which allows representative conditions of a photonics component application to be simulated (i.e., heat loads varying from 2 W to 7 W and ambient temperatures ranging from -5°C to 65°C). Finally, experimental results for a TEM-VCHP subjected to these conditions are provided to demonstrate achievable power savings. TEM power consumption is shown to be reduced by 38%

on average across all examined conditions and up to 98% in one case when compared to a TEM-constant conductance heat pipe assembly.

Acknowledgments

I would like to first thank my advisor and thesis chair, Marc Hodes, for his guidance and tutelage throughout the duration of this research. Without his support, this thesis would not have been possible. I would also like to thank my co-advisors, Professor Vincent Manno and MIT postdoctoral research associate, Martin Cleary for their input and feedback throughout the project. My colleague, Rui Zhang, cannot go unnoticed for her encouragement, ideas and assistance.

I owe a special thanks to Alan Lyons, professor of chemistry at the College of Staten Island, for his valuable advice and patience regarding the proper way to clean copper and chemical questions in general. I must also acknowledge Matt van Lieshout, a former Tufts M.S. student. This thesis research was a continuation of his hard work. Matt was very helpful in answering all of my questions and helped ease the transition from his work to mine.

I would like to acknowledge the Wittich Energy Sustainability Research Initiation Fund for supporting part of this thesis research. This funding helped support the project and provided valuable capital assets for Marc Hodes's research group.

I would also like to thank the people at Northrop Grumman-Adaptive Optics Xinetics for their financial support of my continued education and for respecting the delicate balance of my work and school schedules. I would like to acknowledge my coworkers for understanding and being supportive of my school work. Without their support, completing the M.S. program while working would have been very difficult.

I will be forever appreciative and gracious of my fiancé and future wife, Audrey, for her

unbound support. I could not have completed the program without her encouragement. I owe her a lifetime of thanks for always being supportive of me. Finally, I cannot thank my parents enough for their help and support. They have always supported all of the educational challenges that I have taken on.

TABLE OF CONTENTS

ABSTRACT ii

ACKNOWLEDGMENTS vi

LIST OF FIGURES ix

LIST OF TABLES xii

LIST OF APPENDICES xiii

NOMENCLATURE xvi

CHAPTER

I. Introduction and Background 1

1.1 Thermoelectric Effects 4
1.2 Thermoelectric Modules 4
1.3 Variable Conductance Heat Pipes 6

II. Model Development 11

2.1 One-Dimensional TEM Model 11
2.2 Flat Front Variable Conductance Heat Pipe Model 15
2.2.1 Heat Pipe Wick Calculations 16
2.3 Integrated TEM-VCHP Model 18
2.3.1 Mass of Non-Condensable Gas 19
2.3.2 TEM Pellet Height Optimization for a TEM-VCHP Assembly 19

III. Design and Fabrication 21

3.1 Preliminary Research 21
3.2 CCHP Fabrication 22
3.2.1 Heat Pipe Wick Characteristics 26
3.3 VCHP Fabrication 27

3.4 Leak Detection . . . 31
3.4.1 Coarse Leak Detection . . . 32
3.4.2 Fine Leak Detection . . . 33
3.4.3 Vacuum Pump System . . . 37
3.5 Evaporator Assembly . . . 40
3.5.1 TEM Specifications . . . 44

IV. Testing . . . 47

4.1 Measuring Equipment . . . 47
4.2 Data Acquisition Systems . . . 50
4.3 Environmental Chamber . . . 51
4.4 Overall Experimental Setup . . . 53
4.5 Experimental Testing . . . 54
4.6 Fabrication Challenges . . . 56

V. Experimental Results and Discussion . . . 59

5.1 TEM-CCHP Experimental Results . . . 59
5.1.1 Horizontal TEM-CCHP . . . 59
5.1.2 Vertical TEM-CCHP . . . 66
5.2 TEM-VCHP Experimental Results . . . 72
5.3 Comparison of Experimental Results . . . 77

VI. Conclusions and Future Work . . . 81

6.1 Conclusions . . . 81
6.2 Future Work . . . 83
6.2.1 Recommendations . . . 83

BIBLIOGRAPHY . . . 86

APPENDICES . . . 88

LIST OF FIGURES

Figure

1.1 Cutaway view of a single stage TEM [1]. 5

1.2 TEM power as a function of heat sink thermal resistance with an ambient temperature range of -5°C to 65°C, a component heat load of 10 W and a setpoint temperature of 75°C [2]. 7

1.3 Cross-sectional view of a CCHP [2]. 7

1.4 Cross-section of a gas loaded VCHP [2]. 9

2.1 Embedded resistive network and nodes representing a TEM [1]. 12

3.1 CCHP section of the heat pipe. 23

3.2 Detail view of a wrapped copper screen wick inserted into the heat pipe. . 25

3.3 Reservoir section of the heat pipe. 27

3.4 Argon cylinder connected to heat pipe for VCHP charging. 30

3.5 Overall view of the heat pipe assembly. 31

3.6 MIT leak detector with calibrated pressure vessel attached. 34

3.7 MIT leak detector with heat pipe attached. 35

3.8 Vacuum pump assembly. 39

3.9 Overall stackup of experimental evaporator. 41

3.10 Overall view of experimental evaporator stackup. 44

3.11 TEM only and TEM mounted to heat pipe evaporator stackup with heater attached. 45

4.1 Ice bath used to maintain the thermocouples' reference temperature. 48

4.2 TEM-heat pipe inside the wind tunnel inside the environmental chamber. . 52

4.3 Overall view of experimental apparatus. 53

5.1 Horizontal TEM-CCHP power consumption vs. heat load (T_{cp} = 63°C). . . 60

5.2 Horizontal TEM-CCHP axial temperature distribution (T_{∞} = 65°C, T_{cp} = 63°C). 61

5.3 Horizontal TEM-CCHP axial temperature distribution (T_{∞} = 30°C, T_{cp} = 63°C). 62

5.4 Horizontal TEM-CCHP axial temperature distribution (T_{∞} = -5°C, T_{cp} = 63°C). 63

5.5 Horizontal TEM-CCHP vapor core to ambient thermal resistance (T_{cp} = 63°C). 64

5.6 Vertical TEM-CCHP power consumption vs. heat load (T_{cp} = 63°C). . . . 67

5.7 Vertical and horizontal TEM-CCHP power consumption vs. heat load (T_{cp} = 63°C). 68

5.8 Vertical TEM-CCHP axial temperature distribution (T_{∞} = 65°C, T_{cp} = 63°C). 69

5.9 Vertical TEM-CCHP axial temperature distribution (T_{∞} = 30°C, T_{cp} = 63°C). 70

5.10 Vertical TEM-CCHP axial temperature distribution (T_{∞} = 0°C, T_{cp} = 63°C). 71

5.11 Vertical TEM-CCHP vapor core to ambient thermal resistance (T_{cp} = 63°C). 71

5.12 Vertical TEM-VCHP power consumption vs. heat load (T_{cp} = 63°C). . . . 72

5.13 Vertical TEM-VCHP axial temperature distribution (T_{∞} = 65°C, T_{cp} = 63°C). 74

5.14 Vertical TEM-VCHP axial temperature distribution (T_{∞} = 30°C, T_{cp} = 63°C). 75

5.15 Vertical TEM-VCHP axial temperature distribution (T_{∞} = 0°C, T_{cp} = 63°C). 76

5.16 Vertical TEM-VCHP vapor core to ambient thermal resistance (T_{cp} = 63°C). 78

F.1 Overall setup of methanol charging apparatus. 102

F.2 Injecting methanol into a heat pipe using a precision displacement pipette. 103

F.3 2.5 in piece of tubing with thermocouple and open valve. 103

G.1 Page 9 of 120 of Swagelok® tube fitting installation guide [3] (installation instructions). 108

G.2 Page 10 of 120 of Swagelok® tube fitting installation guide [3] (tube fittings up to 1 in./25 mm). 109

G.3 Page 12 of 120 of Swagelok® tube fitting installation guide [3] (reinstallation instructions). 110

H.1 Page 1 of 3 of TEM datasheet used in experiments [4]. 112

H.2 Page 2 of 3 of TEM datasheet used in experiments [4]. 113

H.3 Page 3 of 3 of TEM datasheet used in experiments [4]. 114

H.4 Microscope photograph of pellets of TEM used in experiments. 115

H.5 Microscope photograph of lead attachment of TEM used in experiments. . 115

I.1 Page 1 of 2 of Omega® pressure transducer instruction sheet [5]. 118

I.2 Page 2 of 22 of Omega® pressure transducer instruction sheet [5]. 119

K.1 Page 1 of 2 of Laird® Tgrease™ 2500 instruction sheet datasheet [6]. . . . 124

K.2 Page 2 of 2 of Laird® Tgrease™ 2500 instruction sheet datasheet [6]. . . . 125

LIST OF TABLES

Table

5.1 CCHP vs. VCHP TEM Power Consumption Comparison 79

A.1 Compiled Horizontal TEM-CCHP Data 89

B.1 Compiled Vertical TEM-CCHP Data 91

C.1 Compiled Vertical TEM-VCHP Data 93

D.1 Miscellaneous Horizontal TEM-CCHP Data 95

D.2 Miscellaneous Vertical TEM-VCHP Data 96

I.1 Calibration data for Omega® pressure transducer used at the condenser (Serial Number: 82975). 117

I.2 Calibration data for Omega® pressure transducer used at the reservoir (Serial Number: 87291). 117

J.1 Calibration data for MKS® 925 Micro Pirani pressure transducer. 121

LIST OF APPENDICES

Appendix

A. Compiled Horizontal TEM-CCHP Experimental Data 89

B. Compiled Vertical TEM-CCHP Experimental Data 91

C. Compiled Vertical TEM-VCHP Experimental Data 93

D. Miscellaneous Experimental Data 95

E. Heat Pipe Cleaning Procedure (Used on as-built heat pipe) 97

F. Methanol Charging Procedure 101

G. Swagelok® Installation Guide 107

H. Laird Technologies® TEM HT6,7,F2,3030 Datasheet and Microscope Photographs 111

I. Omega® PX209, PX219, PXM209, PXM219 Pressure Transducer Calibration Data and Instruction Sheet 117

J. MKS® 925 Micro Pirani Pressure Transducer Calibration Data 121

K. Laird Technologies® Tgrease™ 2500 Thermal Grease Datasheet 123

Nomenclature

A_p	Cross-sectional area of pellet [m^2]
A_v	Cross-sectional area of vapor core [m^2]
d	Wire diameter of a screen wick [m]
H	Pellet height [m]
I	Electrical current [A]
k	Thermal conductivity [W/(mK)]
K	Thermal conductance [W/K] (or wick permeability [m^2])
L_a	Active condenser length [m]
L_c	Condenser length [m]
m	Mass of non-condensable gas [kg]
N	Number of thermocouples (or mesh number for a screen wick [1/m])
p_{sat}	Saturation pressure of working fluid [Pa]
P_v	Perimeter of vapor core [m]
q	Heat transfer rate [W]
r	Radius [m]
R	Ohmic resistance [Ω]
$R_{ec-\rho}$	Electrical contact resistivity [Ωm^2]
R_{ec-R}	Electrical contact resistance [Ω]
R_g	Gas constant of non-condensable gas [J/(kgK)]
R_{HS}	Heat sink thermal resistance [K/W]
S	Wick crimping factor [1/m]

T	Temperature [K]
t	Thickness [m]
U	Overall radial heat transfer coefficient based on the surface area of a condenser vapor core [W/(m^{2}K)]
V_c	Condenser volume [m^3]
V_r	Reservoir volume [m^3]
V_{TEM}	TEM voltage [VDC]
w	Width as in spacing between wires in a screen wick [m]
$\dot{W}_{TEM}$	TEM power [W]

Greek Symbols

α	Seebeck coefficient [V/K]
ϵ	Wick porosity [m/m]
ρ	Electrical resistivity [Ωm]

Subscripts

∞	Ambient
c	Controlled-side interface (csi)
cp	Control plane
e	Evaporator
eff	Effective
i	Inside
ins	Insulation
l	Liquid
max	Maximum
min	Minimum
o	Outside
s	Substrate
u	Uncontrolled-side interface (usi)

v	Vapor core
w	Wick material
wa	Wall
wi	Wick

CHAPTER I

Introduction and Background

Photonics components such as pump lasers and reconfigurable optical add-drop multiplexers (ROADMs) are temperature sensitive and must be maintained within a narrow temperature range (e.g., ± 2°C) in order to function properly [7]. Moreover, precision temperature control must be maintained over a wide range of ambient temperatures and component heat loads varying between zero and a maximum value [8]. Network Equipment-Building System (NEBS) guidelines specify that the temperature of the inlet air used to cool components in telecommunications circuit packs may vary between -5°C and 50°C. However, the bulk temperature of the air typically rises as much as 15°C as it flows through the circuit pack. Thus, a photonics component may be subjected to a range of ambient temperatures varying from -5°C and 65°C [9].

The required operating (control plane) temperature of a photonics component is maintained by mounting it onto the controlled side of a thermoelectric module (TEM) [1]. A conventional heat sink (CHS) of essentially constant thermal resistance is normally mounted to the uncontrolled side of a TEM. When controlling the temperature of a component, TEM power consumption depends on the ambient temperature, the heat dissipated by the component, the required component temperature, the thermal resistance of the heat sink and the TEM itself (i.e., its thermoelectric properties and geometry of the semiconductor pellets therein). A shortcoming of this configuration is that the power consumed by a TEM is

often as high as the photonics component that is mounted to it. However, for any desired component temperature and heat dissipation, there is a heat sink thermal resistance that minimizes TEM power consumption. For example, the power consumption of a TEM operating in cooling mode is minimized when the heat sink thermal resistance is zero. Conversely, the power consumption of a TEM operating in heating mode is minimized when the heat sink thermal resistance is relatively large.

A key requirement of optoelectronic circuit packs is highly reliable subcomponents (i.e., no single point failures) as circuit packs are commonly found in critical applications such as telecommunications. TEMs are particularly attractive for this application given their ruggedness and lack of moving parts. Another constraint of optoelectronic circuit packs is a limited power budget and an increasing demand for low power consumption. Thus, minimizing the power consumption of TEMs is essential. One approach is to determine the unique combination of TEM pellet height and thermal resistance of a CHS such that the maximum TEM power consumption is minimized over an expected range of ambient temperatures and heat loads [10]. Another solution is to implement a variable speed fan which varies the thermal resistance of a CHS. However, this is typically not viable as the airflow supplied to optoelectronic components is provided by a shelf-level fan which runs at a fixed speed. Moreover, even if such a fan could be used, it might not provide the range of thermal resistance required to fully minimize TEM power consumption. Clearly, having the ability to vary the thermal resistance of a heat sink attached to the uncontrolled side of a TEM can reduce its power consumption, but it must be done based on the preceding constraints.

A variable conductance heat pipe (VCHP) is a temperature control device with a very high effective thermal conductivity (i.e., 10 or more times greater than that of copper) which is able to vary its thermal resistance passively depending on a combination of heat load and ambient temperature. The thermal resistance of a VCHP decreases as the ambient temperature or head load decreases and vice versa [11]. Thus, TEM power consumption may be

minimized by attaching a VCHP rather than a CHS to the uncontrolled side of a TEM. The combined assembly of a TEM and a VCHP is particularly attractive because both components are passive and have no moving parts. Their durability has already been demonstrated in telecommunications and space applications [2]. Competing technologies, for example, vapor compression cycles, compromise reliability as they require moving parts. Thus, this advantage combined with the TEM-VCHP's passive ability to vary its thermal resistance makes it a sensible precision thermal management solution. A significant shortcoming, however, of VCHPs is the potential for "trapping" or temporary "trapping" of condensate in the reservoir which can be a reliability issue as this may cause the thermal resistance of the VCHP to be suboptimal, thus drawing more TEM power than necessary.

Melnick *et al.* [12] have developed an analytical model quantifying the power savings achievable using a TEM-VCHP assembly which optimizes the mass of non-condensable gas (NCG) in a VCHP and TEM pellet height. A comparison is made between a TEM-CHS and a TEM-VCHP assembly for a typical set of operation conditions. The optimization algorithm suggests that an average power reduction of 55% can be accomplished when an optimized TEM-VCHP assembly is utilized in place of a TEM-CHS assembly for representative conditions.

The motivation of this thesis is to experimentally characterize a TEM-VCHP assembly to significantly reduce TEM power consumption. The thermal resistance of a VCHP varies passively to accommodate changing component heat loads and ambient temperatures which allows a TEM's power consumption to always be minimized regardless of its mode of operation. A TEM-VCHP experimental rig is fabricated and tested. The primary objectives of this research are to provide fabrication procedures and to demonstrate reduced power precision temperature control of a TEM-CHS and subsequently, the further power savings achievable with a TEM-VCHP assembly.

1.1 Thermoelectric Effects

When considering electrically conducting materials, thermal energy may be reversibly converted into electrical energy and vice versa by three thermoelectric effects [13]. The Seebeck effect is the generation of a voltage gradient in an electrical conductor subjected to a temperature gradient under open circuit conditions. It is described by

$$dV = \alpha dT, \tag{1.1}$$

where V is voltage, α is the Seebeck coefficient of a conductor (or semiconductor) and T is temperature.

The Peltier effect is the evolution or absorption of heat when electric current flows through an interface between two dissimilar conductors. Moving charge carriers associated with current carry different amounts of electrical energy. The amount of Peltier heating or cooling is material dependent and is described by

$$q = I(\alpha_B - \alpha_A)T, \tag{1.2}$$

where q is the reversible rate of heat transfer, I is current, α_B and α_A are the Seebeck coefficients of conductors, B and A, and T is the absolute temperature at their interface. Heat is absorbed when current is positive (positive charge carriers flow from conductor A to conductor B and $\alpha_B > \alpha_A$). Conversely, heat is released when the opposite occurs. The third thermoelectric effect, the Thompson (bulk) effect [1] is the evolution or absorption of heat when electric current flows through a conductor subjected to a temperature gradient.

1.2 Thermoelectric Modules

TEMs are solid-state devices that when operating in precision temperature control mode utilize the Peltier effect to heat or cool the components that are mounted to them in order

to maintain their setpoint temperature. The magnitude of the rate of heat transfer can be directly controlled by changing the magnitude of the current. As per Eq. 1.2, increasing I will increase q and vice versa. Furthermore, the direction of current determines whether heat is released or absorbed by the Peltier effect. For the configuration shown in Fig. 1.1, positive current corresponds to Peltier cooling at the controlled side interface (csi) [14] of a TEM and negative current corresponds to Peltier heating. On the controlled side of a TEM, the csi is the interface between the semiconducting pellets and the electrical interconnects joining the n-type and p-type pellets. The uncontrolled interface (usi) is defined analogously. On the controlled side electrical interconnects, a ceramic substrate (often alumina) is attached, where the component requiring temperature control is mounted. Similarly, a ceramic substrate is attached to the uncontrolled side electrical interconnects and a heat sink (e.g., CHS or VCHP) is mounted to it.

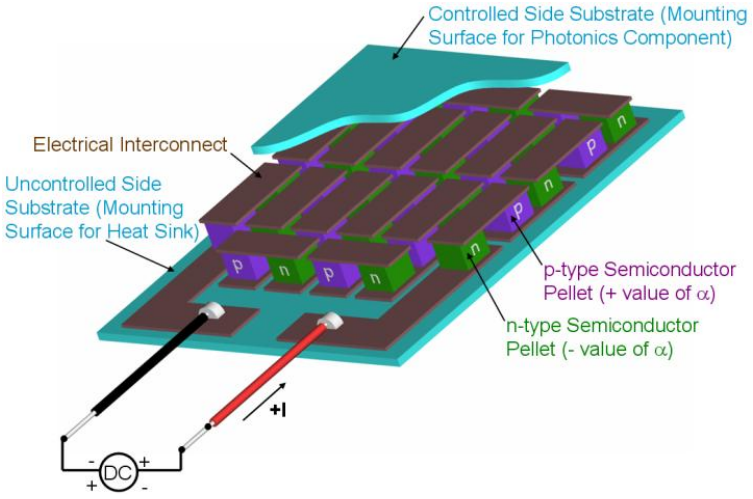

Figure 1.1: Cutaway view of a single stage TEM [1].

TEMs are simply constructed as they feature no moving parts. Additionally, they are lightweight, compact, rugged, moderately priced, modular and acoustically silent [15]. Limitations of TEMs, however, are their inability to generate large temperature differences while operating in cooling mode and the limited rate of heat that can be accommodated in cooling mode. TEMs also have a low thermodynamic efficiency which is further reduced by DC to

DC power conversion losses. Hence, maximizing their efficiency is crucial.

Given the preceding discussion, it is essential to optimize TEM-CHS assemblies to minimize their power consumption when they are subjected to varying combinations of ambient temperature and heat load while maintaining a specified setpoint temperature of a component.

The power consumption of a TEM, $\dot{W}_{TEM}$, is plotted as a function of heat sink thermal resistance, R_{HS}, for a representative set of conditions in Fig. 1.2, where T_∞ = 65°C is a maximum ambient temperature (requiring cooling mode) and T_∞ = -5°C is a minimum ambient temperature (requiring heating mode). In the case of a CHS, the optimal thermal resistance is the intersection of the $\dot{W}_{TEM}$ curves for cooling and heating mode. However, to further reduce TEM power consumption, having the ability to vary R_{HS} is advantageous. For example, when a TEM operates in cooling mode, a relatively low (ideally zero) heat sink thermal resistance minimizes power consumption. However, for certain regions in heating mode, lower values of R_{HS} cause $\dot{W}_{TEM}$ to be higher than optimal. The variable thermal resistance of a VCHP usually allows TEM power consumption to be reduced regardless of the mode of operation. TEMs can be optimized to further minimize power consumption by optimizing their geometry (i.e., the pellet height). Figure 1.2 exemplifies the substantial energy savings that can be accomplished when a TEM operates in series with a VCHP.

1.3 Variable Conductance Heat Pipes

VCHPs are passive thermal management devices commonly used in the precision temperature control of satellites [2]. Their operation is very similar to constant conductance heat pipes (CCHPs), with the exception that they have the ability to vary their thermal resistance, whereas the thermal resistance of a CCHP is constant. A CCHP is comprised of three sections: an evaporator, a condenser and an adiabatic section, which is optional. Figure 1.3 shows a cross-sectional view of a CCHP and its aforementioned sections.

Operation occurs when heat is input to the evaporator section, where it vaporizes working

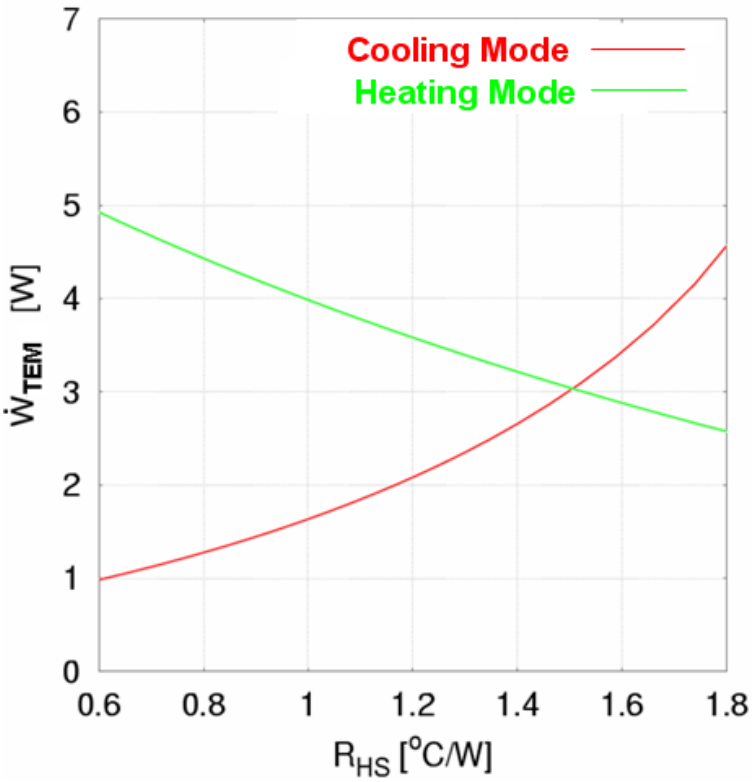

Figure 1.2: TEM power as a function of heat sink thermal resistance with an ambient temperature range of -5°C to 65°C, a component heat load of 10 W and a setpoint temperature of 75°C [2].

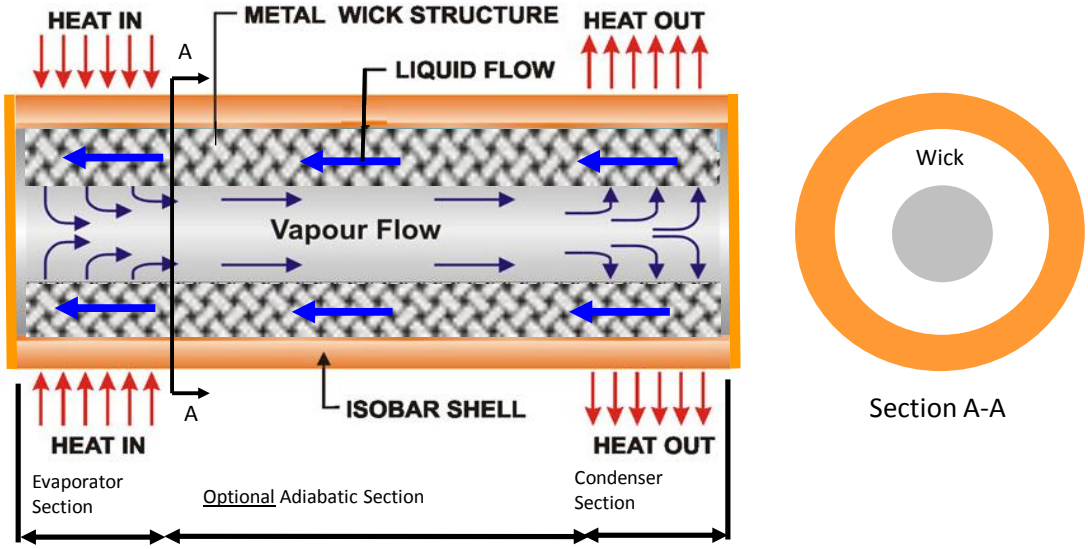

Figure 1.3: Cross-sectional view of a CCHP [2].

fluid (e.g., methanol or acetone) saturated in the wick. The vapor travels through the adiabatic section towards the condenser section where it condenses and releases the heat to the ambient. The direction of return flow of the condensed working fluid (now in a liquid state) from the condenser, through the adiabatic section and back to the evaporator section is driven by an axial pressure gradient in the wick. This pressure is the result of a larger radius of curvature across the liquid-vapor interface in the outer wick pores in the condenser compared to the evaporator due to the continued flow of new condensate in the condenser and vaporization of the condensate in the evaporator [16].

Performing an energy balance on the condenser section of a CCHP shows that

$$q = UP_vL_c(T_v - T_\infty), \tag{1.3}$$

where q is the rate of heat input to the evaporator, U is the overall radial heat transfer coefficient from the vapor core to the ambient, P_v is the perimeter of the vapor core, L_c is the length of the condenser, T_v is the temperature of the vapor core and T_∞ is the ambient temperature. The length of the condenser in a CCHP is constant and its overall radial heat transfer coefficient is assumed to be constant as well. Thus, its thermal resistance remains constant. However, as per Eq. 1.3, the temperature of the vapor core varies linearly with respect to changes in heat load or ambient temperature.

Gas-loaded VCHPs are identical to CCHPs with the exception that they include a reservoir filled with a non-condensable gas (NCG) [16]. The NCG is an inert gas such as nitrogen or argon. VCHPs operate very similarly to CCHPs except that when their working fluid is vaporized, the resulting pressure forces NCG into the condenser and reservoir sections. It is noted that although the reservoir may lack a wick, vapor may still be transported into it by diffusion. A mixture of NCG and vapor exists in the active region of the condenser and in the reservoir. The penetration of this front of vapor-gas depends on heat load and ambient temperature. Active control of the extent of vapor-gas expansion may be accomplished through the use of a heated reservoir (which can be optimized to achieve power savings).

However, this study examines a passive reservoir which is in equilibrium with the ambient along with the inactive length of the condenser. A cross-section of a gas loaded VCHP is illustrated in Fig. 1.4.

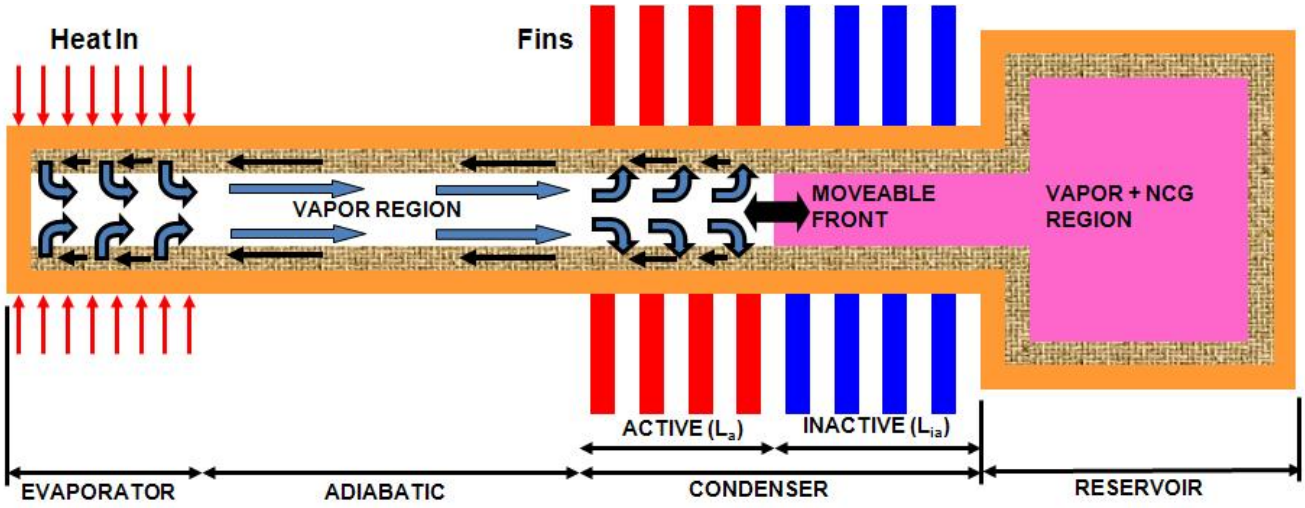

Figure 1.4: Cross-section of a gas loaded VCHP [2].

To describe its operation, consider a VCHP subjected to a decrease in heat load. The temperature of the saturated vapor in the evaporator decreases. Thus, the pressure in the evaporator decreases. This decreased pressure causes the vapor-gas front to expand further into the condenser section. Thus, the exposed section (or active length) of the condenser decreases which increases the thermal resistance of the VCHP. This interfacial vapor and gas front continues to reduce the active length of the condenser (i.e., the area of the condenser available for condensation) until a thermal equilibrium is reached. This passive changing of the condenser thermal resistance somewhat maintains the vapor core temperature. Although slightly more complicated, a decrease in ambient temperature also causes the thermal resistance of a VCHP to increase. In this case, the temperature of the reservoir which is at equilibrium with the ambient decreases. This reduces the partial pressure of the vapor in the reservoir. However, the pressure of the vapor in the active length decreases more than the partial pressure of the vapor in the inactive length of the reservoir. This is due to

the monotonically increasing slope of the pressure-temperature saturation curve for typical working fluids. Thus, the net effect is that the vapor-gas front expands further into the condenser, decreasing its active length and thus increasing its thermal resistance. Again, this passive behavior passively maintains the vapor core temperature to some extent. It is noted that VCHPs are better suited for situations pertaining to a varying heat load rather than a varying ambient temperature.

The ability of a VCHP to passively maintain the temperature of the vapor core temperature in its evaporator section is dependent on the ratio of the reservoir to condenser vapor core volumes, V_r/V_c [12]. As this ratio approaches infinity, a VCHP is most able to passively maintain steady state temperature control. VCHPs with a ratio of $V_r/V_c = 25$ behave nearly the same as those with an infinitely large reservoir [16].

Although VCHPs have the ability to temperature control passively, they are not precise enough to meet the performance specifications required by photonics components [7] even when the component temperature is higher than the upper range of ambient temperature. It has been shown that this is because the specified ambient temperature range is too large [11]. Other experiments have shown that even when a heated reservoir is implemented, the level of temperature control is insufficient [17]. Another shortcoming of VCHPs is the substantial thermal capacitance associated with their wall and wick. This leads to a slow transient response to temperature and head load changes [16]. This makes a VCHP disadvantageous when it is operating as the only temperature control device in a system. Finally, VCHPs lack the ability to refrigerate components to sub-ambient temperatures, which makes them unsuitable for most photonics applications.

Although a VCHP is unable to maintain a sub-ambient setpoint temperature and does not provide adequately precise temperature control, combining it with the rapid response of a high precision TEM presents a feasible and power minimizing thermal management assembly.

CHAPTER II

Model Development

A one-dimensional model of a TEM-CHS assembly controlling the temperature of a component under varying ambient temperatures is first presented. Then, the flat front model of a VCHP is presented. Finally, the two models are integrated to provide a complete singular model of a TEM-VCHP assembly.

2.1 One-Dimensional TEM Model

A thermal resistance network with a TEM embedded in it is shown in Fig. 2.1. A TEM consists of an array of adjacent pairs of positively-doped (p-type) and negatively-doped (n-type) semiconductor pellets. Each pair of p and n type pellets is referred to as a thermocouple and there are N thermocouples in a TEM. The thermocouples are connected electrically in series. The thermocouples are attached by copper electrical interconnects and the interconnects are attached to ceramic substrates. The substrate to which a photonics component to is attached is defined as the controlled-side substrate and the opposite substrate is referred to as the uncontrolled-side substrate. It is on the uncontrolled-side that a heat sink is mounted. The uncontrolled-side is also the side where the electrical leads are connected. As per Fig. 2.1 the controlled side-interface (csi) in a TEM is defined as that between the thermocouples and conductors forming the interconnects on the controlled-side substrate. The uncontrolled-side interface (usi) is defined analogously.

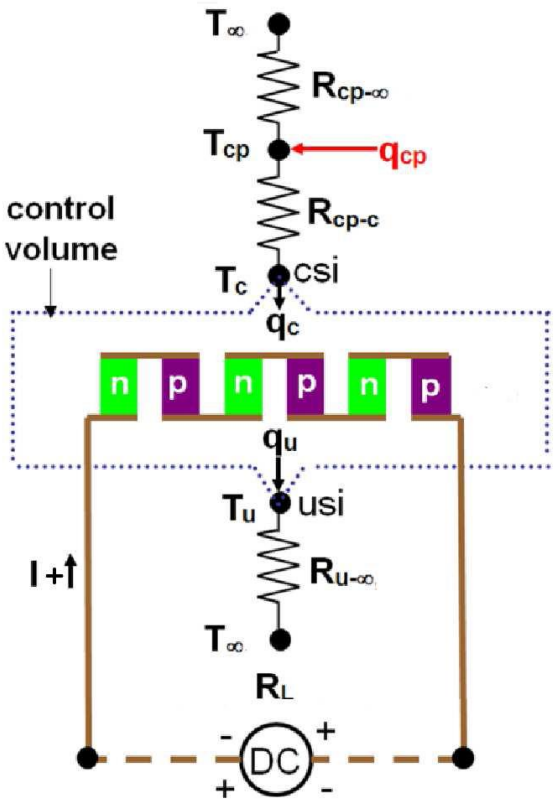

Figure 2.1: Embedded resistive network and nodes representing a TEM [1].

Current is positive when positive charge flows from n-type to p-type pellets at the csi. α_p and α_n are positive and negative in magnitude. Based on this, heat is absorbed through the Peltier effect at the csi and is released at the usi. This is also referred to as cooling mode. Analogously, when current is negative, heat is absorbed at the usi and is released at the csi. This is known as heating mode. The third major mode of operation, generation mode, is not of interest for the purpose of generating power in this analysis. Rather, it is a characteristic that proves to eliminate TEM power consumption altogether in certain situations.

T_∞, T_{cp}, T_c and T_u are defined as the ambient, control plane, csi and usi temperatures, respectively. The required operating temperature of a component is set equal to T_{cp}. The head load dissipated by the component is modeled as a planar heat source and is denoted as q_{cp}. Energy balances at the csi and usi may be performed to determine the external heat transfer rates to and from the TEM, (i.e., q_c and q_u respectively).

The thermal resistances shown in Fig. 2.1 between the control plane and ambient, control plane and controlled-side interface and uncontrolled-side interface and ambient are denoted by $R_{cp-\infty}$, R_{cp-c} and $R_{u-\infty}$, respectively. It is noted that constriction and spreading resistances in the ceramic substrates are accounted for in R_{cp-c} and $\mathrm{R}_{u-\infty}$. The thermal resistance of a heat sink resistance, R_{HS}, is included in $R_{u-\infty}$. For the proceeding analyses, thermal conductances are used in place of thermal resistances. They are defined as $K_{i-j} = 1/R_{i-j}$.

The flow of heat transfer in a TEM is assumed to be one-dimensional as provided in the analysis by Hodes [18]. Because of this, it is implied that neither the "aisles" between the pellets nor "sidewetting" of solder onto them introduces significant multidimensional effects. Additionally, the Peltier effect and interfacial Ohmic heating are assumed to occur exclusively at the csi and usi. It is also assumed that bulk Ohmic heating in the diffusion barrier, solder and copper portions of the interconnects in a TEM are negligible. The thermo-physical properties of the p- and n- pellets are assumed to be constant and equal with the exception that the Seebeck coefficient is positive and negative in p- and n- type pellets, respectively. For this reason, the Thompson (bulk) effect is neglected.

As per Fig. 2.1, a surface energy balances at the control plane yields

$$q_{cp} = K_{cp-c}(T_{cp} - T_c) - K_{cp-\infty}(T_{cp} - T_\infty), \tag{2.1}$$

where the terms, K_{cp-c} and $K_{cp-\infty}$, account for the thermal resistances between the control plane and controlled side-interface and the control plane and ambient, respectively. Surface energy balances at the csi and usi yield, respectively,

$$K_{cp-c}(T_{cp} - T_c) = N\left[I\alpha_{p,n}T_c - K(T_u - T_c) - \frac{I^2R}{2} - \frac{I^2R_{ec-R}}{2}\right], \tag{2.2}$$

$$\frac{T_u - T_\infty}{R_{u-\infty}} = N\left[I\alpha_{p,n}T_u - K(T_u - T_c) + \frac{I^2R}{2} + \frac{I^2R_{ec-R}}{2}\right], \tag{2.3}$$

where $\alpha_{p,n} = \alpha_p$ - α_n and the term, $R_{u-\infty}$, accounts for the thermal resistance between the

uncontrolled side-interface and ambient. The bulk Ohmic resistance, R, thermal conductance, K, and electrical contact resistance of a thermocouple, R_{ec-R}, are, respectively,

$$R = \frac{2\rho H}{A_p}, \tag{2.4}$$

$$K = \frac{2kA_p}{H}, \tag{2.5}$$

and

$$R_{ec-R} = \frac{4R_{ec-\rho}}{A_p}, \tag{2.6}$$

where ρ, H, k, A_p and $R_{ec-\rho}$ are the electrical resistivity, pellet height, thermal conductivity, cross-sectional area of a pellet and electrical contact resistivity, respectively. Performing an energy balance on a control volume surrounding the pellets shows that the electrical power consumed by a TEM is the difference between heat flowing out of the pellets through the usi and that which is flowing into the csi (q_u - q_c). Calculating this difference yields the following equation for TEM power, $\dot{W}_{TEM}$

$$\dot{W}_{TEM} = N\left[\alpha_{p,n}(T_u - T_c) + I(R + R_{ec-R})\right]. \tag{2.7}$$

where Eq. 2.7 is calculated by subtracting Eq. 2.2 from Eq. 2.3. As per the preceding equations, the power required by a TEM to maintain the control plane temperature, T_{cp} is a function of the heat dissipated by a component, q_{cp} and ambient temperature, T_∞. First, Eq. 2.1 is solved for T_c. Then Eqs. 2.2 and 2.3 are analytically solved for T_u and then numerically for I. TEM power follows from Eq. 2.7.

2.2 Flat Front Variable Conductance Heat Pipe Model

In actual VCHPs, operation is multidimensional and it includes simultaneous and conjugate heat and mass transfer [19], [20], [21]. However, to a first order approximation, it can be assumed that a flat front exists between the pure vapor and vapor plus (non-condensable) gas regions in the condenser of a VCHP. This results in a thermally inactive region of the condenser as per Fig. 1.4. Provided by Marcus and Fleischman [22], this "flat" front model is the simplest analytical model of a variable conductance heat pipe. It assumes that a VCHP operates at steady state conditions with negligible mass diffusion and axial conduction and that the total pressure throughout the VCHP is uniform and equal to the saturation pressure corresponding to the liquid-vapor interface in the evaporator. Furthermore, it is assumed that the NCG behaves ideally and that its partial pressure increases stepwise from zero to the difference between the vapor pressure in the active and inactive regions at a flat, active-inactive interface. It is assumed that the partial pressure of the NCG is equal to the difference between the total pressure in the VCHP and the vapor partial pressure at the ambient temperature. The analysis also assumes that heat released to the ambient occurs by forced convection and that the overall radial heat transfer coefficient is constant. Finally, the sensible temperature rise of a fluid passing over the condenser is neglected.

As per the ideal gas law, the mass, m, of NCG in a VCHP is

$$m = \frac{\left[(p_{sat}(T_v) - p_{sat}(T_\infty)\right]\left[(L_c - L_a)A_v + V_r\right]}{R_g T_\infty}, \tag{2.8}$$

where the saturated vapor pressure at the vapor core temperature, T_v, and partial pressure at the ambient temperature, T_∞, are typically calculated by invoking the Clausius-Clapeyron relation. However, tables may also be used as per the analysis by Melnick *et al.* [12]. Solving Eq. 2.8 for the active length of the condenser, L_a, yields

$$L_a = L_c - \left[\frac{m R_g T_\infty}{p_{sat}(T_v) - p_{sat}(T_\infty)} - V_r\right] / A_v. \tag{2.9}$$

Performing an energy balance on a control volume surrounding the condenser section of a VCHP yields

$$q = UP_vL_a(T_v - T_\infty), \tag{2.10}$$

where the overall heat transfer coefficient, U, consists of a series combination of wick, wall and ambient-side thermal resistances of the condenser. This relationship for a VCHP is identical to Eq. 1.3 for a CCHP (when the condenser of a VCHP is fully active).

It is assumed that the thermal resistances between the evaporator wall and wick are radial and one-dimensional as with conduction through an annulus. The effective thermal conductivity of the wick, k_{eff}, depends on the type of wick (e.g., sintered copper powder), porosity, thickness and material. The thermal conductivity of the working fluid (e.g., methanol) also affects k_{eff} [16]. The thermal resistance from the active vapor core to the ambient may be extracted from Eq. 2.10 and is denoted as

$$R_{v-\infty} = \frac{1}{UP_vL_a}. \tag{2.11}$$

2.2.1 Heat Pipe Wick Calculations

The primary purpose of a wick in a heat pipe is to provide a mechanism for the return of condensate [2]. Additionally, a wick evenly distributes the working fluid over the evaporator and condenser surfaces for efficient heat transfer within a heat pipe. Desirable characteristics of a wick include a small effective capillary radius (r_{eff}) to generate large capillary pressure, high permeability (K) to minimize a liquid-phase pressure drop and a high effective thermal conductivity (k_{eff}) to minimize the thermal resistance of a heat pipe. While many types of wicks are common (e.g., sintered powder or axially grooved), the easiest to fabricate for the purpose of this experimental setup is a wrapped copper screen wick. This requires no special sintering processes or any specialty tools or manufacturing. An additional benefit of the wrapped screen wick configuration is that the spring tension of the wick itself holds it

in place. However, a drawback of this design is a low k_{eff}. To calculate the effective pore radius for a screen wick, the following equation may be used [23]

$$r_{eff} = \frac{w + d_w}{2} = \frac{1}{2N}, \tag{2.12}$$

where w is the spacing (presumed square) between the wires in the mesh and d_w is the diameter of the wire in the screen. The wick effective radius may be used to calculate the mesh screen number, N. It is required for the calculation of the permeability (K) of a wick which is given by the equation [23]

$$K = \frac{d_w^2 e^3}{122(1-e)^2}, \tag{2.13}$$

where e is the porosity of the wick. e may be calculated by the equation [23]

$$e = 1 - \frac{\pi S N d_w}{4}, \tag{2.14}$$

where S is the wick crimping factor. $S = 1.05$ is assumed for tightly wrapped wicks [23] which is considered to be the case for the heat pipe used in this thesis work. Porosity is necessary for calculating the amount of working fluid required to properly wet a wick.

With the porosity determined from Eq. 2.14, it is necessary to calculate the effective thermal conductivity (k_{eff}) of a wick. k_{eff} is necessary when determining the radial thermal resistances of the wick. The series combination of this thermal resistance in addition to the wall and ambient side thermal resistances are part of the overall heat transfer coefficient, U, found in Eq. 2.10 . It is an effective quantity that represents the total, effective thermal conductivity of the working fluid and the wick material. For a wrapped screen wick, the following equation may be used to calculate its effective thermal conductivity [23]

$$k_{eff} = \frac{k_l \left[(k_l + k_w) - (1-e)(k_l - k_w)\right]}{(k_l + k_w) + (1+e)(k_l - k_w)}, \tag{2.15}$$

where k_l is the thermal conductivity of the working fluid.

The preceding wick calculations are required to determine the radial thermal resistances of a heat pipe. They are necessary to calculate the properties of a known, as-built wick so that the model as described in Section 2.2 may be implemented based on actual hardware.

2.3 Integrated TEM-VCHP Model

A model for combining a TEM-VCHP assembly is derived by relating the thermal resistance from the usi to the ambient, $R_{u-\infty}$, to the specifications and required parameters for a TEM-VCHP assembly and by I and T_u. It is noted that $R_{u-\infty}$ includes a thermal resistance from the usi to the outer evaporator wall, R_{u-e}, due to conduction through the TEM substrate and contact resistance due to the means by which the TEM and VCHP are joined (e.g., epoxy or thermal grease). Thus, $R_{u-\infty}$ is

$$R_{u-\infty} = R_{u-e} + R_{e,wa} + R_{e,wi} + R_{v-\infty}. \tag{2.16}$$

Substituting Eq. 2.11 into Eq. 2.16 and defining R_{u-v} as $R_{u-e}+R_{e,wa}+R_{e,wi}$ results in

$$R_{u-\infty} = R_{u-v} + \frac{1}{UP_vL_a}. \tag{2.17}$$

Substituting the expression for L_a from Eq. 2.9 into the above result yields

$$R_{u-\infty} = R_{u-v} + \frac{1}{UP_vL_c} - \left[\frac{mR_gT_\infty}{p_{sat}(T_v) - p_{sat}(T_\infty)} - V_r\right]/A_v. \tag{2.18}$$

Additionally, matching the heat transfer rate out of the usi into the vapor core shows that

$$N\left[I\alpha_{p,n}T_u - K(T_u - T_c) + \frac{I^2R}{2} + \frac{I^2R_{ec-R}}{2}\right] = \frac{(T_u - T_v)}{R_{u-v}}. \tag{2.19}$$

Solving Eq. 2.19 for T_v and inserting the result into 2.18 yields

$$R_{u-\infty} = R_{u-v} + \frac{1}{UP_v}\left[L_c - \left(\frac{mR_gT_\infty}{p_{sat}\left\{T_u - NR_{u-v}\left[I\alpha_{p,n}T_u - K(T_u - T_c) + \frac{I^2R}{2} + \frac{I^2R_{ec-R}}{2}\right]\right\} - p_{sat}(T_\infty)} - V_r\right) / A_v\right]. \quad (2.20)$$

Substituting Eq. 2.20 into Eq. 2.3 allows the simultaneous solution of Eqs. 2.1, 2.2 and 2.3 for T_c, T_u and I for any component setpoint temperature, T_{cp}, ambient temperature, T_∞ and heat load, q_{cp}. The corresponding TEM power, $\dot{W}_{TEM}$, results from Eq. 2.7.

2.3.1 Mass of Non-Condensable Gas

The optimal mass of NCG in a VCHP is assumed to correspond to a fully active condenser (i.e., $L_a = L_c$), with the VCHP subjected to the harshest cooling conditions (i.e., $q_{cp,max}$ and $T_{\infty,max}$). This may be achieved by setting $L_a = L_c$, i.e., $R_{u-\infty} = R_{u-v}+1/(UP_VL_c)$, as per Eq. 2.17, $q_{cp} = q_{cp,max}$ and $T_\infty = T_{\infty,max}$. This allows Eqs. 2.1, 2.2 and 2.3 to be simultaneously solved for T_c, T_u and I. The corresponding value of T_v may be determined from Eq. 2.19. Finally, with the preceding variables known, the mass of NCG, m, may be determined by Eq. 2.8.

2.3.2 TEM Pellet Height Optimization for a TEM-VCHP Assembly

TEM power consumption in the most demanding cooling condition is typically higher than that consumed during the most demanding heating condition. This is dependent on common factors such as a limited allowable volume of VCHPs used in optoelectronic circuit packs and the relatively large air-side and wick thermal resistances that limit a VCHP's overall radial heat transfer coefficient. To reduce the maximum TEM power consumed, the pellet height of a TEM may be optimized such that the TEM is most energy efficient when

it is used in a TEM-VCHP assembly under the harshest cooling conditions[1]. In the most demanding cooling conditions, $L_a = L_c$; therefore, the thermal resistance from the usi to the ambient, $R_{u-\infty}$, is known. Equations 2.2 and 2.3 form a system of two equations with three unknowns: T_u, I and H. First, this system of equations is solved analytically for T_u, then numerically for I as a function of H. Finally, $\dot{W}_{TEM}$ is calculated as a function of H and is numerically differentiated with respect to H and set equal to zero to find the pellet height that minimizes the maximum TEM power consumption for a TEM-VCHP assembly that consumes the most power in the most demanding cooling conditions. After the optimal TEM pellet height is determined, the mass of NCG, m, must be recalculated following the preceding procedure.

[1]Zhang *et al.*[10] have shown in certain cases that the optimal TEM pellet height which minimizes the maximum power consumption is the lowest value for which $\dot{W}_{TEM}(q_{cp,max},T_{\infty,min}) = \dot{W}_{TEM}(q_{cp,max},T_{\infty,max})$ rather than that which minimizes $\dot{W}_{TEM}(q_{cp,max}$ and $T_{\infty,min})$.

CHAPTER III

Design and Fabrication

Typical heat pipes are fully closed systems with permanent seals (e.g., solder and crimped joints). Proper construction is critical to ensure a long operating life [16]. For experimental purposes, however, a design has to be conceived that can be readily and easily assembled (and disassembled if need be). Additionally, the chosen design must be able to accommodate instrumentation such as temperature probes and pressure transducers. Thus, it was concluded for this thesis research that a design consisting of simple construction and versatile components was the optimal approach from an experiment standpoint. TEMs, on the other hand, are readily available in a multitude of sizes and geometry. Thus, the majority of efforts was concentrated on the design and fabrication of the heat pipe portion of the assembly.

3.1 Preliminary Research

Preliminary research was required to gather information on the associated subcomponents required of the heat pipe to be constructed. Furthermore, research was performed to examine the equipment necessary to fabricate the heat pipe and then to measure pertinent data such as temperature and pressure. A means of accurately and semi-automatically collecting and recording steady state also had to be considered. Along with these requirements were cost and time constraints. That is, the chosen overall design had to be reasonably priced (e.g., molding a monolithic heat pipe body and condenser fin stack was possible, but costly) and

needed to be constructed within a reasonable timeframe. With the overall design constraints defined, it was next necessary to examine sub-component designs (e.g., how to attach the TEM to the evaporator section of the heat pipe). The final chosen design was selected after addressing top level concerns first and then filtering the requirements down to the component level. Efforts were made to drive the sizes of the components and the overall envelope of the assembly to a realistic and feasible volume. It was concluded that fabricating an assembly somewhat representative of that found in typical photonics equipment was a sensible approach for application to actual hardware and conditions.

The primary purpose of this thesis research was to demonstrate reduced power precision temperature control for a TEM assembled to a VCHP compared to a TEM assembled to a heat sink of fixed thermal resistance. For consistency purposes, it was decided that the fixed thermal resistance heat sink would be represented by a CCHP. Upon completion of the TEM-CCHP experiments, it would then be converted to a VCHP by attaching a reservoir and then the identical experiments would be repeated to demonstrate the achievable power savings associated with a VCHP. Thus, the initial fabrication step began with the CCHP.

3.2 CCHP Fabrication

The CCHP was constructed using readily available components. Care was taken to avoid invoking the need for custom or hard to find components. All of the components were designed with relatively simple features to keep machinability feasible and to minimize costs and lead time. First, the primary component of the heat pipe (i.e., the annular body) was selected to be representative of typical heat pipe geometry used in photonics components. An alloy 101 copper pipe with a 3/8 in ($9.525\text{x}10^{-3}$ m) outer diameter (OD) with a 0.065 in ($1.651\text{x}10^{-3}$ m)wall thickness was selected such that its inner diameter (ID) was large enough to insert the wick somewhat easily and to accommodate Swagelok® compression tube fittings that were required to assemble the entire heat pipe. Selecting a pipe with walls that were too thin could result in potential leaks downstream during assembly or experimental phases

of the project. Aside from the excellent thermal conductivity of copper (k = 391 W/mK), another benefit of using copper from a manufacturing standpoint was that it was a softer material than the stainless steel ferrules used in the compression tube fittings as per the recommendations of Swagelok®. The copper tubing served as both the evaporator and adiabatic sections of the heat pipe and the base for the condenser. The overall length of the copper tubing was 10.375 in (263.525x10^{-3} m). An overall view of the fabricated CCHP is shown in Fig. 3.1.

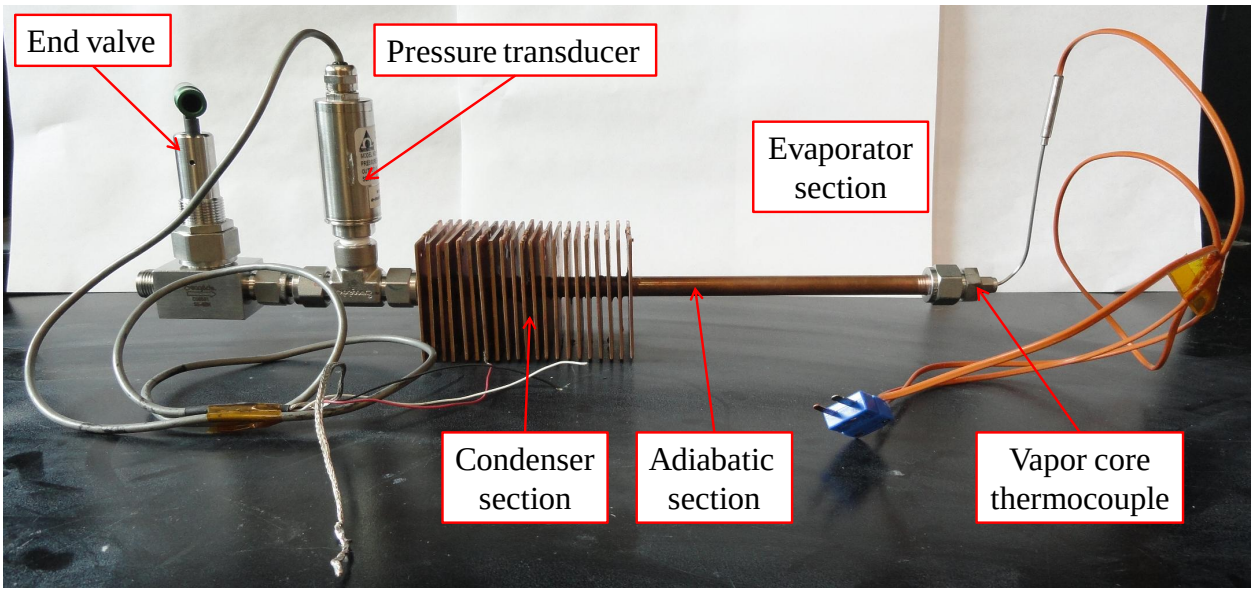

Figure 3.1: CCHP section of the heat pipe.

To complete the condenser section of the heat pipe, 21 copper fins were attached to one end of the copper tube. The geometry of the fins was 2.161 in by 2.161 in (54.889x10^{-3} m by 54.889x10^{-3} m) with a 0.061 in (1.549x10^{-3} m) thickness. At first, the through hole diameter in the center of the fins was also 0.375 in (9.525x10^{-3} m) ,the same as the OD of the tubing, for press fit assembly, but this proved difficult as the circular runout of the through holes in the fins did not match the total runout of the tubing. The copper tubing was drawn and was not finish machined. This may be the reason for the fins not being easily press fit over it. There was some benefit to this, however, as a press fit interface between the wall of

the tubing and the fins would induce significant thermal contact resistance into the design. Thus, the fins were redesigned with a larger clearance hole that allowed an annulus of epoxy to be applied to join the fins to the copper tubing. Thus, thermal contact resistance was reduced[1]. The 21 fins were a result of determining a representative geometry of an actual heat pipe and were not based on an optimization algorithm. This coincided with the primary purpose of the research to characterize an as-built TEM-VCHP assembly and not necessarily an optimized assembly.

With the fins attached, the next fabrication step was to insert the copper screen wick into the copper tubing. A piece of screen 10.375 in by 3.5 in (263.525x10^{-3} m by 88.900x10^{-3} m) was cut out from sheet stock (McMaster-Carr part number: 9224T919). The wire diameter, d_w, was 0.0045 in (0.114x10^{-3} m) and the square spacing between the wire was 0.006 in by 0.006 in (0.152x10^{-3} m by 0.152x10^{-3} m). This volume of copper screen corresponded to the screen wrapped around four times inside of the tube and an inner vapor core radius of r_v = 0.119 in (3.023x10^{-3} m). To physically insert the wick into the tube, it was necessary to very tightly wrap it around a 3/16 in (4.763x10^{-3} m) diameter mandrel (i.e., a solid piece of copper rod stock). Precision was exercised to very carefully insert the wick into the tubing. It was essential to not allow the wick to become crimped or folded during insertion. Twisting the wick in was also avoided to prevent inconsistencies along the axial length of the heat pipe. Once the wick was fully inserted, the copper mandrel was easily slid out without the risk of pulling the wick back out. This was due to the natural tendency of the resilient screen to unwrap and return to a flattened state. Thus, it behaved as a spring which caused it to be pressed firmly along the inner wall of the tubing. This allowed the wick to be considered to be tightly wrapped which allowed a tightly wrapped wick crimping factor ($S = 1.05$) to be used for calculational purposes [16]. Additionally, the volume of screen material seemed optimal given that there was not too little such that the spring force was too weak and there was not too much such that the wick was too difficult to insert or that it would create a

[1]It is noted that the CCHP design and fabrication was performed by former M.S. student, Matt van Lieshout. Thus, he is acknowledged here for his efforts and contributions to this thesis research.

very small vapor core. A detail view of the wrapped screen wick inserted into the tubing is shown in Fig. 3.2.

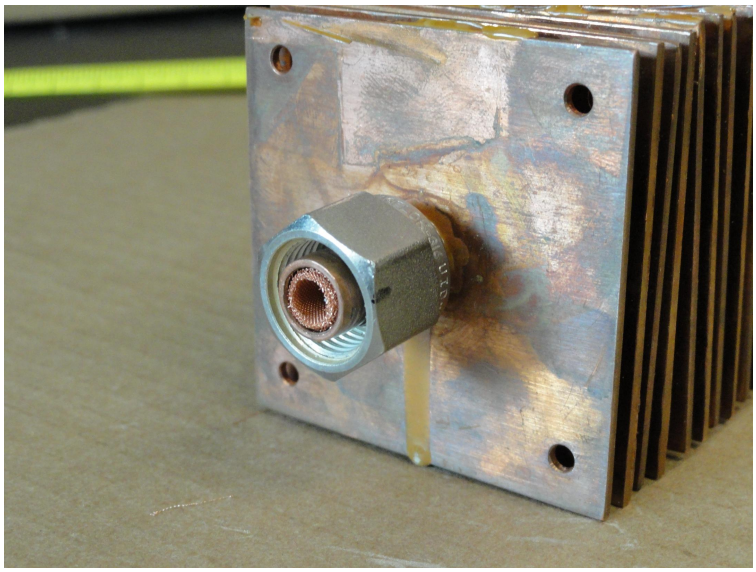

Figure 3.2: Detail view of a wrapped copper screen wick inserted into the heat pipe.

To monitor the vapor core temperature of the heat pipe, a Swagelok® 3/8 in to 1/16 in ($9.525\text{x}10^{-3}$ m to $1.588\text{x}10^{-3}$ m) tube-to-tube fitting reducer was attached to the evaporator section of the heat pipe. A 1/16 in ($1.588\text{x}10^{-3}$ m) diameter sheathed type T thermocouple was attached to the smaller end of the tube fitting reducer. To further safeguard against leaks, the inside of the fitting where the thermocouple was attached was potted with JB Weld® epoxy. To monitor the pressure inside of the heat pipe, a pressure transducer was required to be attached to it. This was accomplished by attaching a tee with two 3/8 in ($9.525\text{x}10^{-3}$ m) tube fitting ends and a 1/4 FNPT (female national pipe thread) top for attaching the pressure transducer (Omega® model PX209).

The final component of the CCHP was a valve to close off the heat pipe. This valve served two purposes. First, it was used to maintain the vacuum pressure inside of the heat pipe and to keep the ambient pressure out after it had been charged with methanol (see Appendix F). Methanol was chosen based on its ability to operate well within the triple and critical points for the expected range of vapor core temperatures to allow for adequate

liquid-vapor phase change. Secondly, it was used to separate the two sections of the heat pipe (i.e., the evaporator/condenser and the reservoir) to maintain the argon pressure used to preserve the cleanliness of the reservoir section out of the condenser. Although the entire VCHP was assembled together, it remained as a CCHP (with a blocked off reservoir) until the valve separating the two sections was opened which then allowed the exposed reservoir and argon gas (NCG) to transform the CCHP into a VCHP. Initially, a 1/4 turn plug valve was used, but it was later discovered that although this valve was designed to hold back pressure in a closed configuration, it was not designed to hold vacuum pressures. This was discovered during leak testing (see Section 3.4) and a bellows sealed valve was required. This valve (Swagelok® part number: SS-6BK) was helium leak tested according to SCS-00020, a Swagelok® procedure, where the valve was leak tested for five seconds to a maximum leak rate of 4x10^{-9} STD. cc/sec at the valve seat, envelope and all seals. As per a representative of Swagelok®, vacuum rated valves are difficult to design because the moving parts associated with them makes it difficult to maintain the negative gage pressure. Thus, selectivity was limited, but fortunately commercial-off-the-shelf (COTS) parts were readily available.

3.2.1 Heat Pipe Wick Characteristics

With the dimensions of the wick material known, it was necessary to calculate the wick characteristics as described in Section 2.2.1. Using Eq. 2.12, the effective pore radius, r_{eff}, was calculated as 0.133x10^{-3} m. The wick permeability, K, was calculated as 2.32x10^{-10} m^2 using Eq. 2.13. Based on the amount of screen used for the experimental heat pipe, the total volume of the wick was 5.335 mL. Multiplying this volume by the wick porosity, which was found to be 0.646 from Eq. 2.14, the required volume of working fluid (methanol) was 3.46 mL. This was the volume of methanol used to charge the heat pipe. See Appendix F for details regarding the methanol charging/air evacuation process. Finally, the effective thermal conductivity of the wick, k_{eff}, was calculated using Eq. 2.15. Assuming $k_l = 0.2024$ W/mK for methanol and $k_w = 391$ W/mK for 101 alloy copper for the thermal conductivity

of the wick material, the effective thermal conductivity was calculated as 0.423 W/(mK).

3.3 VCHP Fabrication

The VCHP utilized the identical evaporator, adiabatic section and condenser section from the CCHP and is shown in Fig. 3.1. However, a reservoir was necessary to contain the non-condensable gas (argon, which was chosen based on its availability in the lab and its proven success in previous work [17]) which was required to vary the thermal resistance of the heat pipe. This section was assembled independently of the condenser section and then the two parts were eventually combined to create one heat pipe. After being leak tested and combined, the two sections were cleaned at the same time as described in Appendix E. An overall view of the reservoir section is shown in Fig. 3.3.

Figure 3.3: Reservoir section of the heat pipe.

To minimize the effect of undesired axial conduction down the length of the reservoir, it was constructed from stainless steel ($k = 16.3$ W/mK) tubing and components. The primary annular portion of the reservoir was constructed from 3/4 in (19.050x10^{-3} m) diameter 321

stainless steel tubing. A larger diameter was selected to achieve the required reservoir volume while minimizing the overall length of the heat pipe. The condenser section featured all 3/8 in (9.525x10^{-3} m) diameter tube fittings and the maximum size increase for a Swagelok® tube-to-tube compression fitting from 3/8 in (9.525x10^{-3} m) was 3/4 in (19.050x10^{-3} m) (for COTS parts) which is why this diameter was selected for the reservoir. With the volume of the condenser known as 2.73x10^{-6} m^3 from the length and vapor core radius, the required length for the reservoir was calculable. Assuming a ratio of $V_r/V_c = 25$ [16], the required length of the reservoir tube section was calculated as 10.533 in (267.538x10^{-3} m) based on an inner diameter of 0.71 in (18.034x10^{-3} m). However, this ratio was slightly exceeded after the volume of the fittings and other components were summed and included; thus, the heat pipe could be assumed to have a nearly infinite large volume reservoir as described in Section 1.3. The actual, as-built V_r/V_c was 29.7.

For leak testing purposes (as a way to monitor pressure over time), the reservoir section was also outfitted with a pressure transducer. An identical valve to the one used on the condenser was also used on the end of the reservoir furthest from the condenser to seal off the heat pipe. When the heat pipe was converted into a VCHP, the entire system was under vacuum pressure as a result of evacuating all of the air during the methanol charging. The total pressure of the entire heat pipe, which consisted of a combination of the saturation pressure of methanol and charged argon pressure (approximately 38,610 Pa), was well below atmospheric pressure. Thus, the same type of vacuum rated valve required for the condenser section was also required for the reservoir section to prevent atmospheric air from entering the heat pipe.

During the CCHP experiments, the valve separating the two sections remained closed. The reservoir was charged with approximately 35 psig (241,316 Pa) of argon pressure to preserve the cleanliness of the reservoir. For the VCHP experiments, only one pressure transducer was required as the valve separating the condenser and reservoir sections was open and thus, the pressure readings across the pressure transducers were identical.

To convert the CCHP into a VCHP, the mass of argon required was first calculated based on the volume of the reservoir and the ideal gas law (see Eq. 2.8). Based on TEM-CCHP characterization experiments, where the assembly was subjected to the harshest cooling conditions (as described in Section 2.3.1), the vapor core temperature was known. The corresponding saturation pressures of methanol were calculated from tabular data [24]. Thus, with the vapor core temperature and the maximum ambient temperature known, the mass of argon was calculated using Eq. 2.8. With the required mass of argon and the room temperature known, the corresponding argon pressure was therefore known. To be conservative, it was intended that half of this pressure would be initially charged into the reservoir and the TEM-VCHP would then be subjected to the maximum cooling conditions and the fin temperatures, thermal resistances and TEM power would be evaluated. The reservoir pressure transducer would be used to measure the level of charge pressure. Then, using a needle valve from the supply tank, small amounts of argon would be incrementally added and the harshest experimental cooling conditions for the TEM-VCHP would be repeated each time until there was a slight change in its characteristics (i.e., the last fin temperature had a small decrease, the TEM power required to maintain T_{cp} decreased slightly and the vapor core to ambient thermal resistance increased slightly). Thus, the mass of argon would be "crept" up on until the optimal amount had been achieved as demonstrated by the experiments.

In actuality, the VCHP charging occurred rather differently than what would have ideally happened. It was very difficult to control the very small amount of argon pressure calculated (0.742 psia or 5111 Pa based on a mass of 6.783×10^{-6} kg) to be released into the heat pipe. The argon was contained in a large steel cylinder under approximately 2000 psig (13.789×10^{6} Pa) of pressure. A high pressure regulator was attached to the reservoir which was rated to 200 psig (1.379×10^{6} Pa). Because the required argon pressure was less than atmospheric, it was very difficult to regulate a very small amount into the heat pipe, while also ensuring that argon rather than air was released. In retrospect, a vacuum rated regulator would have been more appropriate than the high pressure regulator. However, three valves were in series

with the high pressure regulator to help minimize the pressure into the heat pipe. Directly after the regulator was a ball valve that was just barely opened which was followed by a needle valve that was also barely opened. After the needle valve was a section of 3/8 in ($9.525\text{x}10^{-3}$ m) diameter tubing which was connected to the end of the heat pipe. The third valve which was attached to the end of the heat pipe was the Swagelok® valve to keep the vacuum pressure inside of the heat pipe. This valve was also just barely opened and then was immediately closed to allow minimal argon inside of the heat pipe. An overview of the heat pipe being charged with argon is shown in Fig. 3.4.

Figure 3.4: Argon cylinder connected to heat pipe for VCHP charging.

During operation, a heater was attached to the reservoir and was wrapped in insulation to prevent methanol from condensing and collecting in the reservoir. Two thermocouples were attached to the reservoir; one near the condenser and one at the opposite end of the

reservoir. During operation, a small amount of heat was applied to the reservoir to keep the two reservoir temperatures above the condenser temperature which was represented by the vapor core thermocouple. This was the experimental procedure provided by Cleary *et al.* [17]. To ensure all of the methanol was in the condenser and none had displaced into the reservoir, the reservoir was heated for an hour with 25 W from the heater while the heat pipe remained in a vertical orientation. Afterward, only a small amount of heat was required to prevent potential condensate from entering the reservoir.

An overall view of the entire heat pipe assembly (i.e., the evaporator, adiabatic, condenser and reservoir sections) is shown in Fig 3.5.

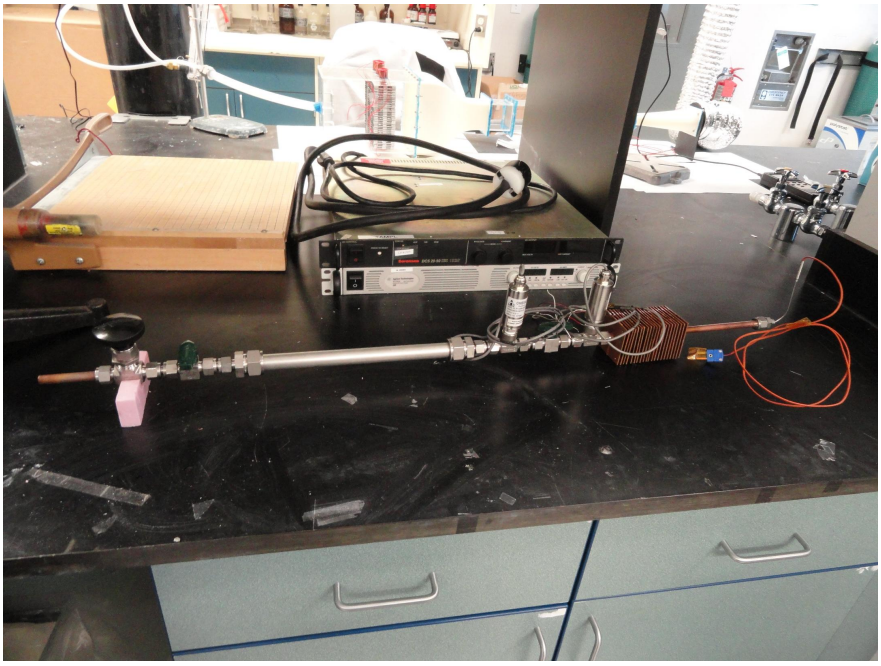

Figure 3.5: Overall view of the heat pipe assembly.

3.4 Leak Detection

As per Faghri [16], a critically important process step in the fabrication of heat pipes is leak detection. It is essential that a heat pipe be verified to be leak free prior to proceeding with its fabrication as leaks will introduce air which will adversely affect its performance.

From initial experiments performed in this research, it was shown that leaks in the heat pipe would significantly change the pressure inside of it (i.e., its pressure was no longer consistent with the saturation pressure of methanol) which would unfavorably change its thermal resistance and thus would increase TEM power consumption to maintain the setpoint temperature.

3.4.1 Coarse Leak Detection

After each section was assembled, they were individually pressurized with approximately 30-40 psig (206,842 Pa to 275,789x10 Pa) of argon. Argon was used rather than air to maintain cleanliness of the components. The first of two leak detection methods was used at this point. It served as a coarse leak check where the pressurized sections were submerged in water and large leaks would be shown by a constant stream of bubbles exiting the heat pipe. It is noted that the pressure transducers were removed for these tests as they were not rated for use with liquids. Replacing them with pipe fitting plugs during these tests caused a potential oversight (i.e., the pressure transducers themselves couldn't be leak tested), but it was determined at a later point that they did not leak. It is noted that alternative methods such as utilizing a soap solution were attempted (where gross leaks would cause soap bubbles to grow at the surface of a leak area), but the magnitude of the leaks was not large enough to efficiently use this method.

After adjustments were made to the heat pipe that removed any traces of bubbles during the coarse leak tests, the pressure transducers were reattached to each section. Then, each section was filled with 30-40 psig (206,842 Pa to 275,789 Pa) of argon pressure. The pressure transducers were monitored over the course of a week to examine the change in pressure. After making adjustments, some small changes in pressure were recorded as the result of the effect of ambient temperature fluctuation per the ideal gas law, but the pressures remained fairly constant and did not decrease over time (e.g., one day the pressure was 302,113 Pa and seven days later, it was 302,955 Pa). At this time it was concluded that both sections of the

heat pipe were leak free and were ready for cleaning. After cleaning, they were checked again and no leaks were found. The heat pipe was then deemed suitable for methanol charging and experiments.

With the heat pipe assembled and charged with methanol, the pressure recorded by the pressure transducer in the condenser section matched the saturation pressure of methanol at room temperature, which showed that all of the air had been evacuated. Experiments were then conducted to characterize the heat pipe. However, over time, the pressures began to drift apart and at a certain point, it was observed that the pressure inside the heat pipe was approximately 3.8 psia (26,200 Pa) when the pressure should have been on the order of 1.8 psia to 2.0 psia (12,411 Pa to 13,789 Pa) depending on the temperature in the room. Unfortunately, earlier leak testing had not caught extremely small leak(s) despite rigorous efforts. It was decided that the available leak testing methods in the lab were insufficient for the assumed small leak(s). Thus, more accurate leak testing equipment available at the Massachusetts Institute of Technology (MIT) was required. This served as the second method of leak detection, which was considered to be a fine leak check.

3.4.2 Fine Leak Detection

At MIT, a vacuum leak testing machine was used to check the heat pipe for leaks. The machine used a mass spectrometer to determine the rate of the leak(s) inside of the heat pipe under vacuum pressure. Specifically, the heat pipe was put under vacuum pressure and helium gas was sprayed around the joints of heat pipe. Any areas with leaks caused the helium to be pulled into the vacuum and thus into the machine's mass spectrometer. The machine was then able to determine the rate of the leaks in standard cubic centimeters per second (STD. cc/sec). To first check the validity of the readout of the machine (i.e., the leak rate), a baseline had to be established with a known, calibrated device. A calibrated pressure vessel with a known leak rate of $4.5\text{x}10^{-8}$ STD. cc/sec was attached to the machine and a vacuum was pulled down on it. An overview of the leak detector machine with the

calibrated pressure vessel is shown in Fig. 3.6.

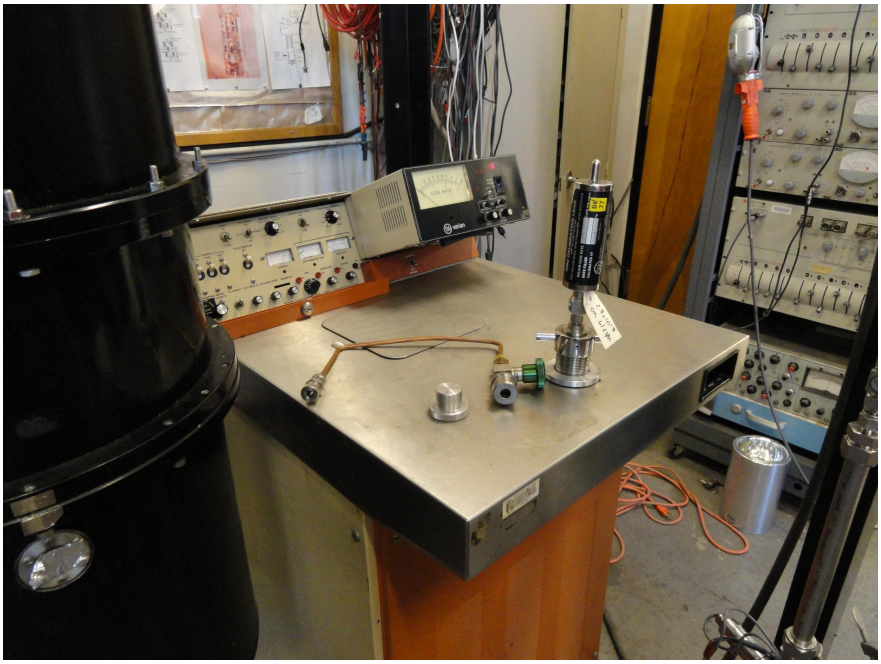

Figure 3.6: MIT leak detector with calibrated pressure vessel attached.

After spraying the connection point between the machine and the pressure vessel with helium, the leak rate was shown to be on the correct order-of-magnitude (i.e., in agreement with the calibrated pressure vessel rating). Because the machine was quite old, specific numbers were not very accurate. Rather, the order of magnitude was the value of interest when assessing the leak rate.

Next, with the machine deemed suitable for leak testing, the heat pipe was attached as an entire assembly (i.e., the evaporator, adiabatic, condenser and reservoir sections). The valve separating the two heat pipe sections was left open. The fitting with the embedded thermocouple probe in the evaporator section was left in to test its ability to withstand leaks. Thus, the first test was performed just to check the overall heat pipe for leaks. After pumping down the entire heat pipe, helium gas was sprayed around the connecting points of the heat pipe one at a time and the output was observed on the machine. All points passed the leak testing as they showed a leak rate on the order of 10^{-8} STD. cc/sec. An overview of the leak detector with the heat pipe attached is shown in Fig. 3.7.

Figure 3.7: MIT leak detector with heat pipe attached.

After the entire heat pipe was checked for leaks and none were found, the next tests to be performed were individual leak tests of the two sections: the CCHP section (evaporator, adiabatic and condenser sections) and the reservoir section. The heat pipe was separated at the valve between the two sections. The valve remained open and was left attached to the CCHP section which was the first to be leak tested. The valve end was then attached to the leak detector tube and the opposite remained the same with the embedded thermocouple fitting. A plastic bag was tied around the entire CCHP section and filled with helium, thus creating a helium rich environment. Any leaks would pull this helium rich environment into the mass spectrometer. However, the result of the leak testing remained the same at an order of magnitude of 10^{-8} STD. cc/sec. Positive results were being shown that leak detecting at the Tufts lab were being confirmed at the MIT lab.

However, this was proven otherwise when the reservoir section was leak tested. The valve

separating the two sections was attached to the reservoir in a closed position to make the heat pipe a closed pressure vessel and to simulate the CCHP tests where the reservoir would be attached, but at a higher pressure than the condenser section which would be under vacuum pressure. Thus, vacuum leak testing was essential to verify that the valve was not the troublesome area that caused the pressure inside of the heat pipe to rise unexpectedly over time in the previous experiments. The opposite end of the reservoir section (the quarter turn plug valve) was attached to the leak testing machine. Again, the helium filled bag was used to improve the stability of the leak rate reading on the machine.

However, when trying to pull a vacuum down on the reservoir section with the closed valve, the leak rate could not even be read out on the machine as the leak rate was too high to pull a vacuum down. Since all other connection points on the reservoir section had already been checked, it was concluded that the valve separating the two sections was the source of the leaks. The valve did not leak during the previous overall test because it was in an open position, but leak testing it under a closed position showed otherwise.

It was concluded that the valve separating the two sections could hold positive pressure in a closed configuration as was its intent. However, it was unable to maintain vacuum pressure. This explained why the pressure did not change when the heat pipe was leak tested under positive argon pressure (it was deemed leak free) and why it did change over time after it was charged with methanol and was under vacuum pressure. It is noted that the direction on this valve as well as other valves is more for throttling purposes and it does not affect the valves' ability to hold back pressure regardless of its orientation with respect to the high pressure side. This was the explanation provided by a Swagelok® representative.

After speaking with Swagelok®, it was confirmed that the quarter turn plug valve design is not rated for vacuum applications, particularly in a closed configuration. Although not many valves are available due to moving parts of valves making it difficult to be vacuum rated, Swagelok® was able to recommend a vacuum rated valve as described in Section 3.2. Two of these valves were used. The first was used to address the leak issue between the

condenser and reservoir sections, particularly in a closed configuration when CCHP only tests were being performed. The second valve was used on the end of the reservoir to keep atmospheric pressure out of the heat pipe. Once the heat pipe became a VCHP, the absolute pressure inside of the heat pipe would still be below atmospheric pressure. Thus, a vacuum rated valve suitable for use in a closed configuration was also required.

3.4.3 Vacuum Pump System

The Swagelok® recommended valves as described in Section 3.4.2 seemed sufficient for preventing argon or air from entering the condenser section of the heat pipe as opposed to what happened with the quarter plug valves. However, the new replacement valves presented a new problem in that a small amount of air was initially being trapped inside of the heat pipe when they were closed during the methanol charging procedure. This problem did not exist with the quarter turn plug valves (i.e., the pressure transducer reading was very close to the saturation pressure of methanol at ambient) and multiple attempts were made to charge the heat pipe to get the air out. At one point, the methanol was allowed to boil off for over two minutes , in a vertical orientation with the end valve open, to ensure all of the air had been pushed out. Eventually, it was determined that it was not exactly obvious as to how some air was being initially trapped and thus the experiments had to resume with the understanding that the small amount of air was not enough to adversely affect the performance of the heat pipe.

To make the heat pipe behave as a CCHP, a vacuum was pulled down on the reservoir section and the valve separating the condenser and reservoir sections was opened. Essentially, the CCHP was an air-methanol VCHP with a very large reservoir given the relatively small amount of air inside. Thus, it was assumed that the volume of the heat pipe was so large that the air-methanol flat front was far from the finstack and that it was not enough to affect the theoretical constant thermal resistance of the heat pipe and thus a CCHP could be assumed.

As per Faghri [16] and industry recommendations, a vacuum pump with the ability to pump down to a magnitude of 10^{-5} Torr is required to make a good heat pipe. A Oerlikon Leybold® pump (model number: 91265-2) was purchased with the capacity to pump down to 8x10^{-5} Torr.

Aside from the pump itself, other vacuum components were required to complete the vacuum system. An oil mist eliminator was implemented to keep the lab environment clean. Although it was not required, especially given the relatively small amount of time it was being run, it was good practice to have the oil mist eliminator attached from a cleanliness standpoint. From the outlet port of the pump, a toggle valve was required to safely bring the pump back to atmospheric pressure once it was done pumping down. Downstream of the toggle valve was a vacuum rated (rated to 10^{-5} Torr) ball valve that allowed the pump to be isolated from the system. After the ball valve was a vacuum rated MKS® Micro Pirani pressure transducer (model number: 925) capable of measuring 10^{-5} Torr to atmospheric pressure. This pressure transducer was required to accurately measure the level of vacuum achieved by the pump and also of the heat pipe once the ball valve was closed. The Omega® pressure transducer attached to the reservoir section of the heat pipe had the ability to measure vacuum pressure, but it did not have the resolution to measure down to 10^{-5} Torr accuracy. Assuming a minimum voltage reading of 1 mV, the lowest reading from the Omega® transducer was 0.014 psia (96.5 Pa or 0.724 Torr), far from the accuracy required. A specific set of calibration data unique to the purchased pressure transducer is provided in Appendix J.

The final connection point was a KF25 flange to 3/8 in (9.525x10^{-3} m) compression tube fitting which connected the vacuum system to the heat pipe through a length of thick walled stainless steel tubing. It is noted that all tees and vacuum components utilized KF25 flange fittings (for 1 in or 0.025 m OD tubing) to maintain as large a length/diameter ratio as possible and minimize the time required to pump the heat pipe down to the required vacuum pressure. An overview of the vacuum system is shown in Fig. 3.8.

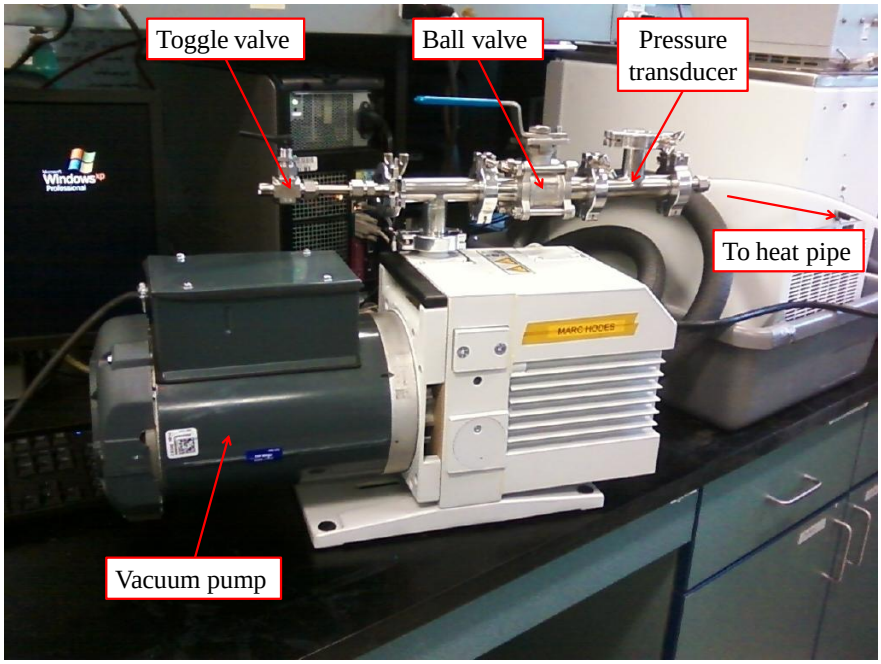

Figure 3.8: Vacuum pump assembly.

The vacuum was turned on and allowed to pump the system down to 8x10^{-5} Torr. This was confirmed with the vacuum pressure transducer. Because of the large capacity of the pump (13.4 CFM or 0.0063 m^3/sec) and the use of large fittings (1 in or 0.025 m OD) until the heat pipe (3/8 in or 9.525x10^{-3} m OD), the pump did not take very long to pump down to the desired pressure. Once the pressure was achieved, the ball valve was closed and the pressure was monitored as it represented the pressure in the heat pipe reservoir. Once it was concluded that the maximum amount of air had been evacuated from the reservoir section, the valves separating the heat pipe from the vacuum system were closed and the pump was shut off. The valve separating the reservoir from the condenser section was then opened and the small amount of air in the condenser was allowed to disperse into the reservoir, thus effectively making the CCHP a VCHP with a reservoir volume so large that did not allow the air to affect the thermal resistance of the condenser. The final step was to open the ball valve separating the heat pipe from the vacuum system and to slowly open the toggle valve on the vacuum system to allow the pump to be safely ramped back up to atmospheric pressure.

To summarize the procedure: only the reservoir section was pulled down to vacuum pressure. It was assumed that the vacuum rated valve (which was initially closed) which separated the CCHP section from the reservoir did not allow methanol to be pulled through it. Therefore, the potential loss of methanol was not a concern. Once the reservoir had been evacuated, the valve was opened which exposed the small amount of air inside of the CCHP section to the much larger volume of the reservoir. It was assumed that this would have a minimal effect on the expected constant thermal resistance of the CCHP.

3.5 Evaporator Assembly

Typically, heat pipes use some sort of heat spreader or a similarly thermally conductive interface between a heat source and the heat pipe. This allows heat to be transferred efficiently from the source to the heat pipe; thus, heat is properly drawn away towards an appropriate release area. This was also true in the case of the experimental TEM-CCHP/TEM-VCHP assembly. It was necessary to conduct the total heat from both the heat source (Kapton® heater) and the heat dissipated by the TEM through its uncontrolled side substrate during cooling and heating modes to the evaporator section of the heat pipe. However, as this was also an experimental apparatus, key temperatures were required to be measured and recorded. Thus, thermocouples were required and had to be accounted for and taken into consideration when designing the evaporator assembly.

An evaporator stackup was designed to address all of these requirements. Additionally, the evaporator stackup and its components were designed to be of relatively simple geometry to keep machining feasible and to ease the assembly and disassembly processes. It was not designed to be a one time, permanent setup. An overview of the stackup is shown in Fig. 3.9.

First, the heat dissipated by a photonics component was simulated experimentally by attaching a 1 by 1 in (25.4 mm by 25.4 mm) adhesive-backed Kapton® heater to copper block (k = 391 W/mK) with a cross-sectional area of 1.181 by 1.181 in (30 by 30 mm)

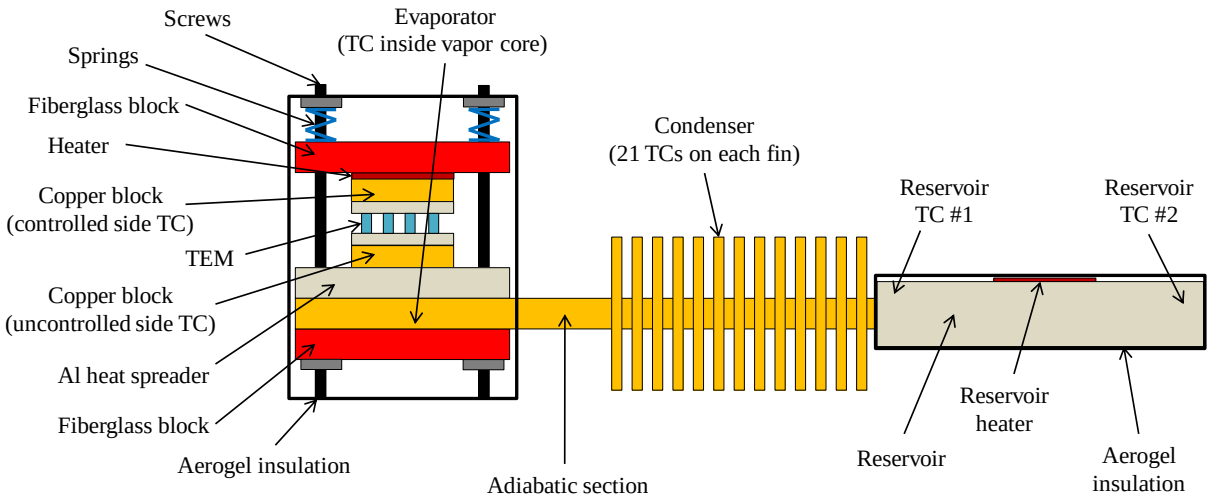

Figure 3.9: Overall stackup of experimental evaporator.

with a thickness of 0.125 in (3.175x10^{-3} m). A tight fit hole for a 1/16 in (1.588x10^{-3} m) diameter sheathed, type T thermocouple was drilled into the center of the copper block. The thermocouple was coated with Laird® Tgrease™ 2500 thermal grease and was then inserted into this copper block to measure the control plane temperature of the simulated component (T_{cp}, i.e., the temperature being controlled). With the heater and copper block having similar cross-sectional areas and given the relatively small thickness of the copper block, it was assumed to be isothermal and thus the temperature reading of the thermocouple represented the control plane temperature.

Above the heater was an insulating block made from GPO-3 fiberglass with a thermal conductivity of 0.274 W/mK. The dimensions of this block were 3.775 in by 1.960 in (95.885x10^{-3} m by 49.784x10^{-3} m) with a thickness of 0.5 in (12.7x10^{-3} m). The reason for the block being oversized compared to the heater was to allow room for through holes required to allow the entire stackup assembly to be held together with four bolts in a "sandwich" configuration. This is described later on in this section.

Below the heater and copper block was a layer of Laird® Tgrease™ 2500 thermal grease followed by a Laird® TEM with its ceramic substrates having a cross-sectional area of 30 by 30 mm. The grease allowed the copper block and TEM to be as thermally conductive as

possible while minimizing contact resistance (regardless of the TEM substrates being lapped and the copper being machined flat). Next, was another layer of thermal grease followed by another 1.181 by 1.181 by 0.125 in (29.997x10^{-3} m by 29.997x10^{-3} m by 3.175x10^{-3} m) copper block with another embedded thermocouple. This thermocouple was used to monitor the uncontrolled side temperature of the TEM.

Below the TEM uncontrolled side copper block was another layer of thermal grease followed by a block of 6061-T6 aluminum with a similar footprint of the aforementioned fiberglass block (the connecting bolts passed through this as well). The primary purpose of this aluminum block was to act as a heat spreader and thus evenly distribute the heat dissipated by the TEM and heater over the length of the evaporator on the heat pipe (3.775 in or 95.885x10^{-3} m). The thermal conductivity of the aluminum was 167 W/mK. On the opposite of the copper block, a slot was machined using a 3/16 in (4.763x10^{-3} m) radius ball end mill, which matched the outer radius of the copper tubing used for the heat pipe. Thermal grease was used as an interface between the aluminum heat spreader and the copper tube. Finally, a second insulative fiberglass block was used to complete the evaporator stackup assembly. The purpose of this block was to allow the "sandwich" to be completed and to also ensure that a majority of the heat dissipated by the TEM through the aluminum heat spreader continued to be conducted into the heat pipe and not elsewhere. To aid in this, the fiberglass block had a V-notch milled out at a 45° angle. Essentially, the heat pipe was only in contact with this block along two lines of infinitely small area.

To complete the "sandwich" of the evaporator stackup, four long 1/4-20 cap screws, washers and nuts were used to fasten the entire assembly together. The heads of the bolts were oriented above the controlled side of the TEM and the nuts below the fiberglass block below the heat pipe. Directly below the heads of the screws were flat washers followed by four springs with a stiffness of 110 lb_f/in (19,263 N/m). Based on the thermal resistance (°C/in^2/W) of the thermal grease as a function of pressure (psi), there appeared to be diminishing returns on the level of thermal resistance beyond 50 psi (344,737 Pa) where

the thermal resistance was about 0.017 °C/in^2/W (26.35°C/m^2/W). A datasheet for the Tgrease^{TM} is provided Appendix K which includes a plot of thermal resistance as a function of pressure.

To achieve the desired thermal resistance from the thermal grease, the areas where the grease was used were calculated (i.e., between the copper blocks and the TEM and between the aluminum heat spreader and the heat pipe). With the heat spreader to heat pipe surface area calculated as a larger amount (2.221 in^2 or 1.433x10^{-3} m^2 compared to 1.395 in^2 or 0.900x10^{-3} m^2 for the copper blocks), the force associated with 50 psi (344,737 Pa) was determined as 111.05 lb$_f$ (19,447 N/m). This was done to ensure that the larger surface area thermal grease still was at 0.017 °C/in^2/W (26.35°C/m^2/W) while the smaller surface area would see an even lower thermal resistance. Based on this force, the pressure at the copper block to TEM interface was calculated as 79.61 psi (548,890 Pa which corresponded to 0.015 °C/in^2/W or 23.25°C/m^2/W). With the force and stiffness of the springs known, the displacement required to achieve the aforementioned thermal resistances was thus known and was calculated as 0.252 in (6.401x10^{-3} m). Because the screws had 1/4-20 threads, this translated into a requirement of approximately five turns for each screw to compress the springs the right amount. The screws were turned one turn, one at a time in a cross/diagonal manner to allow even distribution of the load and to keep the evaporated stackup level and parallel. The final spring displacement was checked by recording the preload height from the bottom of the washer to the top of the fiberglass block (measured with a set of calipers) and comparing it to the post-tightening height.

Finally, the entire assembly was covered in aerogel to maximize the heat transfer from the heater to the TEM and from the uncontrolled side of the TEM into the evaporator section of the heat pipe. Aerogel was chosen based on its highly insulative properties with a thermal conductivity of $k = 0.016$ W/mK [25]. An as-built view of the evaporator without the aerogel is shown in Fig. 3.10.

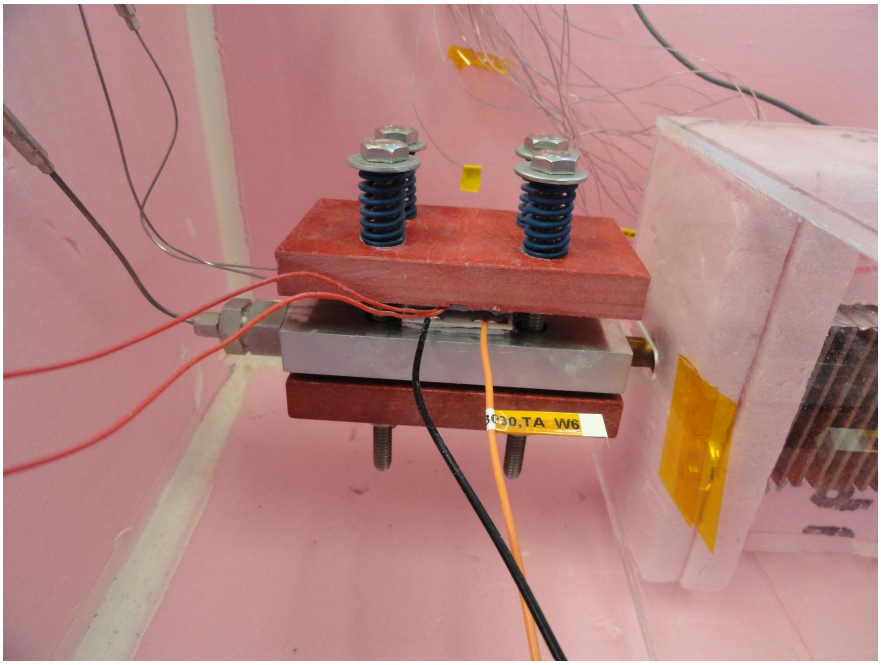

Figure 3.10: Overall view of experimental evaporator stackup.

3.5.1 TEM Specifications

TEMs are much simpler in design when compared to the heat pipe and evaporator assemblies and can be purchased off the shelf. The wide range of available TEM geometry (i.e., pellet height and footprint) is such that COTS TEMs may often be purchased and implemented without the need for custom fabrication. As such, a COTS TEM with comparatively medium-height pellets was selected for the experiments. The chosen TEM was a Laird® HT6,7,F2,3030 model with a nominal substrate area of 30 by 30 mm and a pellet height of 1.651 mm. However, microscopic inspection showed that the actual substrate area was 30.048 by 30.048 mm and the actual height of the pellets was 1.578 mm. The actual cross-sectional area of the pellets was 1.364 by 1.364 mm. There were a total of 142 pellets or 71 thermocouples. The actual thickness of the ceramic substrates was measured as 0.803 mm. Microscope photographs used for measuring the actual geometry of the TEM may be found in Appendix H.

This TEM was selected based on its pellet height which fell in the middle of the available test samples provided by Laird® (other pellet heights available were 1.097, 1.855 and 2.377

mm). It is noted that these TEMs were known as a "porch" style in informal Laird® terminology, meaning the uncontrolled side substrate extended beyond 30 mm in one direction and the electrical leads were exposed. The uncontrolled side substrate was actually 30.048 by 34.036 mm, but the pellets were only attached to the 30.048 by 30.048 mm area, so this was considered as the uncontrolled side substrate dimensions as Peltier cooling and heating could only happen there. This also signified a high temperature capacity TEM that featured a nickel diffusion barrier to help protect the pellet to substrate solder joints. A complete datasheet of the experimental TEM is provided in Appendix H.

The TEM was placed inside of the evaporator stackup as described in Section 3.5. The controlled side substrate interfaced with the heater block to maintain the setpoint temperature and the uncontrolled side (with the attached electrical leads as shown in Fig. 1.1) was attached to another copper block near the evaporator section of the heat pipe. A view of the TEM only and the TEM mounted to the copper block and aluminum heat spreader with the heater block on its controlled side substrate is shown in Fig. 3.11.

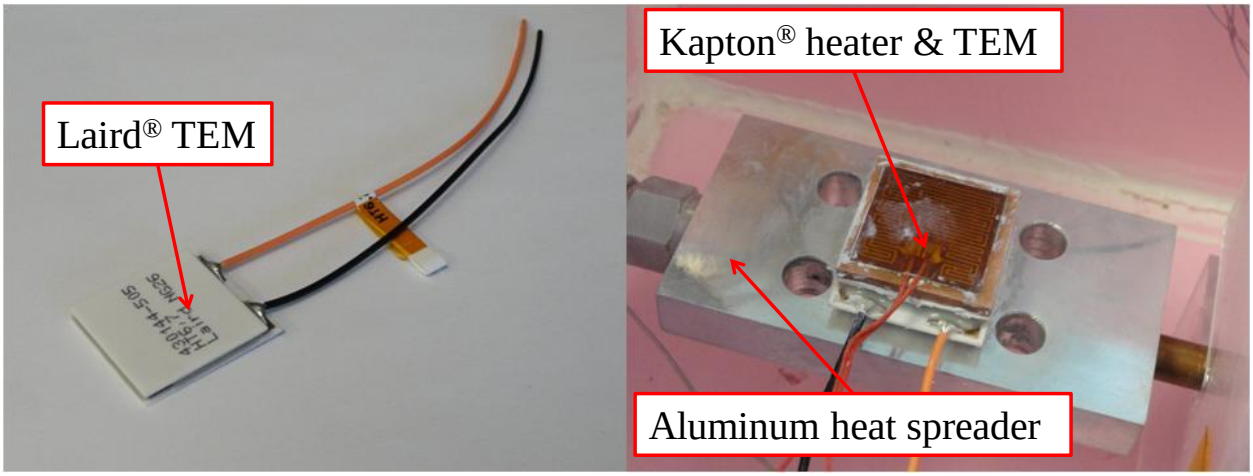

Figure 3.11: TEM only and TEM mounted to heat pipe evaporator stackup with heater attached.

CHAPTER IV

Testing

With the heat pipe fully assembled and combined with the TEM, the experimental rig was ready to be outfitted with the equipment necessary to measure key temperatures and pressures. Once outfitted with the proper measuring equipment, a means of recording the data was designed and set up. Finally, an environmental chamber to simulate the wide range of environmental conditions was assembled and the TEM-heat pipe was subjected to required conditions.

4.1 Measuring Equipment

As described in Chapter III, the heat pipe had pressure transducers to measure the condenser and reservoir absolute pressures and it had sheathed type T thermocouples embedded into copper blocks to measure relevant temperatures on the controlled and uncontrolled sides of the TEM. It also had a thermocouple attached to a tube fitting to measure the vapor core temperature of the heat pipe. Other pertinent temperature locations included each of the tips of the fins on the condenser finstack and the two thermocouples measuring the temperature of the reservoir (as described in Section 3.3). Given the geometry and thermal conductivity of the fins, a fin efficiency of 100% was assumed, so that the tip temperature represented the temperature of each fin. The thermocouples were attached to the fins using thermal grease and aluminum tape. They were not epoxied on as a permanent bond would

have prevented the thermocouples from being reused. The reason for this was that all of the thermocouples had been carefully calibrated as per the research performed by Zhang [26]. The thermocouples were calibrated using a reference temperature of 0°C. Thus, an ice bath was required to control the reference junction of the thermocouples. Two calibrated thermistors were available. One was used to measure the temperature of the ice bath and the other was used to measure the ambient temperature of the environmental chamber. A photograph of the ice bath is shown in Fig. 4.1. Note, a cover made from 2 in thick foam was used to cover the ice bath, but it is not shown for clarity.

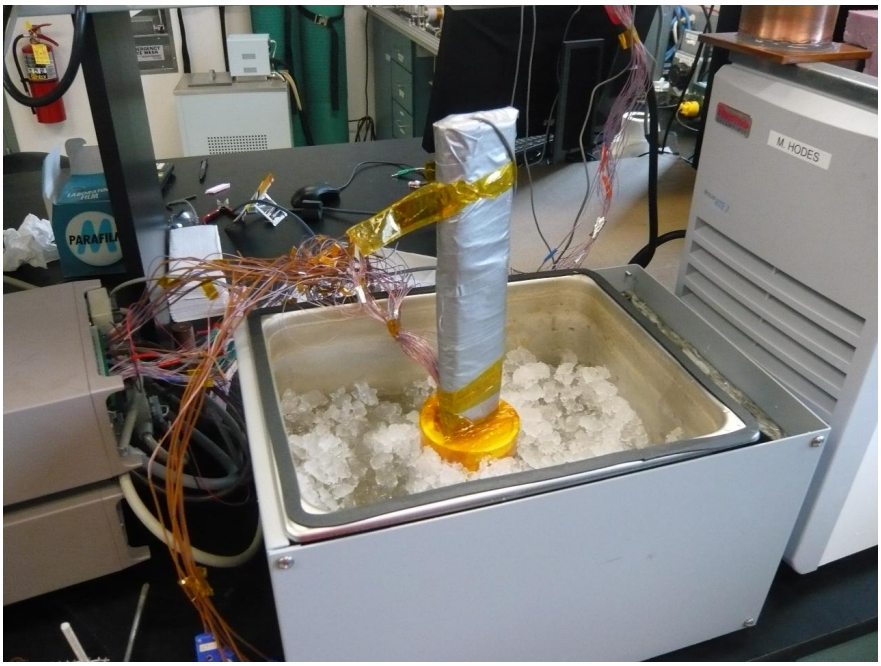

Figure 4.1: Ice bath used to maintain the thermocouples' reference temperature.

Other important data to be measured included the heaters and TEM voltages and currents. This was required to determine the heat dissipated by the heaters on the controlled side of the TEM and at the reservoir (to maintain a higher temperature at the reservoir over the condenser) and to determine the TEM power consumed required to maintain the prescribed setpoint temperature. To maintain the setpoint temperature in certain situations, the TEM had to operate in generation mode. To achieve this, a potentiometer was connected across the leads of the TEM and its electrical resistance was varied until the setpoint tem-

perature was maintained. Thus, the electrical resistance of this potentiometer was measured when it was required. All of the aforementioned electrical properties were measured using a multimeter (Fluke® model number: 179). A "permanent" (i.e., it was not removed during the extent of the experiments) multimeter was run in series with the TEM's electrical connection to a power supply to measure its current draw. It is noted that it was discovered the multimeter behaved as an additional electrical resistor as it had a certain level of electrical impedance associated with its internal components which affected the TEM's performance when it was turned on. Because the multimeter had an automatic shutoff feature, it was kept off until the current was to be measured (after data collection) for consistency (i.e., the system could reach the desired steady state conditions with the multimeter turned on, but then would change once the automatic shutoff feature occurred).

The electrical resistance of the multimeter set to measure DC current was measured across its leads with an identical multimeter. This was done with it on and off and the result was the same with the electrical resistance being 0.2 Ω. After speaking with a technical representative at Fluke®, it was confirmed that the electrical resistance varied to a small degree when the multimeter was turned off. Although this change was too small to be measured based on the resolution of the other (identical) multimeter, it was still a sufficient amount such that it caused a variation in the controlled side temperature of the TEM.

To maintain the ambient temperature inside of the environmental chamber, a temperature controllable recirculating bath (Thermo Scientific® Neslab RTE 7) was connected to a heat exchanger (Lytron® part number: 6105G1SB) with a fan. The temperature of the digital readout on the recirculating bath was recorded. No measurements were performed for this temperature. The heat exchanger fan was powered with 120 VAC from a Variac®. The voltage required to power the fan was also recorded.

4.2 Data Acquisition Systems

With the measuring devices setup as described in Section 4.1, a means of recording the data was required. As the purpose of the experiments was to demonstrate steady state operation of a TEM-VCHP assembly, data was recorded for at least 10 minutes without making adjustments and after all temperatures had leveled off. The temperatures and pressures were recorded over the course of this steady state period using LabView. Specifically, the temperatures voltages (in mV) were recorded through a Keithley nanovoltmeter. This nanovoltmeter was also used during the thermocouple calibration [26]. The voltages were later converted to Celsius using Seebeck integrals [26] or temperature as a function of voltage sixth order polynomials specific to each thermocouple. The pressures were also recorded using LabView. Based on the calibration report specific to each individual Omega® pressure transducer, the voltage output of the transducer was converted to pressure (in psia) using a second order polynomial in LabView.

Regarding the two thermistor (Fluke® serial numbers: B072717 and B072719) temperatures, their data was reported in Celsius and not voltage as they were calibrated within 0.01°C which was a sufficient tolerance. It was simpler and far less time consuming to have the ice bath and ambient temperatures reported in real time in Celsius to make necessary adjustments to the recirculating bath to maintain the desired ambient temperature inside of the environmental chamber and to know when the ice bath had reached steady state. The output of the data recorded by LabView was easily converted in an Excel spreadsheet, where further analysis (i.e., computing the average of each temperature and pressure over the steady state time) could be performed.

The heaters' and TEM's voltages and currents were not recorded over a period of time and were simply written down after being measured as they were fixed parameters after making necessary adjustments. The same holds true for the heat exchanger voltage.

4.3 Environmental Chamber

To simulate the environmental conditions a TEM-heat pipe would normally be subjected to in a photonics component application, an environmental chamber was constructed to achieve a wide range of ambient temperatures (-5°C to 65°C). It consisted of simple construction as the exterior of the chamber was made from 1/2 in thick plywood with 2 in thick insulating foam lining the interior. Two holes were cut in one side to allow access for the inlet and outlet of the heat exchanger. The ambient temperature was achieved by adjusting the recirculating bath setpoint temperature until the ambient temperature thermistor matched the desired temperature (e.g., -5°C). It is noted that the recirculating bath temperature had to be set slightly above the desired ambient temperature for above ambient temperature experiments and below it for sub ambient temperature experiments. For example, to achieve 65°C inside the chamber, the bath had to be set to 68.25°C and to achieve -5°C, the bath had to be set to -10.45°C in two particular tests. Insulating foam was used to minimize undesired heat transfer to the room from the bath inlet and outlet tubes.

Electrical terminals were attached to the side of the chamber to access the heater, TEM and heat exchanger electrical leads which could be easily connected to power supplies. To complete the chamber, a cover was constructed from plywood and foam and was screwed down to minimize temperature losses.

Inside of the chamber, a "homemade" wind tunnel constructed of clear acrylic was centered around the condenser finstack portion of the heat pipe for concentrated ambient temperature control. Foam was used to block all passages around the fins so that air flow could only pass through the fins to enable the use of parallel plate internal flow correlations. This portion of the environmental chamber was considered to be the ambient temperature as it was concentrated around the heat pipe and was carefully controlled. The ambient temperature thermistor was located within this wind tunnel. The heat exchanger was connected to this wind tunnel so that its fan pushed air away from the wind tunnel. This was done to recirculate the airflow within the environmental chamber and prevent disruptive, turbulent

flow within the tunnel and over the fins. An overview of the heat pipe inside of the wind tunnel inside of the environmental chamber is shown in Fig. 4.2.

As per Fig. 4.2, the insulated evaporator stackup is shown on the left hand side. Going bottom to top, the finstack is shown inside of the wind tunnel with all passages blocked except those through the fins themselves. The pressure transducers and reservoir section follow. In the bottom center of Fig. 4.2, the heat exchanger fan connected to the recirculating bath inlet and outlet tubes is visible. The thermocouples are routed through the bottom of the chamber, the electrical leads terminate towards the right side and the pressure transducer leads are routed through the bottom right hand side.

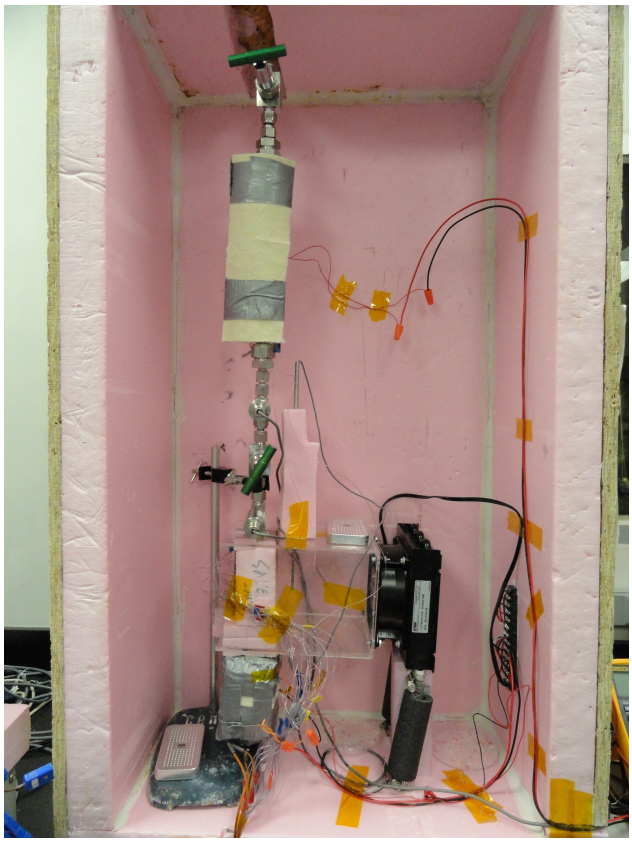

Figure 4.2: TEM-heat pipe inside the wind tunnel inside the environmental chamber.

To minimize moisture inside of the chamber, desiccant was placed inside next to the heat exchanger. This was particularly important for the -5°C and 0°C (as described in Section 4.5) experiments where ice would build up on the fins of the heat exchanger. Upon completion of

these experiments, the ice would melt and would condense inside of the chamber. The cover of the chamber would be removed and the puddles would be wiped up. The desiccant color changed when it became saturated with moisture (it would turn from blue to pink). The desiccant was baked out using an oven set to approximately 140°C until the color turned back to blue.

4.4 Overall Experimental Setup

With each subcomponent of the experimental apparatus described in Sections 4.1, 4.2 and 4.3, a complete overall view of the entire experimental apparatus is shown in Fig. 4.3.

Figure 4.3: Overall view of experimental apparatus.

In Fig. 4.3 going left to right, a computer with LabView to record the thermocouple voltages and thermistor temperatures, the recirculating bath, thermocouple reference junction ice bath, environmental chamber with the TEM-heat pipe inside, heater and TEM power supplies, Variac® power supply for the pressure transducers and a computer with LabView to record the pressure are shown.

4.5 Experimental Testing

The procedure for conducting experiments was fairly simple. The primary objective of the experiments, regardless of the TEM-CCHP or TEM-VCHP configuration, was to maintain the setpoint temperature (T_{cp} = 63°C) for a combination of specified heat load and ambient temperature. Note, 63°C was chosen to demonstrate sub-ambient cooling at $T_{\infty,max}$ = 65°C. A matrix of experiments was conducted to cover a range of heat loads and ambient temperatures representative of an actual photonics application. Specifically, nine experiments were conducted for the TEM-CCHP configuration and then were repeated for the TEM-VCHP to illustrate the power savings associated with the ability to alter the thermal resistance of the heat pipe. These nine experiments were based on heat loads of 2 W (0.22 W/cm^2), 4.5 W (0.50 W/cm^2) and 7 W (0.78 W/cm^2) and ambient temperatures of -5°C, 30°C and 65°C.

To perform an experiment, the recirculating bath was set to a temperature that corresponded to the desired ambient temperature inside of the environmental chamber. The heat exchanger fan was turned on and the Variac® was turned up all the way for consistency across the experiments. It is noted that the Variac® was supposed to provide 120 VAC, but for reasons unknown, the recorded voltage across it often ranged from 130-140 VAC on average (the actual voltage draw was fairly "noisy"). Turning the Variac® all the way up was the only way to maintain somewhat consistent airflow. As a future reference, a DC fan may be a better solution than the AC fan used as the voltage can be controlled more carefully (i.e., with a good power supply rather than a fairly old Variac®). Implementing a hotwire anemometer will also help contribute to more consistent airflow across experiments.

It took about two hours for the chamber to reach the set ambient temperature from room temperature. The ice bath was also set up in parallel as it took some time to reach steady state. This was because the copper cylinder to which the thermocouples' reference junctions were attached had a large thermal capacitance. The heater was adjusted to a voltage to dissipate the desired heat load.

As T_{cp} was monitored in real time, adjustments were made to the TEM voltage in order to maintain this temperature. The TEM was connected to a power supply to Peltier cool or heat depending on the experiment. Positive current was supplied to the TEM in cooling mode and the polarity was reversed to provide Peltier heating as shown in Fig. 2.1. The control plane heater and TEM voltages were checked (then adjusted if required) using a multimeter. The digital readouts on the power supply were not referred to. The power supply powering the pressure transducers was turned on to 24 VDC (excitation voltage was 7 to 35 VDC as per the Omega® datasheet in Appendix I) and the computer recording the pressure transducer readings was set up with LabView running. No adjustments were made to the pressure transducers as it was a passive attribute of the heat pipe.

In LabView, three data files were recorded for the thermocouple voltages, the pressure and the two thermistors (ice bath and ambient temperatures) and were saved as ".lvm" files which could easily be converted to Excel files. For consistency, these files were named by month, day, year, data being recorded and number in the format: "MM-DD-YY-TC-#", "MM-DD-YY-P-#" and "MM-DD-YY-BS-#", respectively. This allowed the data files to be traceable to the experimentation date and to the master Excel spreadsheet that compiled all of the data.

The individual adjustments made to maintain the setpoint temperature affected other parameters which required further adjustments to be made. For example, increasing the TEM power in cooling mode to reduce T_{cp} from 66°C caused the ambient temperature to decrease slightly and increasing the bath temperature was required. A decrease in T_{cp} would reduce the ambient temperature despite the increased TEM power needed to do so. Constant temperature monitoring and adjustments were necessary until steady state conditions were achieved.

Using LabView allowed real time monitoring of the voltages of the thermocouples and the temperatures of the thermistors. Once the setpoint temperature was achieved, the ambient temperature was controlled within 0.1°C and all of the temperatures were at steady state,

data was collected for a minimum of 10 minutes. The data files were saved in the format previously described. After the data was recorded, the voltages and currents were measured. This was done afterward to avoid disrupting the experiments when data was being recorded. For example, measuring the current draw from the heater required the circuit to be broken so that a multimeter could be attached in series.

It is noted that for the -5°C experiments, the recirculating bath and heat exchanger were left on for a minimum of three hours at 0.6°C. This was the only way that the -5°C ambient temperature inside the environmental chamber could be achieved and controlled. Moisture would accumulate on the fins of the heat exchanger and attempting to ramp down to the bath set temperature of -9 to -11°C from room temperature or any other temperature significantly above freezing would cause the fins in the heat exchanger to build up with ice at an excessive rate. The ice would block the fins which reduced the effectiveness of the heat exchanger. If this occurred, it was not possible to control the ambient temperature below -4°C. The temperature would become close to -5°C, but then would increase and would not be controllable regardless of the setpoint temperature of the recirculating bath.

Upon the completion of -5°C experiments, the desiccant was baked out to maintain its effectiveness as described in Section 4.3.

4.6 Fabrication Challenges

Despite attempting to maintain strict control of each fabrication step, unforeseen events caused the actual experimentation steps to be conducted differently than initially anticipated. Specifically, the addition of the new vacuum rated Swagelok® valves alleviated the issue of atmospheric pressure slowly entering the heat pipe over time, but a small amount of air somehow got trapped inside of the heat pipe during methanol charging. The vacuum pump was not designed for pumping down on combustible or flammable gases or vapors so it could not be used to remove the air during methanol charging or afterward.

To remedy this issue, the valve which separated the condenser section from the reservoir

section was opened. Effectively, this exposed the small volume of air to a substantially larger volume ($V_r/V_c = 29.7$) of evacuated space and thus made it almost insignificant (i.e., the methanol-air front was far from the finstack and did not block off any fins). This made the CCHP essentially a VCHP with an infinite reservoir volume. While this alleviated the effect of the air on the CCHP, it also caused some methanol to condense in the reservoir and thus the heat pipe did not work properly when operating in a horizontal orientation. Earlier experiments with the valve closed with the heat pipe in a horizontal orientation established a baseline in terms of TEM power consumption. The setpoint temperature could not be controlled and the TEM power consumption was not repeatable after the section separating valve was opened.

Once the heat pipe was oriented vertically, the setpoint temperature was controllable again. The TEM power consumption results were also more consistent with the baseline experiments. Thus, it was concluded that the heat pipe was indeed operating as a CCHP and not a thermosyphon which uses gravity assistance to aid in the reflow of condensate back to the evaporator section. A small amount of heat was applied to the reservoir (which was also wrapped with aerogel) to ensure that methanol did not condense in the reservoir and to prevent a similar problem from happening again.

Because the CCHP was demonstrated to operate as a heat pipe and not a thermosyphon, the TEM-VCHP experiments were also conducted in a vertical orientation. This was done to maintain consistency across the two experiments so that the results were comparable. Under ideal circumstances, the Swagelok® valve would not have introduced any air into the system in addition to holding back atmospheric pressure. This would have allowed both experiments to be performed with the heat pipe oriented horizontally.

As described in Section 3.3, the calculated amount of argon required to convert the CCHP into a VCHP was overcharged into the heat pipe. The calculated amount of argon pressure was supposed to be 0.742 psia (5116 Pa) based on Eq. 2.8 and it was supposed to have been achieved in small increments. However, the actual amount of pressure used in the

VCHP was much more than desired at 3.539 psia (24,400 Pa), a significant overcharge. This translated into an actual mass of $3.238\text{x}10^{-5}$ kg, when the desired mass was $6.783\text{x}10^{-6}$ kg. Due to time constraints, the VCHP experiments had to continue with the much higher mass of argon inside of the heat pipe.

There was high confidence in all of the measuring instrumentation with the exception of the calibrated thermocouples. The thermocouples (as is shown in Chapter V) seemed to have the largest inconsistency and variation. Since no suspicious trends were observed during their calibration [26], it is considered that the variation may be due to the way they were attached to the heat pipe and possibly the way that the fins were attached (with epoxy). Although the pressure transducers showed no such issues, it is noted that the resolution of them (i.e., the voltage measured across them) was 1 mV which corresponds to a 0.03 psia (207 Pa) minimum increment. For the argon charging, the goal pressure was 0.742 psia (5116 Pa) which would have been ideally added in 1/10 increments after half was initially charged (0.0371 psia or 256 Pa increments). It would have been extremely difficult to measure this small amount of pressure change given the resolution of the pressure transducers that were used.

For future reference, it is recommended that an uncertainty analysis be performed to better assess the instrumentation. Obtaining an understanding of the uncertainty in the equipment will lead to a better confidence in the results or at least an understanding of the measurement error and error stackup associated with it.

CHAPTER V

Experimental Results and Discussion

TEM-CCHP experiments were performed as described in Section 4.5. Upon the completion of the TEM-CCHP experiments, identical experiments were repeated for the TEM-VCHP configuration to illustrate the power savings associated with the ability of a VCHP to vary its thermal resistance. This chapter discusses the experimental results of the two configurations and compares the data.

5.1 TEM-CCHP Experimental Results

Two sets of experiments were performed for the TEM-CCHP assembly. First, the TEM-CCHP experiments were performed with the heat pipe oriented in a horizontal position with respect to gravity. Then, the experiments were repeated with the heat pipe oriented in a vertical position along with a heated reservoir. In the latter case, the reservoir was above the condenser. Details of these experiments are described in Sections 5.1.1 and 5.1.2.

5.1.1 Horizontal TEM-CCHP

Initially, the TEM-CCHP experiments were conducted with the assembly oriented horizontally. This was done to demonstrate that the heat pipe was indeed operating as a heat pipe and not a gravity assisted thermosyphon. A complete set of data was collected over the entire range of experiments described in Section 4.5. A summary of the TEM-CCHP

power consumption is shown in Fig. 5.1. Note, the horizontal TEM-CCHP experiments were conducted with the reservoir "closed", i.e., before a vacuum was pulled on the reservoir and while the valve separating the condenser from the evaporator sections was still closed. It is reiterated here that a setpoint temperature of 63°C was chosen to demonstrate sub-ambient cooling of the TEM. It could not be much smaller of a value as this would exceed the performance capability of the TEM for the range of heat loads and ambient temperatures.

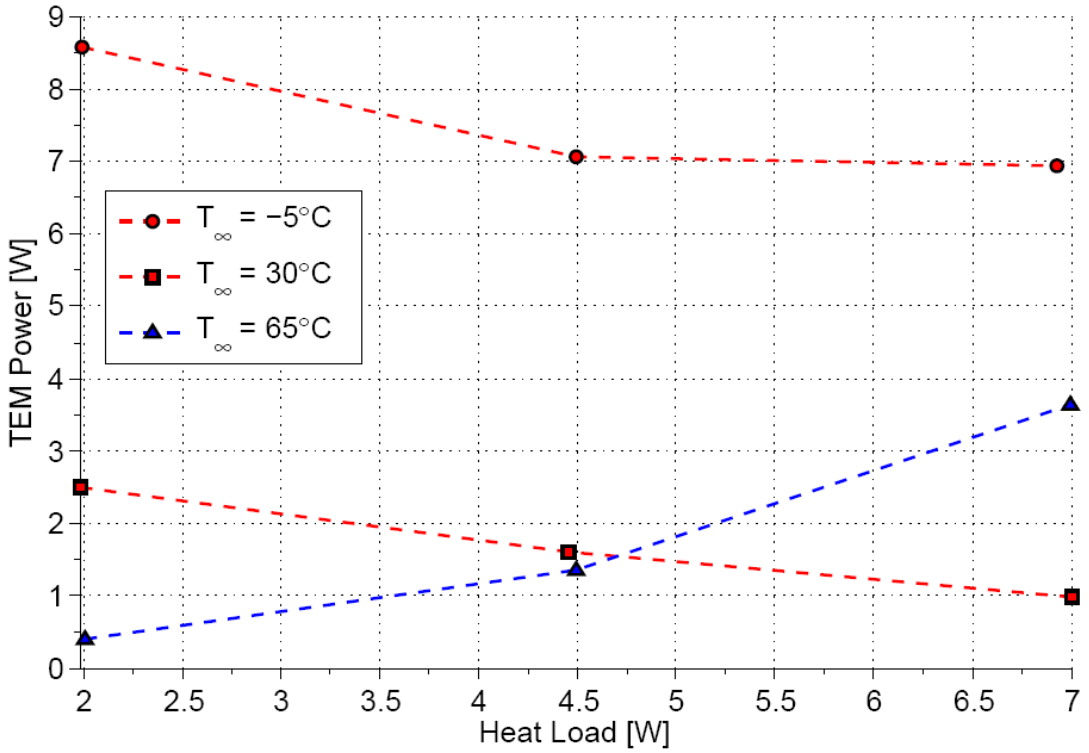

Figure 5.1: Horizontal TEM-CCHP power consumption vs. heat load ($T_{cp} = 63°C$).

As per Fig. 5.1, the TEM power consumption appears to follow an appropriate trend. For -5°C, the TEM operated completely in heating mode which makes sense given the low ambient temperature. As the heat load increased, the TEM power consumption decreased as less power was required to heat the control plane and maintain the setpoint temperature. Similarly for 30°C, the TEM operated completely in heating mode. However, its power consumption was significantly lower as the demand was not as high given the significantly higher ambient temperature. Finally, for 65°C, the TEM operated completely in refrigeration

mode. Thus, as the heat load increased, the power consumed by the TEM increased given the larger demand for Peltier cooling to maintain the prescribed setpoint temperature. As TEM power consumption depends on the temperature difference across it as per Eq. 2.7, it seems plausible that the maximum power consumption would occur at -5°C. Based on the experimental data recorded, the -5°C experiments had the largest temperature difference between the controlled side and the uncontrolled side of the TEM.

As the purpose of this experiment was to demonstrate a TEM-CCHP assembly, the fin temperature profile was expected to be very close together. This was based on the assumed fin efficiency of 100% based on their geometry and the assumption that the fins were all attached the same way with the same amount of epoxy and equal thermal contact resistance. Axial temperature profiles for ambient temperatures of 65°C, 30°C and -5°C are provided in Figs. 5.2, 5.3 and 5.4 respectively, where the temperature is plotted away from the evaporator towards the condenser and includes the vapor core temperature first then all of the 21 fins.

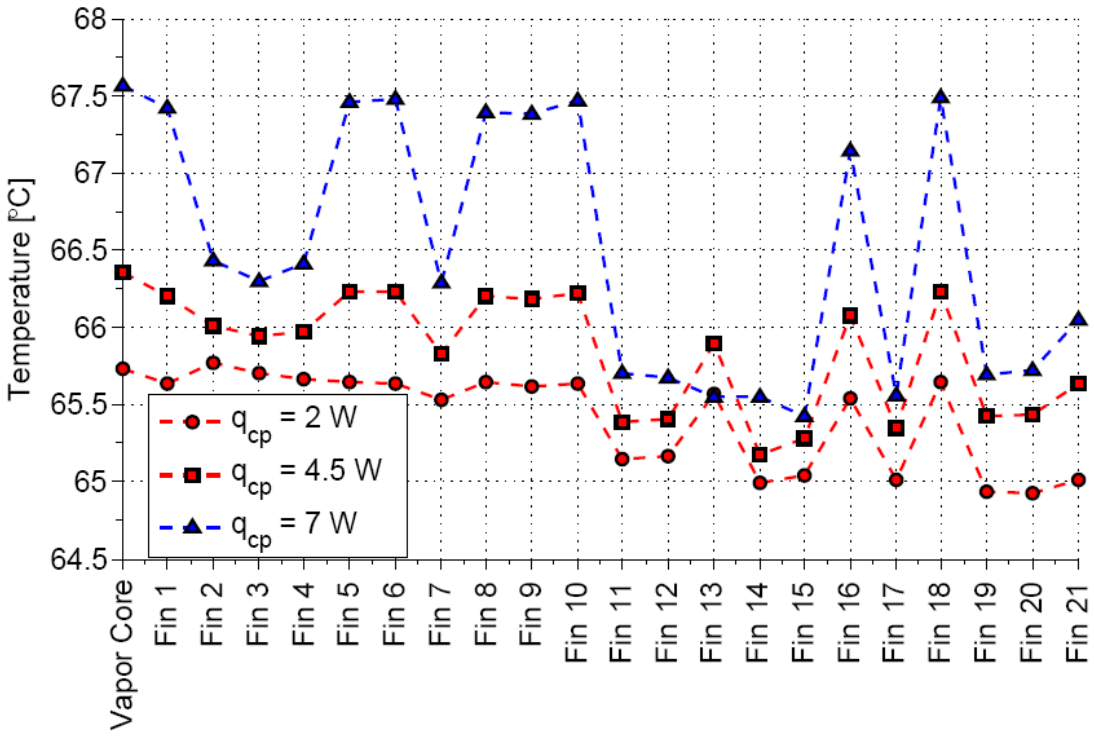

Figure 5.2: Horizontal TEM-CCHP axial temperature distribution ($T_\infty = 65°C$, $T_{cp} = 63°C$).

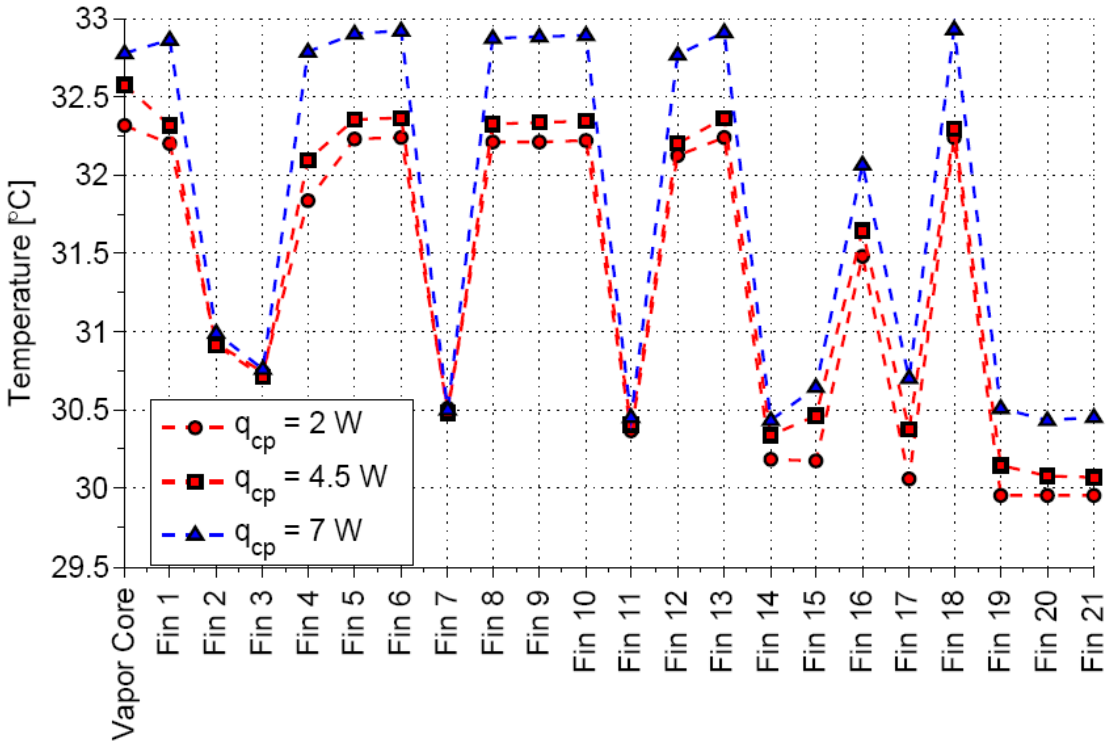

Figure 5.3: Horizontal TEM-CCHP axial temperature distribution ($T_\infty = 30°C$, $T_{cp} = 63°C$).

When examining the vapor core and fin temperatures, it is observed that relatively large fluctuations (i.e., among the fin temperatures) were apparent in the CCHP, particularly at -5°C. This behavior is assumed to be based on a fault with the thermocouples that could not be determined. Suboptimal fin attachment and thermocouple attachment are presumed to be the primary root causes, but errors with the thermocouples themselves are considered as well. This is supported by fin temperatures that fell slightly below the ambient temperature which is not possible. It is observed that the general trends were repeated for each experiment in terms of temperature peaks and valleys. Although the temperature profiles appear to be somewhat oscillatory, the important conclusion is that in general, the temperature appears to be "flat" axially down the length of the heat pipe away from the evaporator. This suggests that the CCHP was in fact operating with constant conductance. If it had not been, there would have been a noticeable drop in temperature near the end of the finstack.

An additional key trend across the temperature distribution for $T_\infty = 65°C$ and $T_\infty =$

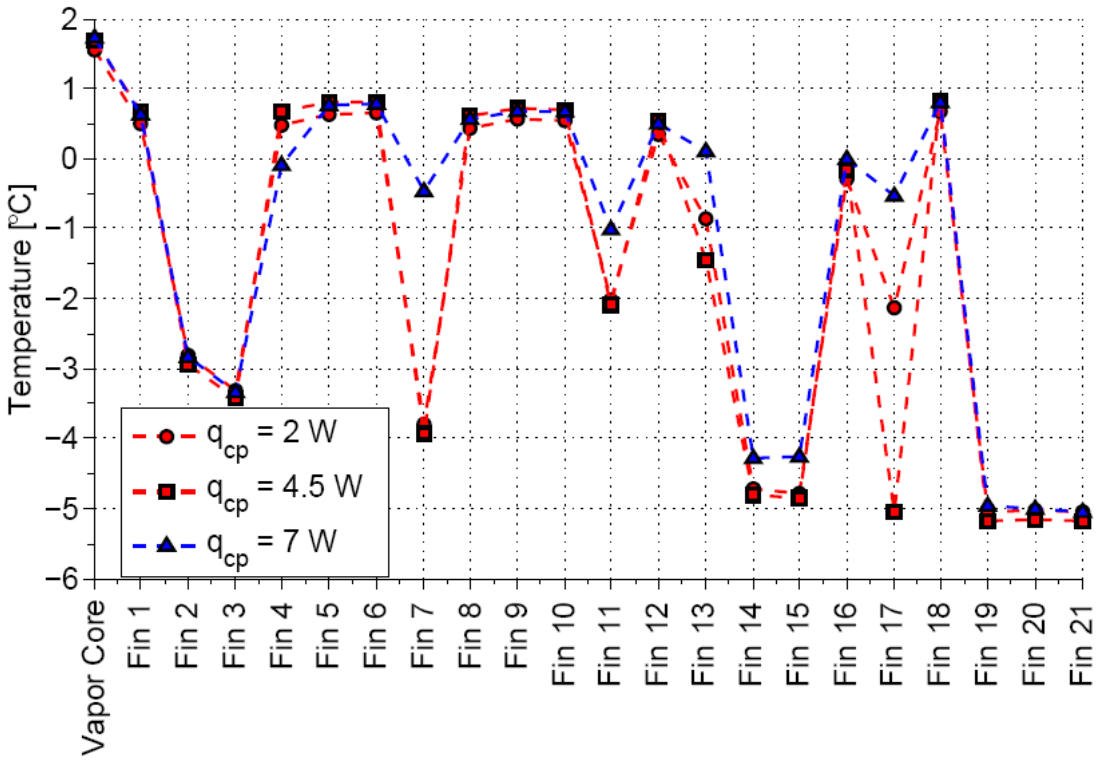

Figure 5.4: Horizontal TEM-CCHP axial temperature distribution (T_∞ = -5°C, T_{cp} = 63°C).

30°C is the noticeable separation between temperatures for each heat load (i.e., as heat load increases, the temperature increases) and total power (i.e., heat load and TEM power consumption) which also follows the same trend. These differences for each heat load are less noticeable for T_∞ = -5°C. Complete data for the total TEM-CCHP power consumption may be found in Table A.1 in Appendix A. The temperature "spikes" near the end of the condenser for each temperature distribution suggests that the CCHP was fully open despite some apparent issues with the thermocouples.

Across the wide range of ambient temperatures (-5°C to 65°C), a modest change in air density would be expected. Since density would decrease as ambient temperature increased, the expected result would be a decreased mass flow rate of air through the wind tunnel. However, the actual trend is shown to be the opposite across the temperature distribution plots as ambient temperature increases. This is exhibited by the increased separation in the vapor core and fin temperatures for each heat load as the ambient temperature increases.

For T_∞ = -5°C, the temperatures are nearly identical regardless of applied heat load.

Based on the recorded temperatures, a multitude of thermal resistances could be calculated. Specifically, the vapor core to ambient thermal resistance was of primary interest (U from Eq. 1.3). To calculate the thermal resistance, the difference between the vapor core temperature and the ambient temperature was divided by the total power, which was the sum of the heat dissipated by the heater and the power consumed by the TEM. A plot of the thermal resistances for the horizontal TEM-CCHP experiments is shown in Fig. 5.5.

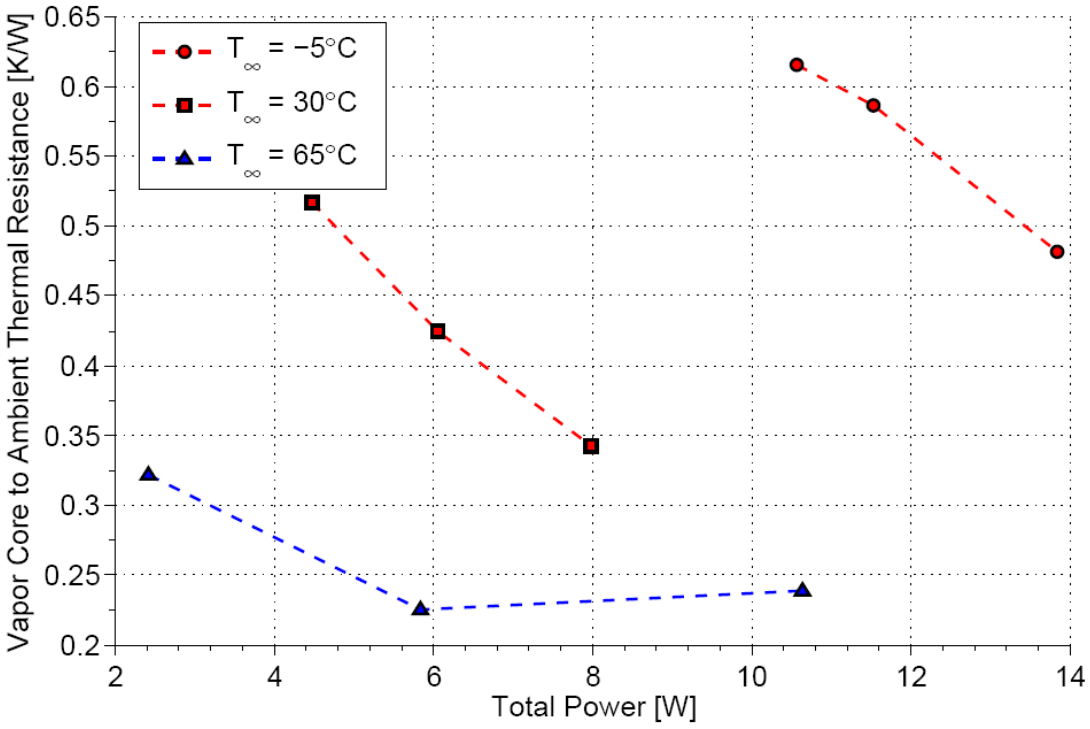

Figure 5.5: Horizontal TEM-CCHP vapor core to ambient thermal resistance (T_{cp} = 63°C).

It is sensible that the vapor core to ambient thermal resistance, for T_∞ = 65°C, is noticeably lower than the thermal resistances for the other ambient temperatures because TEM power consumption increases as heat load increases. While the total power increases in Fig. 5.5, which results in the decreasing trend shown for all ambient temperatures, the power demand in cooling mode was higher at those heat loads and ambient temperatures. Thus, the vapor core to ambient thermal resistance curve for T_∞ = 65°C decreases at a higher rate.

It is evident that the CCHP was not operating with constant conductance across ambient

temperatures and heat loads. However, within each ambient temperature, the thermal resistance remained relatively "flat" to some degree. This explains why there were no dramatic fin temperature drops within each ambient temperature experiment. The thermal resistances decreased as the total power increased. This seems to follow the expected behavior of a VCHP where an increased heat load causes it to decrease its thermal resistances (i.e., as the heat load increases, the VCHP's thermal resistance decreases to allow the heat to be dissipated more easily). It is reiterated that it was known that there was a small amount of air inside of the heat pipe. On average, a percent difference of 16% was observed between the measured vapor core pressure and the saturation pressure of methanol at the temperature of the room on that particular day. Thus, it is known that the assembly behaved as a methanol-air VCHP to some degree as opposed to a true CCHP.

It is known that there were errors with the thermocouple readings (presumably due to poor attachment). However, if there were other anomalies with the thermocouples themselves it is possible that they were also translated to the sheathed thermocouple used to measure the vapor core temperature (as well as the controlled and uncontrolled sides of the TEM). Thus, if this is true, it would have an effect on the vapor core to ambient thermal resistance since this is a calculated value based on the measurement of the vapor core temperature (and the ambient temperature as well, but that was measured with a thermistor which was assumed to be problem free). It is assumed that the primary reason for the somewhat erroneous temperature readings is due to poor thermocouple attachment in the fins as these thermocouples (including the sheathed thermocouples) were all calibrated and no problems were found. Thus, since the vapor core and ambient temperatures were monitored using a sheathed thermocouple and a thermistor, respectively, the estimated error associated with the vapor to ambient thermal resistance is a function of the tolerance stackup associated with the accuracy of the instruments and the precision of the multimeters and the data acquisition software.

Upon examining the experimental results of the horizontal TEM-CCHP, it was decided

that pulling a vacuum down on the reservoir and exposing the heat pipe to the much larger volume of the heat pipe would make the methanol-air "VCHP" operate with an infinite volume reservoir, where the flat front between methanol vapor and air would be so far from the last fin in the condenser that it would not affect the vapor core to ambient thermal resistance. However, proceeding with this caused the need for new requirements which ultimately lead to the heat pipe being oriented vertically as discussed in Section 4.6. This is described in Section 5.1.2. A complete set of compiled data for the horizontal TEM-CCHP experiments may be found in Table A.1 in Appendix A.

5.1.2 Vertical TEM-CCHP

As described in Section 4.6, the TEM-CCHP was oriented vertically with a small amount of heat applied (0.665 W to 1.080 W) to the reservoir. This section outlines the results for measurements similar to those presented in Section 5.1.1, but with the heat pipe oriented vertically.

Aside from the orientation, the only difference between the vertical and horizontal TEM-CCHP experiments was the lowest ambient temperature. For the horizontal tests, an ambient temperature of -5°C was achievable. However, this temperature could not be obtained again with the vertical tests. The same procedure of allowing the recirculating bath to run overnight at 0.6°C (just above freezing) was repeated, but the -5°C ambient temperature simply could not be achieved again. It was decided that 0°C would have to suffice as the new minimum ambient temperature and it would have to be used for the TEM-VCHP as well for comparison purposes. Unfortunately, it could not be directly compared to the horizontal TEM-CCHP experiments, but the trends were expected to be similar across different TEM operating conditions.

The resulting TEM power consumption as a function of heat load for 65°C, 30°C and 0°C ambient temperatures is shown in Fig. 5.6. While the power consumption was comparable to the horizontal orientation for the 65°C ambient tests, it was substantially less for the

30°C. This could be because the 65°C ambient temperature tests were the harshest cooling conditions for the heat pipe and thus the flat front interface of methanol and air was beyond the last fin based on the small known mass of air. However, at 30°C, this front became more influential and could have possibly blocked off some fins, thus decreasing the power demand from the TEM to maintain the setpoint temperature.

It makes sense that TEM power consumption was lower for $T_{\infty,min}$ = 0°C for the vertical TEM-CCHP compared to it for $T_{\infty,min}$ = -5°C for the horizontal TEM-CCHP as the heating demand on the TEM was decreased. A comprehensive comparison of TEM power consumption for the TEM-CCHP in the vertical and horizontal orientations is shown in Fig. 5.7.

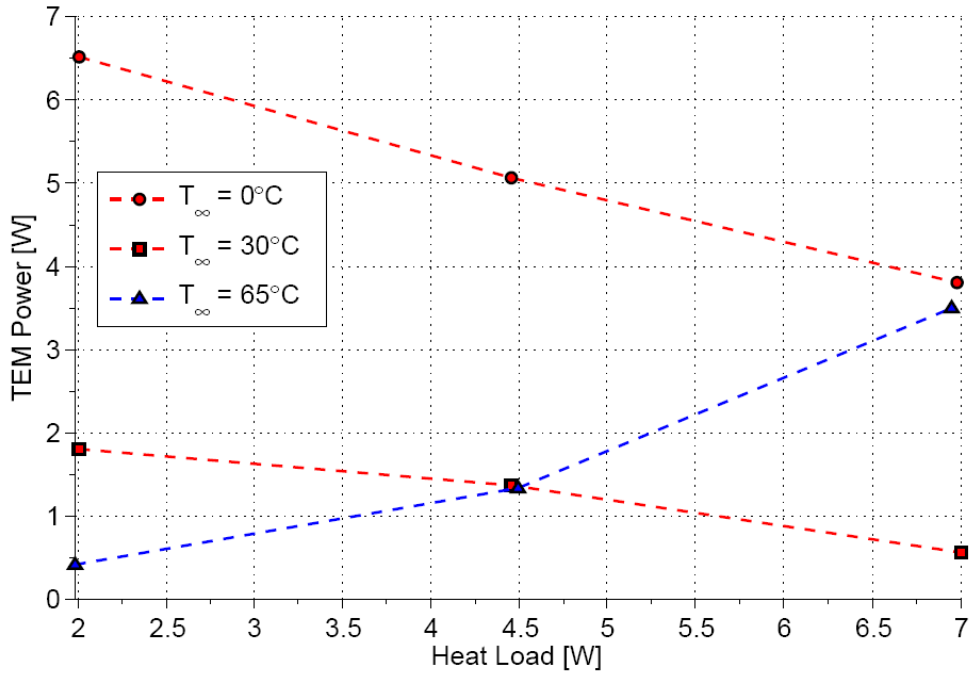

Figure 5.6: Vertical TEM-CCHP power consumption vs. heat load (T_{cp} = 63°C).

Again, with the vertical orientation, the heat pipe was expected to operate as a CCHP (i.e., with minimal change to the vapor core to ambient thermal resistance). Thus, the fin temperatures were expected to be close to each other within each experiment. After making some adjustments to the fin thermocouples, the TEM-CCHP tests were repeated.

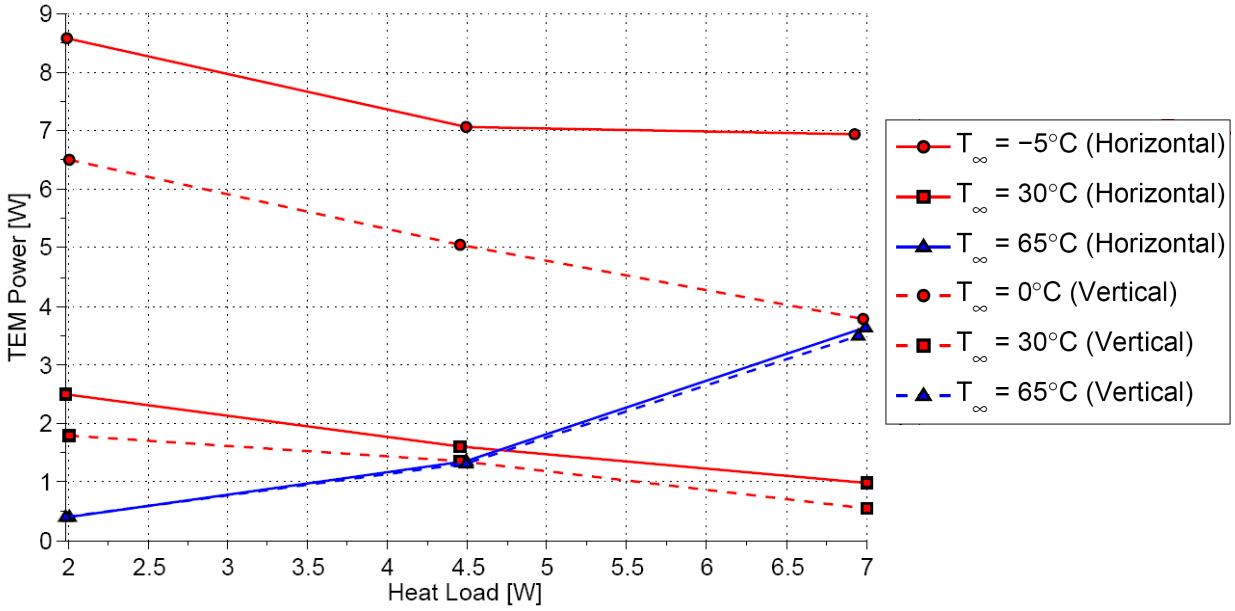

Figure 5.7: Vertical and horizontal TEM-CCHP power consumption vs. heat load (T_{cp} = 63°C).

The experimental results for the fin temperatures for ambient temperatures of 65°C, 30°C and 0°C are shown in Figs. 5.8, 5.9 and 5.10 respectively. It is noted that these plots are very similar to the ones shown in Section 5.1.1. However, there are two additional temperatures plotted which represent the reservoir thermocouples located near the condenser and at the end of the heat pipe. These two temperatures were monitored in real time and heat was increased to the reservoir heater to maintain reservoir temperatures above the vapor core temperature as described in Section 3.3. These two temperatures are represented by "1st Reservoir" and "2nd Reservoir", respectively, in the plots.

In contrast to the horizontal TEM-CCHP temperatures, the vertical fin temperatures were much closer together with less drastic variation and fluctuations. However, some thermocouples continued to show temperatures below the ambient temperature. Overall, the temperature profiles looked much improved over the horizontal TEM-CCHP results. The relatively constant temperatures also meant that similar or improved vapor core to ambient thermal resistances were expected. It is noted that prior to conducting the vertical TEM-

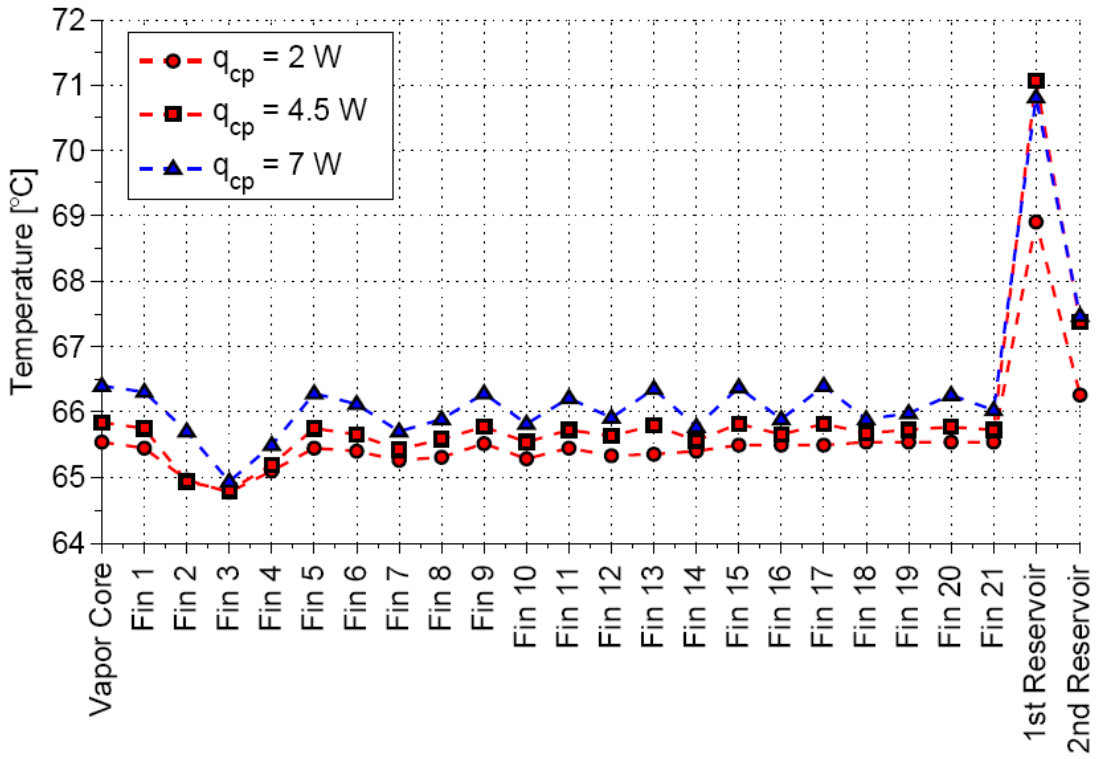

Figure 5.8: Vertical TEM-CCHP axial temperature distribution ($T_\infty = 65°C$, $T_{cp} = 63°C$).

CCHP experiments, some fin thermocouples were either reattached or checked which helped contribute to an improved temperature distribution.

With an expanded volume provided by the open reservoir, the vapor core to ambient thermal resistances were expected to be even closer in proximity compared to the configuration with the closed off reservoir which was oriented horizontally. With the horizontal orientation, the range of this thermal resistance was 0.225 K/W to 0.615 K/W. Alternatively, the vertical TEM-CCHP thermal resistances were a lot closer to constant with a range of 0.121 K/W to 0.235 K/W. It is reiterated here that potential problems with the thermocouples may lead to misleading values of the vapor core to ambient thermal resistances. However, these problems would at least be consistent between the horizontal and vertical TEM-CCHP (as well as the vertical VCHP) experiments. A plot showing the vapor core to ambient thermal resistance as a function of total power for the three ambient temperatures is shown in Fig. 5.11. It is noted that the total power also includes the small amount from the reservoir heater in order

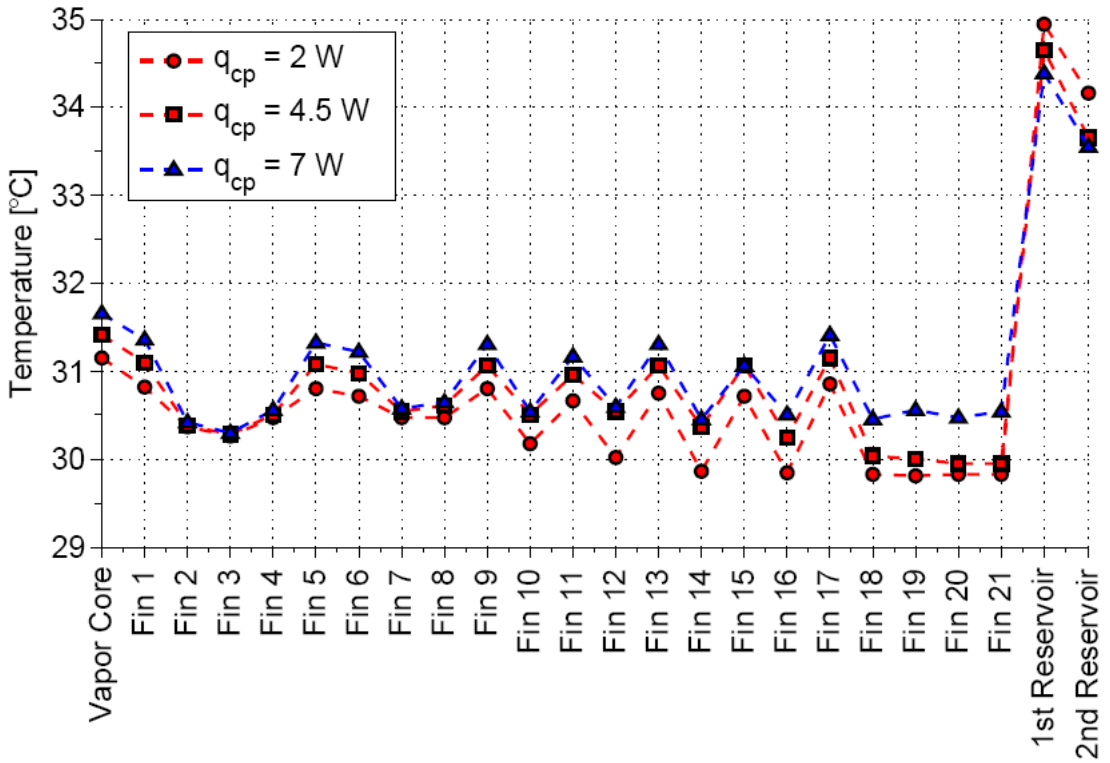

Figure 5.9: Vertical TEM-CCHP axial temperature distribution ($T_\infty = 30°C$, $T_{cp} = 63°C$).

to maintain its temperature above the vapor core temperature.

Based on the results shown in Fig. 5.11, the vapor core to ambient thermal resistance were significantly improved. Based on the assumptions in the flat front model (e.g., neglecting axial conduction), it seems that the thermal resistances shown in Fig. 5.11 could not have been improved much further in practice. Again, it is reiterated that the minimum ambient temperature for the vertical TEM-CCHP was 0°C and it was -5°C for the horizontal configuration, so those thermal resistances aren't fully comparable. A complete set of compiled data for the vertical TEM-CCHP experiments may be found in Table B.1 in Appendix B.

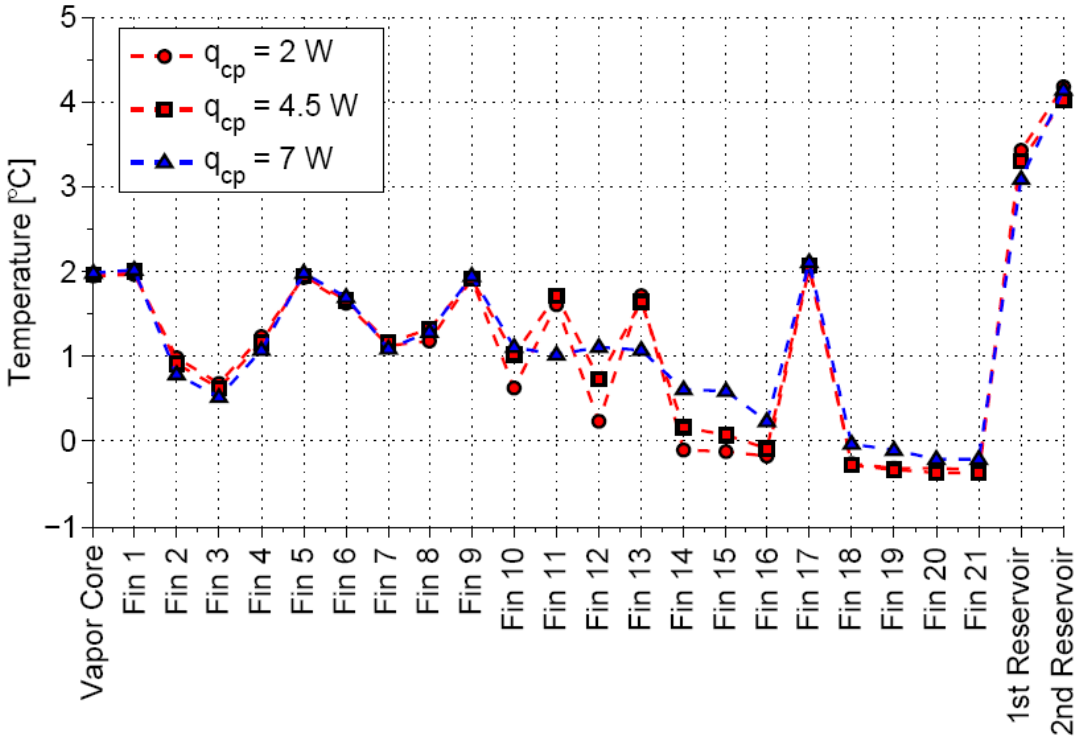

Figure 5.10: Vertical TEM-CCHP axial temperature distribution ($T_\infty = 0°C$, $T_{cp} = 63°C$).

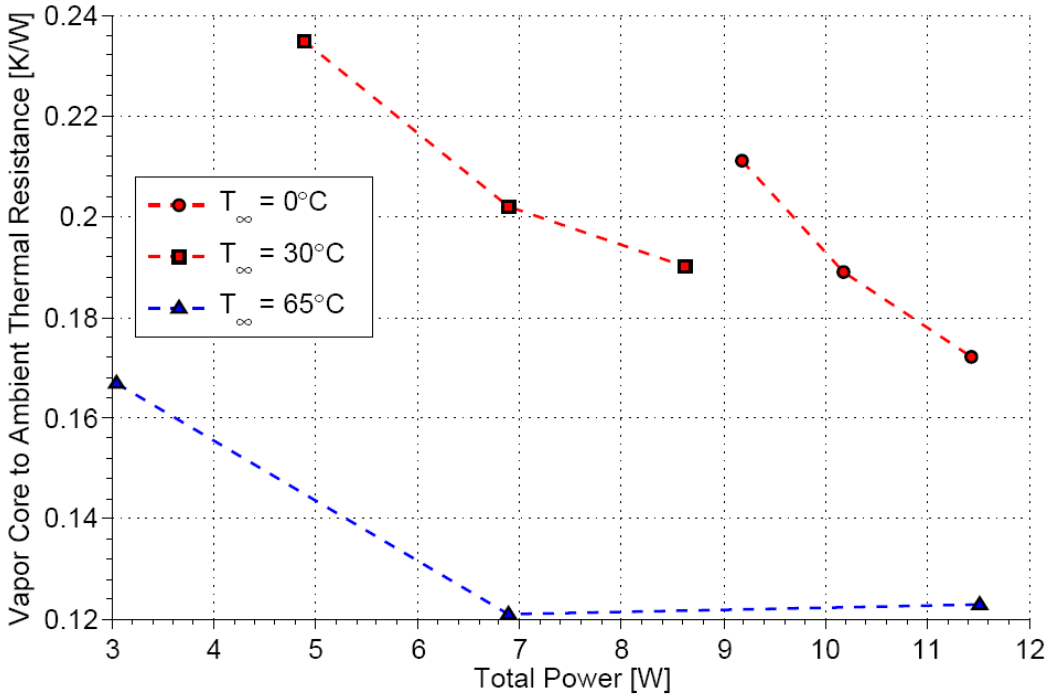

Figure 5.11: Vertical TEM-CCHP vapor core to ambient thermal resistance ($T_{cp} = 63°C$).

5.2 TEM-VCHP Experimental Results

Experiments identical to the vertical TEM-CCHP were repeated for the TEM-VCHP configuration to demonstrate the power savings achievable from varying the thermal resistance of a TEM's heat sink. This section describes the results of them.

As with the horizontal TEM-CCHP, experiments were performed with ambient temperatures of 65°C, 30°C and 0°C at heat loads of 7 W, 4.5 W and 2 W. It is noted that the VCHP was overcharged with argon as described in Section 3.3. Had an optimal mass of argon been charged into the VCHP, the expected power consumption would have been less than the CCHP. However, due to the overcharging of argon in the VCHP, the expected power consumption was not predictable. The resulting TEM power consumption as a function of heat load is shown in Fig. 5.12.

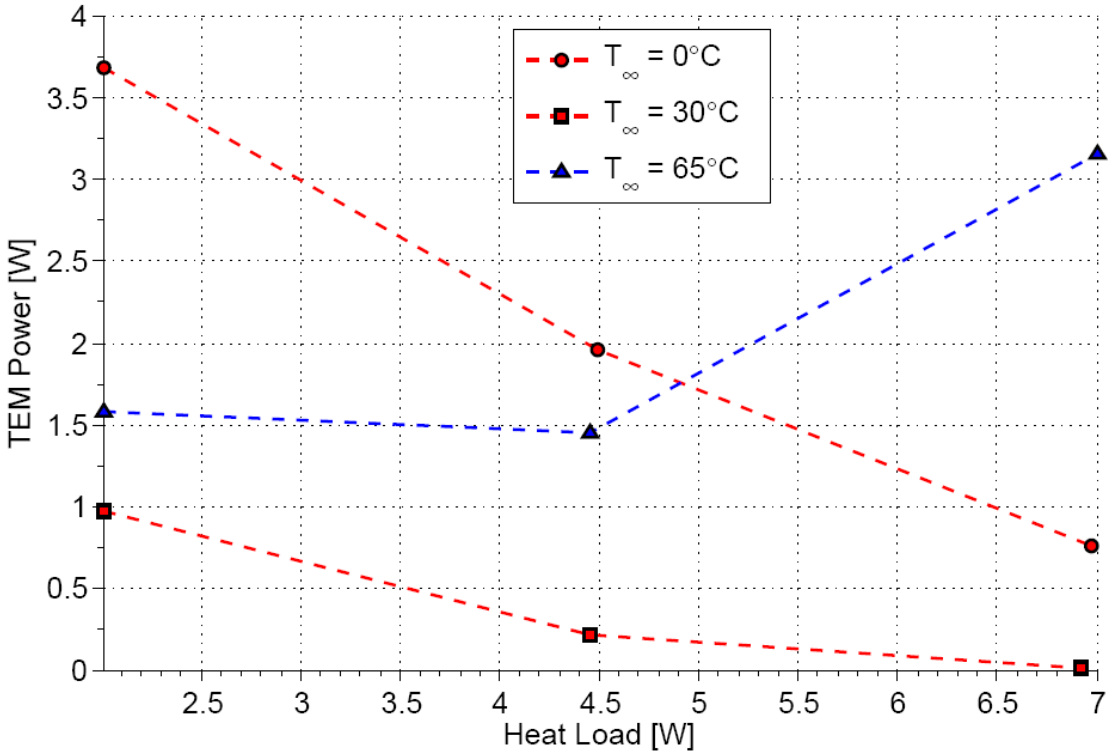

Figure 5.12: Vertical TEM-VCHP power consumption vs. heat load ($T_{cp} = 63°C$).

The experimental results for TEM power consumption at each ambient temperature

for the VCHP follow the same trends as in the case of the CCHP (shown in Fig. 5.6) with the exception that the power consumption was significantly less in heating mode and was comparable in cooling mode. This could be based on the overcharging of argon into the VCHP. While the TEM power consumption at the harshest cooling conditions (i.e., 65°C and 7 W of heat load) was similar to the CCHP, the TEM power actually increased slightly in other experiments requiring cooling mode. The overcharging of argon would cause an undesired increase of blocked off fins and would increase TEM power consumption during cooling mode as the optimal heat sink thermal resistance for these conditions is a relatively small value. The increased amount of blocked off fins would cause the thermal resistance of the condenser section of the VCHP to behave more insulatively, thus reducing the effectiveness of the heat pipe to dissipate heat from the uncontrolled side of the TEM.

In contrast, the power consumption for the TEM-VCHP operating in heating mode was substantially less than that for the TEM-CCHP assembly at the same conditions. This may be explained based on the preceding discussion with the exception that the overcharging of argon may have worked in favor of further reduced power consumption. A TEM operating in heating mode requires a heat sink of relatively large thermal resistance (i.e., more insulative) to minimize power consumption. Thus, it seems that the overcharging of argon caused more fins to be blocked off than anticipated which helped reduce power consumption during heating mode.

While the optimal mass of NCG is based upon the harshest cooling conditions, where the TEM power consumption is presumably the largest, overcharging the mass of gas may cause power consumption to increase as shown with the experiments, but it may prove beneficial at ambient temperatures that require the TEM to operate in heating mode to maintain the prescribed setpoint temperature.

The temperature profiles for the TEM-VCHP subjected to the three ambient temperatures varied significantly from the TEM-CCHP configuration. A much larger temperature difference was observed (i.e., the maximum and minimum temperatures observed in the fins).

Based on the temperature profiles, much more fluctuating behavior is shown with a much larger pitch than before with the CCHP. Temperature profiles for the VCHP for ambient temperatures of 65°C, 30°C and 0°C are shown in Figs. 5.13, 5.14 and 5.15, respectively. An improvement was shown in the fin temperatures after correcting the thermocouple attachment prior to the vertical TEM-CCHP experiments. It seems that the aluminum tape lost some of its effectiveness to maintain good contact between the thermocouples and fins over time which would explain why the vertical TEM-VCHP fin temperatures exhibit the same oscillatory behavior as the horizontal TEM-CCHP fin temperatures.

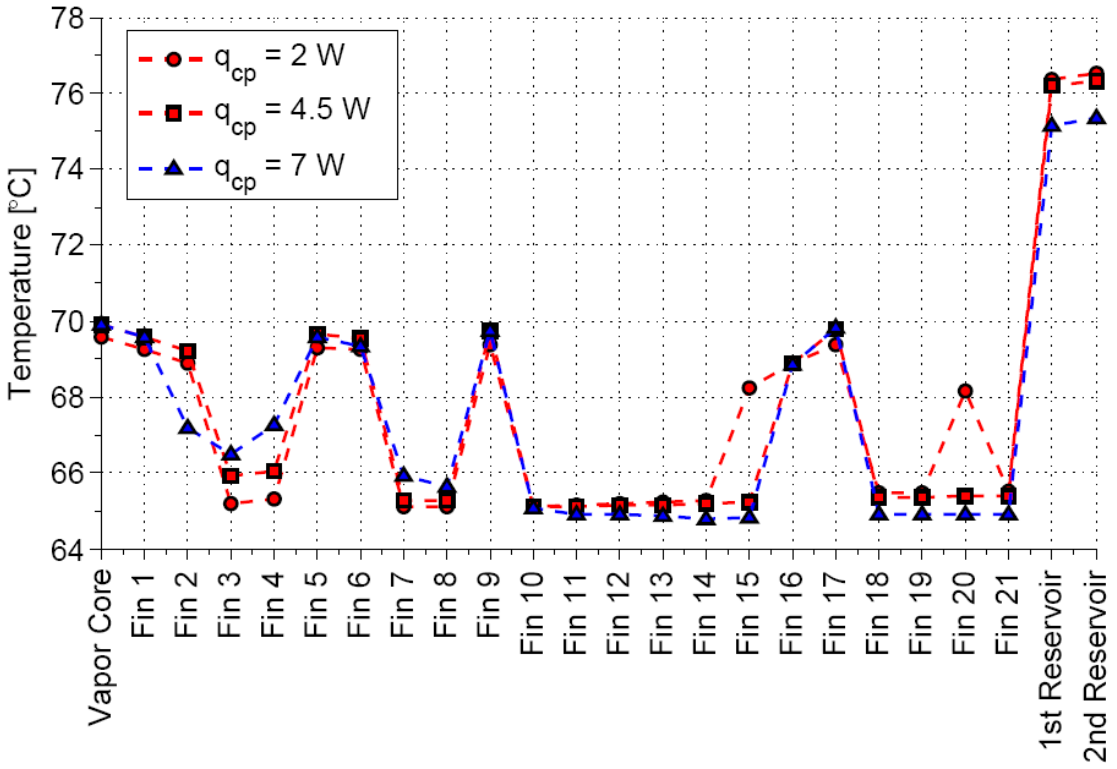

Figure 5.13: Vertical TEM-VCHP axial temperature distribution ($T_\infty = 65°C$, $T_{cp} = 63°C$).

It is noted that a majority of the fin temperatures for all ambient temperatures are very close to that temperature. This suggests that the fin thermocouples essentially measured the ambient temperature surrounding them with some slight sensible heating from the condenser. It is not an unreasonable presumption given that they were only attached with aluminum tape, which when subjected to moisture from the thawing of the ice buildup on the heat

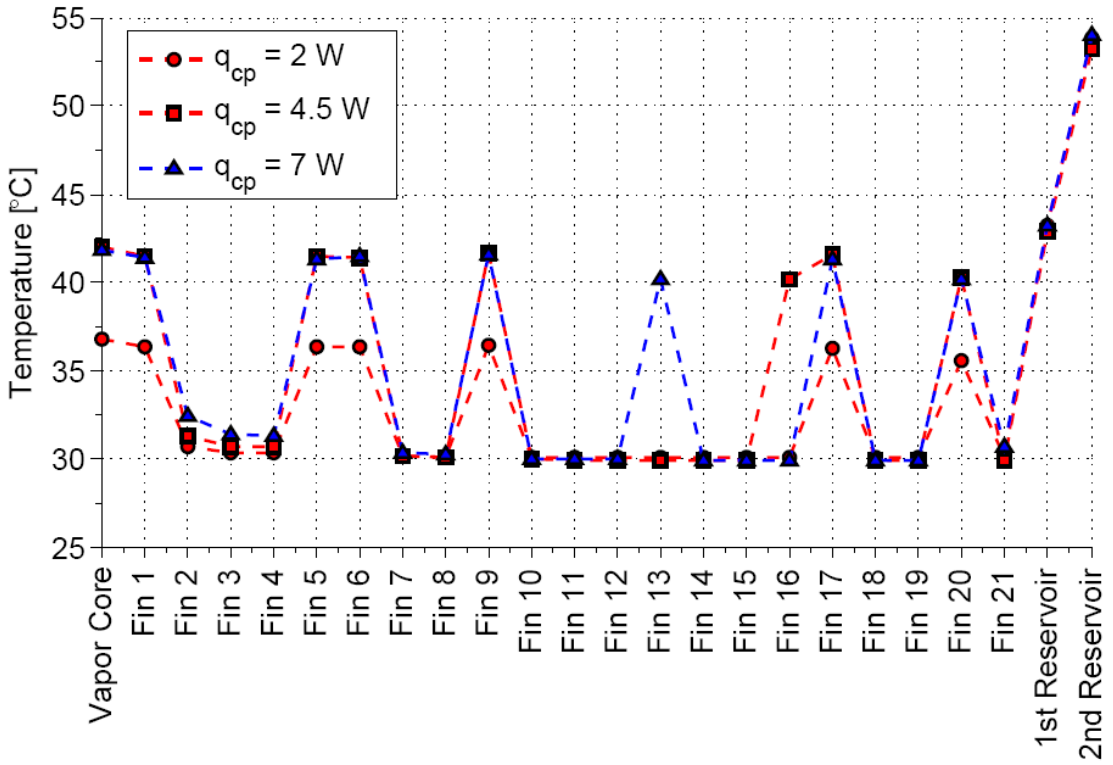

Figure 5.14: Vertical TEM-VCHP axial temperature distribution ($T_\infty = 30°C$, $T_{cp} = 63°C$).

exchanger after a 0°C temperature run, may have reduced the effectiveness of the adhesive. Efforts were made to remove the ice quickly and the desiccant used to maintain a dry environment within the chamber was baked out after each 0°C run as described in Section 4.3.

Ultimately, no obvious indication of the methanol-argon flat front is evident in any of the temperature profiles and it cannot be determined where this interface was. An improvement of the thermocouples' attachment to the fins with perhaps better resolution of the measuring equipment may be the remedy for obtaining the desired level of accuracy.

The vapor core temperature was also much higher for the VCHP than with the CCHP for all ambient temperatures. Again, referring back to the discussion of overcharging the heat pipe (where overcharging caused the thermal resistance of the heat sink to be more than desired), the over-insulative property of the heat pipe may have caused the vapor core temperature to be driven up.

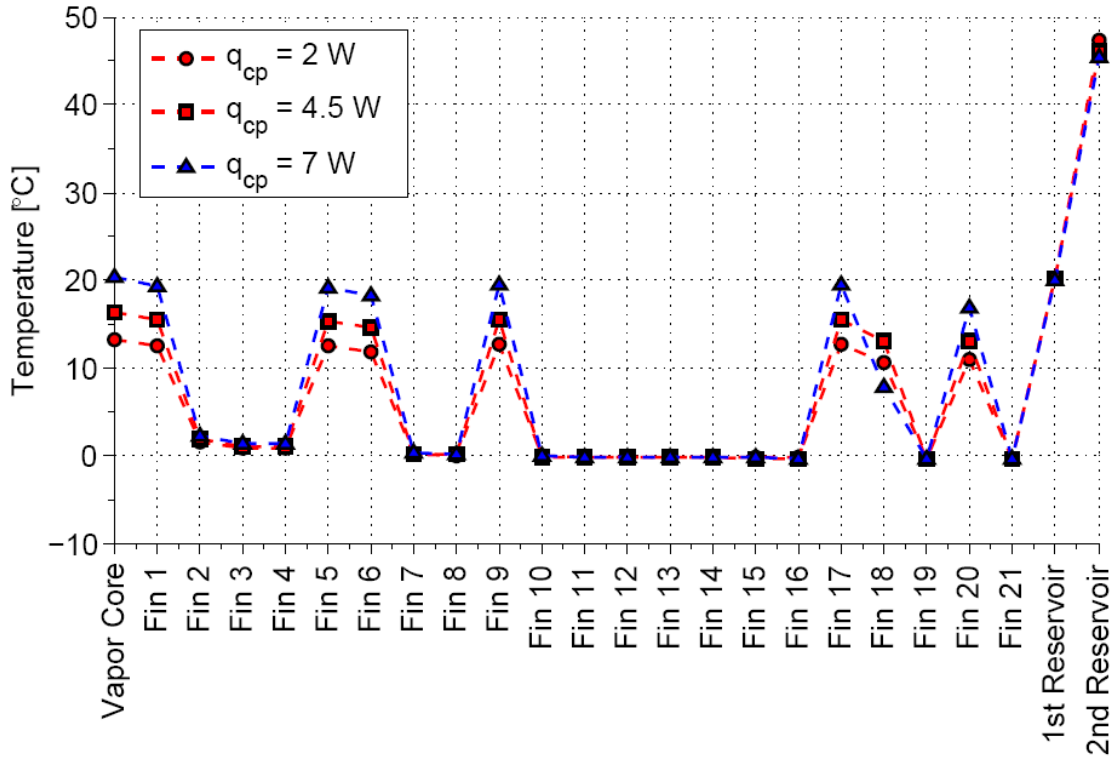

Figure 5.15: Vertical TEM-VCHP axial temperature distribution ($T_\infty = 0°C$, $T_{cp} = 63°C$).

The vapor core to ambient thermal resistance was calculated for the TEM-VCHP configuration and varying behavior was expected. The thermal resistance for the CCHP (in Fig. 5.11) was relatively constant as it varied from 0.167 K/W to 0.235 K/W (note, that there was a small amount of air within the heat pipe which would cause it to act as a VCHP to a small degree). The thermal resistance changed significantly after the heat pipe was charged with argon.

As shown in Fig. 5.16, the vapor core to ambient thermal resistance does vary substantially and is significantly different than the CCHP at each combination of heat load and ambient temperature. However, aside from the profile for the 65°C ambient temperature, the thermal resistance curves result in a somewhat unexpected behavior. The 65°C (cooling mode) thermal resistance profile is sensible in that it decreases as heat load increases. That is, as the heat load increases, the heat pipe becomes less insulative which is desired for releasing heat more easily and efficiently. For the 30°C ambient temperature, the same

trend follows with the exception of the lowest heat load point. For the 0°C ambient temperature, the actual trend is completely opposite of what is expected (i.e., the thermal resistance increases as the total head load increases).

The argon overcharging seems to be the best explanation for why the vapor core to ambient thermal resistances behaved irregularly for the most part. Perhaps, the argon caused all of the fins to be blocked off for the smallest heat load (2 W) and 30°C and all of the heat loads for 0°C. Thus, the larger difference between the two temperatures (i.e., the vapor core and the ambient) would cause the thermal resistance to increase as the heat load increased due to a much higher vapor core temperature. Moreover, axial conduction affects the thermal resistance of the heat pipe to some degree. Although it is neglected in the flat front analytical model, it could become significant especially in the event where all or most of the fins are inadvertently blocked and axial conduction becomes more of a primary means for the heat to transfer.

Regardless of what the exact reason is for the peculiar thermal resistance behavior, the underlying point is an obvious change in thermal resistance and much more importantly, reduced power consumption from the TEM. A complete set of compiled data for the vertical TEM-CCHP experiments may be found in Table D.2 in Appendix C.

5.3 Comparison of Experimental Results

The vertical TEM-CCHP was comparable to the horizontal configuration for the 65°C ambient temperature. However, power consumption was significantly less at 30°C. Direct comparison for the minimum ambient temperatures could not be made as the minimum ambient temperature for the horizontal and vertical TEM-CCHP was -5°C and 0°C, respectively. The vapor core to ambient thermal resistance was also improved (i.e., more constant) for the vertical vs. horizontal CCHP. This was largely based on the small amount of air being distributed over the relatively large volume of the reservoir.

The heart of this thesis research is experimental demonstration of reduced power preci-

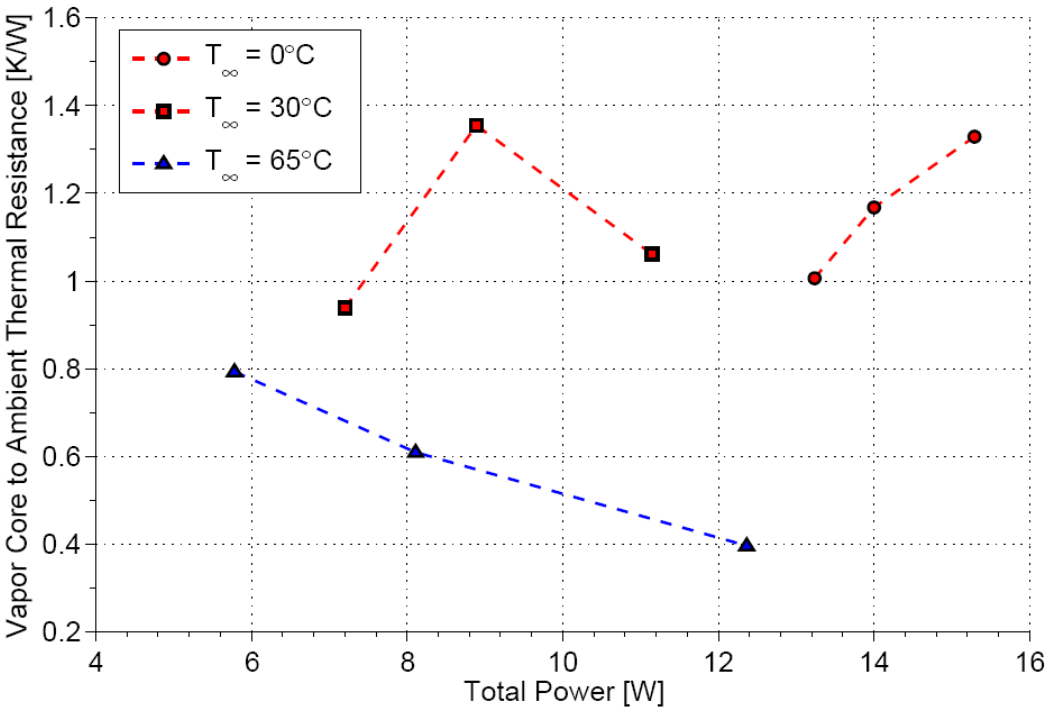

Figure 5.16: Vertical TEM-VCHP vapor core to ambient thermal resistance ($T_{cp} = 63°C$).

sion temperature control. Thus, despite some obscure fin temperatures and peculiar thermal resistance behavior, the underlying fact is that the TEM required less power for most of the combinations of heat load and temperature when coupled to a VCHP instead of a CCHP. Although the overcharging of argon clearly affected the behavior of the VCHP, it still appeared to have a positive effect on the TEM power consumption. Perhaps, further power reduction could have been achieved with an optimal mass of argon inside the heat pipe. A comparison between the vertical TEM-CCHP and vertical TEM-VCHP experiments is shown in Table. 5.1. The relevant data is presented (i.e., TEM power consumption and vapor core to ambient thermal resistance for each combination of heat load and ambient temperature). More thorough, complete data for the vertical TEM-CCHP and TEM-VCHP may be found in Appendices B and C.

The setpoint temperature for all of the experiments shown in Table 5.1 was 63°C. Had this decreased, TEM power consumption would presumably increase in cooling mode (i.e., the demand for Peltier cooling would increase). Conversely, TEM power consumption would

Table 5.1: CCHP vs. VCHP TEM Power Consumption Comparison

Experiment	CCHP $\dot{W}_{TEM}$ [W]	VCHP $\dot{W}_{TEM}$ [W]	CCHP $R_{v-\infty}$ [K/W]	VCHP $R_{v-\infty}$ [K/W]
7 W, 65°C	3.494	3.156	0.123	0.395
4.5 W, 65°C	1.323	1.456	0.121	0.607
2 W, 65°C	0.406	1.583	0.167	0.793
7 W, 30°C	0.551	0.012	0.190	1.059
4.5, W 30°C	1.361	0.215	0.202	1.352
2 W, 30°C	1.803	0.972	0.235	0.938
7 W, 0°C	3.791	0.763	0.172	1.326
4.5 W, 0°C	5.054	1.955	0.189	1.166
2 W, 0°C	6.506	3.686	0.211	1.004

decrease while operating in heating mode because the demand for Peltier heating would decrease to maintain a lower setpoint temperature. The expected trends for a higher setpoint temperature (greater than 63°C) would have an opposite effect. A higher setpoint temperature would decrease the demand for Peltier cooling, but would increase the demand for Peltier heating for a TEM operating in cooling and heating mode respectively.

CHAPTER VI

Conclusions and Future Work

A number of conclusions may be made from the research conducted for this thesis which concerned thermoelectric module-variable conductance heat pipe assemblies to demonstrate reduced power precision temperature control. A model from the literature was presented to analytically predict the power consumption of a TEM based on its material properties and geometry. Detailed steps were provided to fabricate, clean and leak test a heat pipe. It was then demonstrated how to assemble and combine a VCHP assembly with a TEM. A procedure was presented to experimentally test a TEM-VCHP subjected to varying heat loads and ambient temperatures representative of conditions of a photonics component used for telecommunications applications. Finally, results from the experiments were presented.

6.1 Conclusions

The experimental results seem logical. Aside from issues with the thermocouples, the fin temperatures in the horizontal and vertical TEM-CCHP seem reasonable based on a relatively constant temperature across them which makes sense given that the heat pipe was supposed to be operating with constant conductance. It was known that a small amount of air was trapped inside of the heat pipe which shows why the horizontal CCHP behaved with somewhat variable thermal resistance. This thermal resistance became much more consistent with the vertical CCHP as the small amount of air was subjected to the large volume of the

reservoir, thus making it almost insignificant.

The thermocouples appeared to detach from the fins during the VCHP experiments as shown by most of them reporting the same temperature as the ambient temperature. This could also be the result of poor attachment of those particular fins to the heat pipe, but most likely it was the aluminum tape that was used to secure the thermocouples losing its effectiveness. Regardless of the root cause, the thermocouple issues prohibited the methanol-argon flat front from being observed. This was a key trend that would have shown evidence of the flat front had everything gone more smoothly. Although it is neglected for simplicity in the flat front model, it is well known that a certain degree of axial conduction down the length of the heat pipe exists. This could also help contribute to why the methanol-argon flat front was never quite obvious from the VCHP experimental data.

Since the heat pipe was overcharged with argon, the flat front may have never existed anyway within the finstack (at least for lower ambient temperatures). The overcharging appeared to affect the vapor core to ambient thermal resistances in the VCHP and caused it to behave irregularly from that standpoint. However, the overcharging did not have an adverse effect on the power consumption of the TEM and in most cases, the power consumption for the VCHP was reduced up to 98% when compared to the CCHP at identical conditions. Only in two experiments (2 W and 4.5 W both at $T_\infty = 65°C$) did the VCHP consume more power than the CCHP. Across the nine experiments, the average TEM power reduction with the VCHP compared to the CCHP was 38%.

Encouraging experimental data and trends were observed from the results of this thesis. Reduced power precision temperature control was indeed demonstrated through these experiments. To obtain more refined data in the future, following the lessons learned from this research is recommended so that setbacks and mistakes are not repeated. For example, relatively simple fixes such as better attachment of the fins and thermocouples and better control of the argon pressure during VCHP charging are a good starting point to improve the experimental results.

6.2 Future Work

This thesis has been able to successfully characterize a TEM-heat pipe assembly experimentally. A TEM-VCHP one-dimensional model [12] has been provided to make analytical predictions of an actual, as-built assembly. In the future, it is recommended that this model be implemented to make predictions of the experiments and also be used to validate the experimental results. Based on findings throughout the research, improvements may be made to better the heat pipe's design to minimize inconsistencies and yield better performance while still being able to accommodate necessary measuring equipment. It is advisable to consider minimizing the amount of joints and sources of potential leaks when designing future heat pipes. Establishing an improved method for charging the heat pipe with methanol (or any other working fluid for that matter) is recommended to minimize the amount of air that becomes initially trapped inside of the heat pipe. Similarly, improving the method for argon charging is essential to avoid overcharging of the VCHP. Based on what was learned while conducting the experiments, improvements may be made in that area to yield more accurate results. By applying the findings from this thesis, future research may be performed with a good understanding of analytical models, fabrication techniques and representative experiments. By applying lessons learned from this research, improved experimental results and understanding of TEM-VCHP assemblies are expected.

6.2.1 Recommendations

Given time constraints, no analytical modeling was performed to make predictions or validate the experimental results. This was a purely experimental thesis. However, it would have been beneficial to run the model and make accurate predictions then overlay the experimental results onto the analytical predictions to examine the accuracy of the model. Given that the flat front model makes some assumptions that are not 100% accurate, the predictions would not have been expected to be exactly the same as the experimental results, but based on other work that has done by Cleary *et al.* [17] the results would have been expected

to show good agreement. However, this work was compared using a VCHP only and not a TEM-VCHP assembly. It is beneficial to demonstrate the accuracy of an analytical model that can predict the performance of combined TEM-VCHP. However, this may prove challenging as all of the thermal resistances that should have been consistent from experiment to experiment were not. For example, the control plane to controlled-side interface thermal resistance, R_{cp-c}, should be a fixed value regardless of the ambient temperature and heat load, but it was not across the experiments. Decisions will have to be made to determine the best course of action to properly and most accurately correspond all of the experimental data to the analytical model (e.g., perhaps using the average of the aforementioned thermal resistance in the model).

From a fabrication standpoint, it was concluded that the as-built design could have used improvement. With the fins attached to the copper tube with epoxy, it seems that a certain degree of inconsistency and uncertainty existed regarding the thermal contact resistance in the epoxy. Ideally, the entire heat pipe and finstack would have been monolithic and machined or cast from a single piece of copper. This option is challenging however, given the high level of difficulty to machine copper. An alternative solution is to have the fins brazed onto the copper tubing which would be more practical than machining a heat pipe and more effective than epoxied on fins. The wrapped screen copper wick seemed to do a sufficient job of returning condensed methanol back to the evaporator. To improve the performance of the wick inherent in the heat pipe, a sintered powder copper wick is recommended (and is possible to fabricate at Tufts). As per Cleary *et al.* [11], installing a wick inside of the reservoir is recommended to prevent condensation from becoming trapped inside. This could potentially remove the need for a heated reservoir which would further reduce the total power consumption of the system. Although the Swagelok® compression tube fittings eased the fabrication process and were necessary for housing sheathed thermocouples and pressure transducers, they introduced a multitude of joints which increased the likelihood of leaks in the system. A large portion of time was spent troubleshooting and attempting to find these

leaks which were very small and difficult to find. If this process were repeated, alternative solutions would be examined and minimizing the number of joints would be a top priority.

During the methanol charging, one problem that could not be overcome was the small amount of air initially trapped inside of the heat pipe. Despite multiple attempts to correct this, the small amount of air could not be removed. Although this did not seem to adversely affect the performance of the heat pipe, the experimental results could be improved slightly if the vacuum system, for example, could be implemented to completely remove all traces of air. During argon charging to convert the CCHP into a VCHP, the setup was rather crude. The pressure regulator on the argon tank that was rated to 200 psig was too coarse for the very small amount of argon pressure required. It is recommended that a vacuum level pressure regulator be used, preferably one that is controllable so that the mass of argon may be incrementally increased until a small change in vapor core to ambient thermal resistance is observed at maximum cooling conditions.

From an experimental standpoint, the fin thermocouples were sub-optimally attached. Rather than being attached with aluminum tape, a more permanent means of attachment is recommended such as soldering or epoxy. The ice bath reference junction did an efficient job of maintaining a low temperature. However, it never was able to quite get the reference junction temperature down to 0°C. At best, the temperature was able to get down to around 0.55°C. For more consistent maintenance of the reference junction, it is recommended that a temperature controllable recirculating bath be used as was done when the thermocouples were calibrated. A combined improvement of the attachment of the thermocouples and the reference junction may have yielded better results for the temperatures measured by the thermocouples in the finstack.

The heat exchanger, fan system was sufficient for circulating above freezing temperatures within the environmental chamber. However, it was difficult to achieve temperatures below 0°C. Perhaps, for example, the design used in temperature controlled environmental chambers could be incorporated to ensure a wide range of ambient temperatures can be easily

and consistently achieved.

It is recommended that a much finer means of controlling the sub ambient pressure of argon be implemented in future experiments to ensure that the optimal mass of argon gets charged into the heat pipe. Specifically, a simple fix might just be switching out the coarse pressure regulator on an argon cylinder with a vacuum rated regulator.

BIBLIOGRAPHY

[1] M. Hodes. "On One-Dimensional Analysis of Thermoelectric Modules (TEMs)". *IEEE Transactions of Components and Packaging*, **28**(2):218–229, 2005.

[2] M. Hodes. ME110. Class Lecture, Topic:. "Lectures 11-13: Heat Pipes and Variable Conduction Heat Pipes." Department of Mechanical Engineering, Tufts University, Medford, MA, 2010.

[3] Swagelok®. "An Installer's Pocket Guide for Swagelok® Tube Fittings".

[4] Laird Technologies®. "Thermoelectric Cooler". HT6,7,F2,3030 datasheet, Rev 1.01.

[5] Omega®. "PX209, PX219, PXM209, PXM219 Pressure Transducers Instruction Sheet". Product Manual.

[6] Laird Technologies®. "Tgrease™ 2500 Series Thermal Grease". THR-DS-Tgrease-1500 0710 datasheet.

[7] JDSU. "Handling, Mounting, Control, and Operation of High-power Pump Lasers". Tech. Rep., February, 2009.

[8] M. Safavi. "Thermal Design and NEBS Compliance". *Electronics Cooling* [online document], 2006. Available: http://www.electronics-cooling.com/2006/02/thermal-design-and-nebs-compliance/.

[9] GR-63-CORE. "Network Equipment-Building System NEBS Requirements: Physical Protection". Issue 1. (Bellcore, October 1995).

[10] R. Zhang, M. Hodes, D. Brooks and V. Manno. "Optimized Thermoelectric Module-Heat Sink Assemblies for Precision Temperature Control". To appear in Journal of Electronics Packaging, 2012.

[11] M. Cleary, M. Hodes, R. Grimes and M. North. "Design of a Variable Conductance Heat Pipe for a Photonic Component". *Proceedings of ASME International Mechanical Engineering Congress & Exposition*, **377**(2):143–152, 2006.

[12] C. Melnick, M. Hodes, G. Ziskind, M. Cleary and V. Manno. "Thermoelectric Module-Variable Conductance Heat Pipe Assemblies for Reduced Power Temperature Control". To appear in IEEE CPT, 2012.

[13] C.L. Foiles. "Thermoelectric Effects". In Encylopedia of Physics, 2nd ed., R.G.Lerner and G.L. Triggs, Eds. New York: VCH Publishers, INC., 1991, pp. 1263, 1264.

[14] M. Hodes. ME110. Class Lecture, Topic:. "Lectures 8-10: Thermoelectric Effects, Thermocouple Thermometry and Thermoelectric Modules." Department of Mechanical Engineering, Tufts University, Medford, MA, 2010.

[15] M. Hodes. "Optimal Pellet Geometries for Thermoelectric Refrigeration". *IEEE Transactions on Components and Packaging Technologies*, **30**:50–58, 2007.

[16] A. Faghri. *Heat Pipe Science and Technology.* Taylor and Francis, 1995.

[17] M. Cleary, M. Hodes, R. Grimes and M. North. "Characterisation of a Variable Conductance Heat Pipe Prototype for a Photonic Application". *Proceedings of the 2007 ASME-JSME Thermal Engineering Conference*, pages 313–320, 2007.

[18] M. Hodes. "Optimal Pellet Geometries for Thermoelectric Refrigerators Embedded in a Thermal Resistance Network". Submitted to IEEE CPT, 2010.

[19] D. K. Edwards and B. D. Edwards. "Heat and Mass Transfer in the Viscinity of the Vapor-gas Front in a Gas Loaded Heat Pipe'. *Journal of Heat Transfer*, **94**:155–162, 1972.

[20] A. R. Rohani and C. L. Tien. "Steady Two-Dimensional Heat and Mass Transfer in the Vapor-Gas Region of a Gas-Loaded Heat Pipe'. *Journal of Heat Transfer*, **95**:377–382, 1973.

[21] P. F. Peterson and C. L. Tien. "Numerical and Analytical Solutions for Two-Dimensional Gas Distribution in Gas-Loaded Heat Pipes'. *Journal of Heat Transfer*, **111**:598–604, 1989.

[22] B. D. Marcus and G. L. Fleischman. "Steady State and Transient Performance of Hot Reservoir Gas-Controlled Heat Pipes". ASME paper No. 70-HT/SpT-11. 1970.

[23] A. Kraus and A. Bar-Cohen. *Thermal Aanlysis and Control of Electronic Equipment.* McGraw-Hill, 1983.

[24] N. I. of Standards and Technology. "Thermophysical Properties of Fluid Systems". 2011. Available: http://webbook.nist.gov/chemistry/fluid/.

[25] Marketech International. "Silica Aerogels". [online document], 2010. Available: http://www.mkt-intl.com/aerogel/Silica_Aerogels.shtml.

[26] R. Zhang. "Optimized Thermoelectric Module-Heat Sink Assemblies for Precision Temperature Control". M.S. thesis, Dept. Mech. Eng., Tufts Univ., Medford, MA, 2011.

APPENDIX A

Compiled Horizontal TEM-CCHP Experimental Data

Table A.1: Compiled Horizontal TEM-CCHP Data

Experiment #	T_∞ [°C]	T_{cp} [°C]	q_{cp} [W]	V_{TEM} [VDC]	I_{TEM} [A]	$\dot{W}_{TEM}$ [W]	$\dot{W}_{Total}$ [W]
09-07-11-3	-4.95	62.78	1.994	4.491	-1.911	8.582	10.576
09-07-11-2	-5.08	63.05	4.492	4.350	-1.621	7.051	11.543
09-07-11-4	-4.95	61.95	6.924	4.467	-1.551	6.928	13.852
09-06-11-3	30.00	62.93	1.981	2.580	-0.968	2.497	4.478
09-06-11-2	30.00	62.15	4.453	2.196	-0.731	1.605	6.058
09-06-11-1	30.03	62.61	7.000	1.892	-0.522	0.988	7.988
09-08-11-3	64.95	62.09	2.008	0.925	0.445	0.412	2.420
09-08-11-2	65.04	61.92	4.494	1.637	0.827	1.354	5.848
09-08-11-1	65.01	62.22	6.997	2.691	1.356	3.649	10.646

Note, when the TEM current is a negative value, it implies Peltier heating is required to maintain T_{cp}. The TEM power is considered to be a positive value despite the negative current and is calculated as an absolute value. Truly "negative" TEM power implies generation mode (i.e., the reversal of power back into the TEM) when considering an energy balance around a TEM. Peltier heating corresponds to negative current from the TEM, but still requires "positive" power consumption by a TEM to maintain the setpoint temperature.

APPENDIX B

Compiled Vertical TEM-CCHP Experimental Data

Table B.1: Compiled Vertical TEM-CCHP Data

Experiment #	T_∞ [°C]	T_{cp} [°C]	q_{cp} [W]	V_{TEM} [VDC]	I_{TEM} [A]	$\dot{W}_{TEM}$ [W]	$\dot{W}_{Total}$ [W]
10-20-11-3	0.01	62.51	2.007	4.031	-1.614	6.506	9.178
10-20-11-2	0.04	62.37	4.455	3.657	-1.382	5.054	10.174
10-20-11-1	0.03	62.84	6.978	3.308	-1.146	3.791	11.434
10-13-11-3	29.99	63.02	2.007	2.199	-0.820	1.803	4.890
10-13-11-2	30.02	62.82	4.453	2.041	-0.667	1.361	6.894
10-13-11-1	30.02	63.03	7.000	1.501	-0.367	0.551	8.631
10-07-11-1	65.03	62.08	1.982	0.925	0.439	0.406	3.053
10-07-11-3	65.01	62.55	4.492	1.627	0.813	1.323	6.895
10-07-11-2	64.97	62.14	6.948	2.635	1.326	3.494	11.522

Note, the total power ($\dot{W}_{Total}$) column also includes a small amount of heat provided to the reservoir (not shown here) to maintain its temperature above the temperature of the vapor core for each experiment.

APPENDIX C

Compiled Vertical TEM-VCHP Experimental Data

Table C.1: Compiled Vertical TEM-VCHP Data

Experiment #	T_∞ [°C]	T_{cp} [°C]	q_{cp} [W]	V_{TEM} [VDC]	I_{TEM} [A]	$\dot{W}_{TEM}$ [W]	$\dot{W}_{Total}$ [W]
11-02-11-3	-0.05	62.49	2.007	3.100	-1.189	3.686	13.253
11-02-11-2	-0.04	62.16	4.492	2.375	-0.823	1.955	14.007
11-02-11-1	0.03	63.34	6.973	1.677	-0.455	0.763	15.296
11-03-11-1	30.00	63.48	2.007	1.658	-0.586	0.972	7.208
10-28-11-2	29.96	62.21	4.453	0.946	-0.227	0.215	8.898
11-03-11-4	30.05	62.02	6.924	0.626	-0.019	0.012	11.154
10-27-11-3	64.97	62.98	2.007	1.916	0.826	1.583	5.799
10-27-11-2	64.99	63.62	4.453	1.754	0.830	1.456	8.119
10-27-11-1	65.02	62.44	7.000	2.547	1.239	3.156	12.366

APPENDIX D

Miscellaneous Experimental Data

Table D.1: Miscellaneous Horizontal TEM-CCHP Data

Experiment #	T_∞ [°C]	T_{cp} [°C]	q_{cp} [W]	V_{TEM} [VDC]	I_{TEM} [A]	$\dot{W}_{TEM}$ [W]	$\dot{W}_{Total}$ [W]
07-27-11-1	64.96	54.96	5.993	3.496	1.849	6.464	12.457
07-27-11-2	65.01	55.58	3.967	2.859	1.482	4.237	8.204
07-27-11-3	65.01	54.73	1.981	1.987	0.983	1.953	3.934
07-28-11-1	41.71	54.94	10.060	1.905	1.281	2.440	12.501
07-28-11-2	41.63	54.81	7.991	1.274	0.900	1.147	9.138
07-28-11-3	41.72	54.80	5.993	0.775	0.585	0.453	6.446
07-28-11-4	41.68	54.88	4.020	0.295	0.282	0.083	4.103
07-28-11-5	41.65	54.89	2.007	0.330	-0.078	0.026	2.032
09-01-11-1	65.06	54.55	4.020	3.293	1.677	5.522	9.542
09-02-11-1	64.96	63.06	6.948	3.608	1.720	6.206	13.154
09-02-11-2	64.99	62.09	4.453	2.497	1.185	2.959	7.412
09-02-11-3	64.98	63.11	1.981	0.900	0.431	0.388	2.368
09-06-11-1	30.03	62.61	7.000	1.892	-0.522	0.988	7.988
09-06-11-2	30.00	62.15	4.453	2.196	-0.731	1.605	6.058
09-06-11-3	30.00	62.93	1.981	2.580	-0.968	2.497	4.478
09-07-11-1	-5.05	63.31	7.000	4.678	-1.615	7.555	14.555
09-07-11-2	-5.08	63.05	4.492	4.350	-1.621	7.051	11.543
09-07-11-3	-4.95	62.78	1.994	4.491	-1.911	8.582	10.576
09-07-11-4	-4.95	61.95	6.924	4.467	-1.551	6.928	13.852
09-08-11-1	65.01	62.22	6.997	2.691	1.356	3.649	10.646
09-08-11-2	65.04	61.92	4.494	1.637	0.827	1.354	5.848
09-08-11-3	64.95	62.09	2.008	0.925	0.445	0.412	2.420
09-15-11-3	64.98	62.59	7.000	2.468	1.268	3.129	10.129

Note, the original value of T_{cp} was 55°C. The original heat loads were supposed to be 2 W, 4 W, 6 W, 8 W and 10 W. The ambient temperatures were originally intended to be -5°C, 18.33°C, 41.67°C and 65°C. However, the TEM could not physically maintain this

setpoint temperature under the higher heat loads for every ambient temperature (e.g., it was not possible to maintain a setpoint temperature of 55°C at 10 W of heat load at an ambient temperature of 65°C. This explains why the heat loads and ambient temperatures were selected as they are presented in the thesis; to have values of each load that can be tolerated for every ambient temperature while maintain the setpoint temperature.

Table D.2: Miscellaneous Vertical TEM-VCHP Data

Experiment #	T_∞ [°C]	T_{cp} [°C]	q_{cp} [W]	V_{TEM} [VDC]	I_{TEM} [A]	$\dot{W}_{TEM}$ [W]	$\dot{W}_{Total}$ [W]
10-21-11-1	65.04	62.32	6.997	2.535	1.234	3.128	12.335
10-28-11-1	30.05	63.36	6.997	0.409	0.071	-0.029	11.198
10-28-11-3	29.95	62.73	2.007	2.037	-0.716	1.458	7.695
11-03-11-2	30.04	62.88	7.466	7.466	0.614	NA	11.696
11-03-11-3	30.02	62.02	9.777	NA	0.307	NA	14.007

Note, experiment 10-28-11-1 shows the TEM power as a negative value. This is related to the sign convention chosen for an energy balance taken on a TEM. In this case, the TEM is operating in generation mode (requiring an attached electrical load of 6 Ω provided by a potentiometer) which is taken to be a negative value as it is energy out of the system. Due to the allowable tolerance in the setpoint temperature, ambient temperature and heat load, the setpoint temperature was actually controlled utilizing generation mode. However, after performing open and short circuit experiments (11-03-11-2 and 11-03-11-3), which are used to determine the range of q_{cp} that corresponds to generation mode for a given ambient temperature, it was shown that the value of $q_{cp} = 6.997$ W did not fall within this range. The range of q_{cp} for generation mode at $T_\infty = 30$°C was 7.466 W to 9.777 W. To determine these values, the Kapton® heater would be adjusted until T_{cp} was achieved. Thus, the experiment was reexamined in experiment 11-03-11-3, which demonstrated that TEM Peltier heating mode was actually required to maintain T_{cp}.

The total power for experiments 11-03-11-2 and 11-03-11-3 is larger than q_{cp} despite $\dot{W}_{TEM} = 0$ W because of the reservoir heater required to maintain its temperature above the vapor core temperature.

APPENDIX E

Heat Pipe Cleaning Procedure

(Used on as-built heat pipe)

This procedure is for the internal cleaning of copper tubes and fittings, etc. for a VCHP. The apparatus should be placed into a large tub to collect any spills from the cleaning chemicals. The entire cleaning apparatus and procedure should be performed under a fume hood. Nitrile gloves must be worn and replaced as applicable and splash goggles must be worn. Reminder: gloves should be used to protect hands from accidental exposure. They should not be used as an excuse to immerse hands into solvents.

1. Assemble the entire VCHP together. The copper screen wick should already be installed so that it can be cleaned as well.

2. Verify that the VCHP has been leak tested.

3. Check that the valves are compatible for the chemicals to be used.

4. Remove the pressure transducers and other sensitive equipment prior to cleaning.

5. Open all of the valves to allow flushing fluids to go completely through the assembly.

6. Weigh the VCHP and record. (Didn't do. VCHP too long to fit onto scale.)

7. Blow compressed air through the VCHP to remove large debris. (Didn't do. Heat pipe free of large debris. Care taken to prevent burrs, etc. during assembly.)

8. Connect the hand pump outlet tube to the evaporator section of the heat pipe.

9. Connect the end of the VCHP reservoir section to a section of tube.

10. Connect another section of tube to the inlet of the hand pump.

11. Prepare a large bucket of Alcanox for flushing and follow the preparation instructions on the box, mixing with DI water. (Mixed 1500 mL of DI water with 15 grams of Alcanox.)

12. Place the inlet tube of the hand pump into the bucket.

13. Place the outlet tube of the VCHP (at the reservoir) into the bucket to complete the pumping cycle.

14. Pump Alcanox through the VCHP (Alcanox should remove bulk of dirt). (Flushed through for 10 minutes. No visible debris visible after this time.)

15. Properly dispose of the Alcanox in the bucket and replace the bucket contents with DI water.

16. Pump DI water through the VCHP until soap remnants from the Alcanox are gone. Fresh water will most likely need to be supplied. (Flushed with 1500 mL of DI water until no soap bubbles were visible. Did this five times.)

17. Properly dispose of the DI water in the bucket and replace with tetrachloroethyelene. (Used 1500 mL of tetrachloroethylene.)

18. Pump the tetrachloroethyelene through the VCHP. (Flushed through for five minutes.)

19. Properly dispose of the tetrachloroethyelene in the bucket (attempt to save the tetrachloroethyelene as much as possible) and replace with acetone. (Saved tetrachloroethylene and put in flame cabinet. Used 1500 mL of acetone.)

20. Pump the acetone through the VCHP. (Flushed through for five minutes.)

21. Properly dispose of the acetone in the bucket.

22. Flush out the acetone in the VCHP by either flushing with it DI water again or by carefully blowing dry with oil free nitrogen. If nitrogen is used, avoid inhaling the acetone-laden nitrogen. (Used DI water to flush through twice at 2.5 minutes for each flush (1500 mL each time).

23. Properly dispose of the DI water if it was used.

24. Replace the bucket contents with ammonium persulfate, mixing with DI water. (Mixed 370 grams with 1500 mL of DI water.)

25. Pump the ammonium persulfate through the VCHP. (Flushed through for two minutes.)

26. Properly dispose of the ammonium persulfate in the bucket and replace it with DI water.

27. Pump the DI water through the VCHP. (Used three, 1500 mL flushes. The first for two minutes, then one minute, then another minute. No blue tint visible in water after third flush.)

28. Properly dispose of the DI water.

29. Purge the VCHP with nitrogen to dry (most importantly the wick section). (Purged for about eight minutes. Liquid stopped blowing out after two minutes.)

30. Continue to purge the VCHP until its weight is the same as prior to cleaning. Record weight. (Didn't do.)

31. Close the valves to VCHP to prevent atmospheric contamination.

32. Put the entire heat pipe under argon pressure to maintain its cleanliness.

33. The VCHP is now ready for methanol and argon charging.

APPENDIX F

Methanol Charging Procedure

This procedure is for charging methanol (i.e., the working fluid) in a heat pipe. The heat pipe should be suspended vertically in a ring stand to prevent undesired heat conduction to non-applicable areas. The already cleaned reservoir should be separated from the condenser/evaporator which should be kept under argon pressure to preserve their cleanliness. Splash goggles and gloves shall be worn as a safety precaution. It is assumed that the heat pipe has been properly cleaned as specified in Appendix E. Exercise caution when working near the heat pipe once it has been heated up as it can get very hot. The time duration of the entire process should take about an hour, but may vary on the geometry, etc. of the heat pipe being charged. An overall view of the methanol charging setup is shown in Fig. F.1.

1. Calculate the total occupied volume of the wick inside the heat pipe. For a wrapped screen wick, the volume may be calculated as the width times the length of the section of screen times its thickness. For an interwoven screen wick, the thickness should be treated as twice the wire diameter.

2. Multiply the calculated volume by the porosity, ϵ, of the wick to obtain the volume of methanol required for charging. See Section 3.2 on how to calculate the porosity.

3. Orient the heat pipe vertically on a ring stand such that the methanol can flow down towards the evaporator section.

Figure F.1: Overall setup of methanol charging apparatus.

4. As per Fig. F.2, dispense the calculated volume of methanol into the condenser side using a precision displacement pipette, so that the heat pipe behaves as a thermosyphon during charging. It is assumed that a thermocouple probe is embedded into the vapor core and that there is a pressure transducer attached to the heat pipe to monitor its vapor core pressure.

5. Wrap the evaporator section with an AC rope heater and secure it with Kapton® tape and connect the leads to a Variac® or equivalent. The electrical resistance of the rope heater should be known. A 24 in (609.6 mm) long rope heater was used for the thesis work.

6. Wrap the rope heater/evaporator and then the entire heat pipe with insulating foam.

7. Connect a multimeter across the rope heater leads to monitor the AC voltage.

8. With the electrical resistance of the rope heater known as well as the voltage applied from the power supply, the amount of heat applied to the evaporator may be known. For the work done in the thesis, the heater was limited to 60 VAC or 24.9 W.

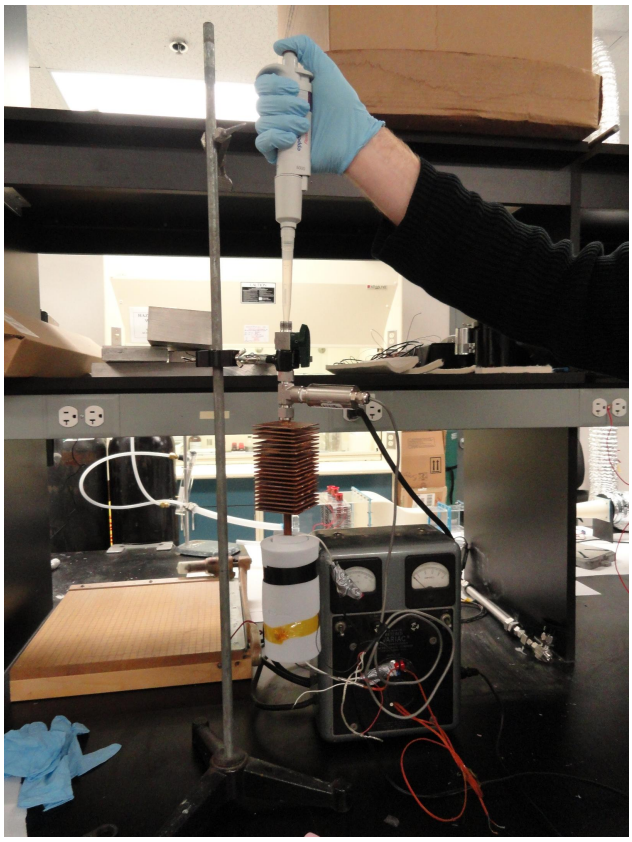

Figure F.2: Injecting methanol into a heat pipe using a precision displacement pipette.

9. Open the valve used to close off the heat pipe from the ambient and attach a 2.5 in (63.5 mm) long piece of tubing to it as demonstrated in Fig. F.3.

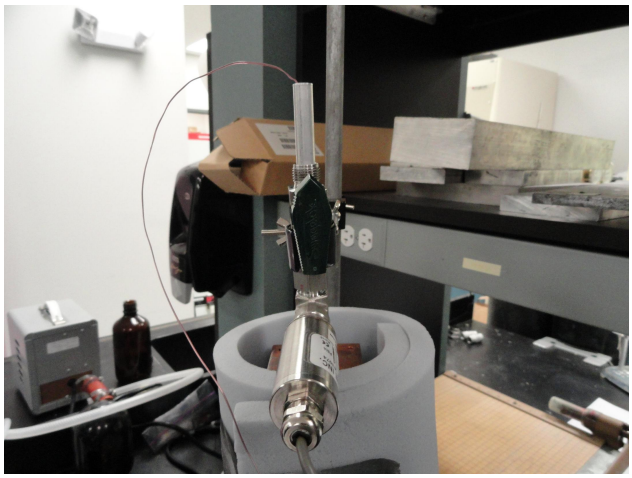

Figure F.3: 2.5 in piece of tubing with thermocouple and open valve.

10. Place a thermocouple near the top (away from the heat pipe) of the piece of tubing.

The purpose of this tubing is to ensure that the temperature of everything below it (i.e., the entire heat pipe) is guaranteed to be at the boiling temperature of methanol when being charged and thus prevent any air from remaining inside of it.

11. Connect the thermocouple in the tube and the thermocouple in the vapor core to a thermocouple thermometer to observe the temperatures during methanol charging.

12. Place an inverted beaker above the piece of tubing so that condensate can be observed when the methanol starts to boil.

13. Turn on the heater power supply and adjust it to 5 W.

14. Slowly increase the heater power by 5 W increments.

15. Observe the two temperatures on the thermocouple thermometer. The thermocouple measuring the vapor core temperature will reach the boiling temperature of methanol at room temperature first (64.7°C).

16. After the vapor core reaches the boiling temperature of methanol at room temperature, the remainder of the heat pipe will take some time to heat up to that temperature (as it has a large thermal capacitance and features stainless steel components).

17. Once the entire heat pipe starts to heat up, the temperature of the thermocouple inside the tube above the condenser valve will immediately increase from room temperature at a fairly steady rate. At this point, the rope heater should be applying the maximum allowed heat load (24.9 W in the case of the thesis work).

18. At the onset of the tube thermocouple reaching the boiling temperature of methanol, condensate should start appearing immediately on the inverted beaker.

19. Allow the methanol to condense for 2.5 minutes. It is assumed that the mass of methanol lost during this time is insignificant compared to the overall amount dispensed into the wick.

20. After 2.5 minutes have elapsed, slowly close the valve near the condenser while continuing to apply the maximum heat load from the rope heater. This is done to ensure a positive pressure gradient so that air cannot enter the heat pipe.

21. Once the valve is firmly closed, the rope heater power may be turned off and the insulating foam may be removed.

22. To accelerate the cooling process, use a fan to bring the heat pipe back down to room temperature.

23. Allow the heat pipe to cool for a few hours back down to room temperature before checking the pressure inside of the heat pipe. Allowing the heat pipe to sit overnight to reach an equilibrium with the ambient is recommended.

24. Record the pressure reading inside of the heat pipe using the pressure transducer and compare it to the saturation pressure of methanol at the temperature of the room. Use a reliable temperature measuring device such as a calibrated thermistor located close to the heat pipe for the most accurate room temperature readings. The vapor core thermocouple may also be referenced.

25. The two pressures should be very close. If they are not, some air may have been trapped inside the heat pipe. If this is the case, the heat pipe needs to be blown out with argon to evaporate all of the methanol and the entire process needs to be repeated until the pressure is deemed satisfactory.

26. It is recommended that the measured pressure of the heat pipe be recorded and compared to the saturation pressure of methanol at room temperature for at least a couple of days to verify that there are no leaks in the heat pipe.

27. Attach the reservoir and slowly throttle argon into it until there is about 30-35 psig of pressure inside of it. DO NOT open the valve separating the two halves until the heat

pipe is ready to become a VCHP. The argon is there to maintain the cleanliness of the reservoir.

28. This concludes the heat pipe methanol charging procedure. It is now ready to be used as a CCHP.

APPENDIX G

Swagelok® Installation Guide

Installation Instructions

Swagelok tube fittings 1 in./25 mm and smaller can be installed quickly, easily, and reliably with simple hand tools.

Over 1 in./25 mm sizes require use of a hydraulic swaging unit to swage the ferrules onto the tubing.

Safety Precautions

- Do not bleed system by loosening fitting nut or fitting plug.
- Do not assemble and tighten fittings when system is pressurized.
- Make sure that the tubing rests firmly on the shoulder of the tube fitting body before tightening the nut.
- Use the correct Swagelok gap inspection gauge to ensure sufficient pull-up upon initial installation.
- Always use proper thread sealants on tapered pipe threads.
- Do not mix materials or fitting components from various manufacturers—tubing, ferrules, nuts, and fitting bodies.
- Never turn fitting body. Instead, hold fitting body and turn nut.
- Avoid unnecessary disassembly of unused fittings.
- Use only long reducers in female Swagelok end connections.

See the instructions starting below for installation of Swagelok tube fittings, O-seal male connectors, caps and plugs, port connectors, tube adapters, positionable elbows and tees, weld fittings, depth marking tool, and preswaging tool.

Figure G.1: Page 9 of 120 of Swagelok® tube fitting installation guide [3] (installation instructions).

Swagelok Tube Fittings

Up to 1 in./25 mm

These instructions apply both to traditional fittings and to fittings with the advanced back-ferrule geometry.

Fully insert the tube into the fitting and against the shoulder; rotate the nut finger-tight.

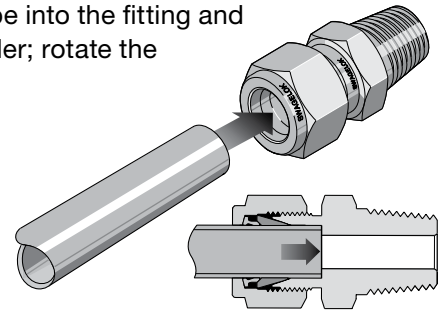

High-pressure applications and high safety-factor systems: *Further tighten the nut until the tube will not turn by hand or move axially in the fitting.*

Mark the nut at the 6 o'clock position.

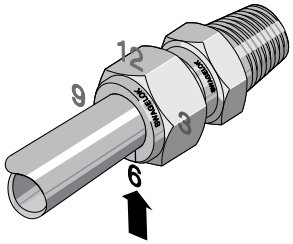

While holding the fitting body steady, tighten the nut one and one-quarter turns to the 9 o'clock position.

For 1/16, 1/8, and 3/16 in.; 2, 3, and 4 mm tube fittings, tighten the nut three-quarters turn to the 3 o'clock position.

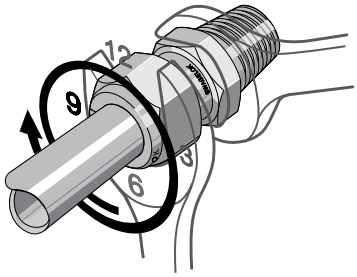

Figure G.2: Page 10 of 120 of Swagelok® tube fitting installation guide [3] (tube fittings up to 1 in./25 mm).

Swagelok Tube Fittings

Reassembly—All Sizes

You may disassemble and reassemble Swagelok tube fittings many times.

⚠ **Always depressurize the system before disassembling a Swagelok tube fitting.**

Prior to disassembly, mark the tube at the back of the nut; mark a line along the nut and fitting body flats.

Use these marks to ensure that you return the nut to the previously pulled-up position.

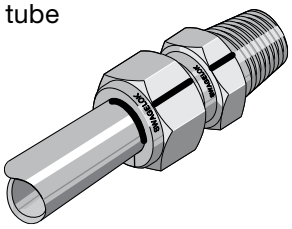

Insert the tube with preswaged ferrules into the fitting until the front ferrule seats against the fitting body.

Over 1 in./25 mm sizes: *If needed, reapply lubricant lightly to the body threads and the rear surface of the back ferrule.*

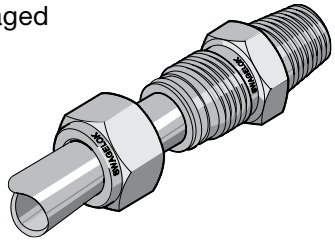

While holding the fitting body steady, rotate the nut with a wrench to the previously pulled-up position, as indicated by the marks on the tube and flats. At this point, you will feel a significant increase in resistance. Tighten the nut slightly.

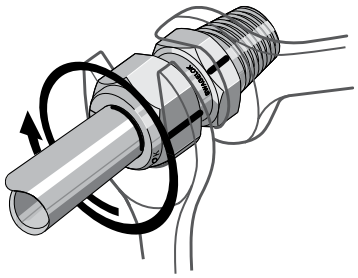

⚠ **Do not use the Swagelok gap inspection gauge with reassembled fittings.**

Figure G.3: Page 12 of 120 of Swagelok® tube fitting installation guide [3] (reinstallation instructions).

APPENDIX H

Laird Technologies® TEM HT6,7,F2,3030 Datasheet and Microscope Photographs

Laird TECHNOLOGIES

Thermoelectric Cooler

HT6,7,F2,3030

Performance Specifications

Hot Side Temperature (°C)	25 °C	50 °C
Qmax (Watts)	29	32.23
DeltaTmax (°C)	67	77
Imax (Amps)	6.0	6.12
Vmax (Volts)	8.1	9.14
Module Resistance (Ohms)	1.23	1.38

Performance Curves – Th = 25°C

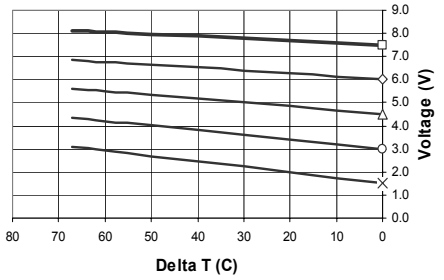

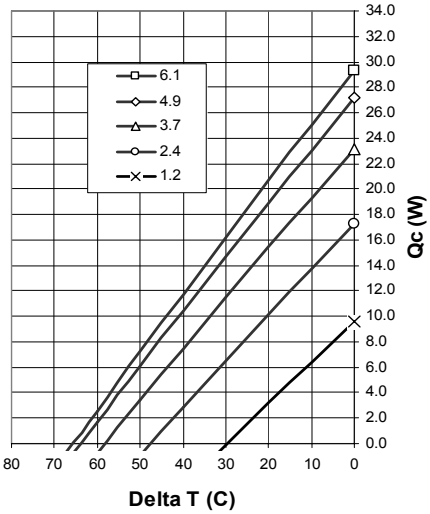

Performance Curves – Th = 50°C

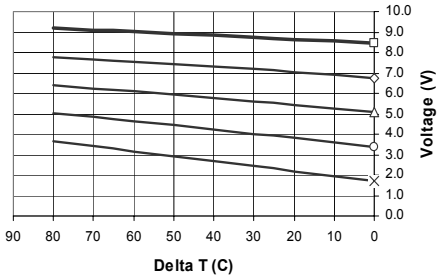

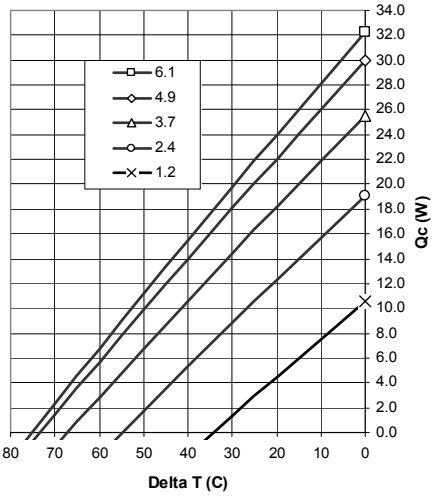

Copyright Laird Technologies. Laird reserves the right to change these specifications without notice. Rev 1.01

Figure H.1: Page 1 of 3 of TEM datasheet used in experiments [4].

Mechanical Drawing

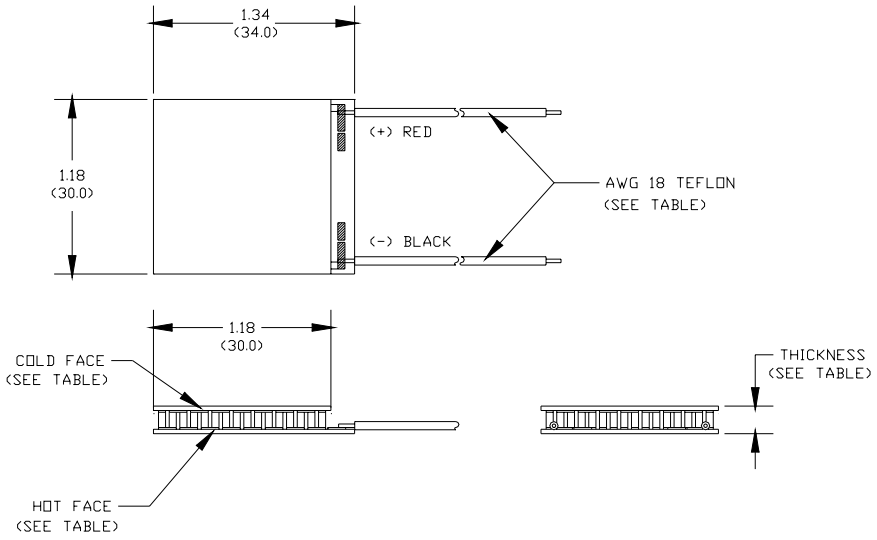

Ceramic: Alumina (Al_20_3)
Solder Construction: 271°C SnSb

Thickness and Surface Finish Specifications

Suffix	Thickness	Flatness & Parallelism	Hot Face	Cold Face	Lead Length
NONE	0.150" +/- 0.015"	0.002" / 0.0035"	Lapped	Lapped	6.0"
-T1	0.150" +/- 0.001"	0.001" / 0.001"	Lapped	Lapped	6.0"
-T2	0.150" +/- 0.0005"	0.0005" / 0.0005"	Lapped	Lapped	6.0"

Operation Tips

- Max Operating Temperature: 175°C
- Max Short Term Temperature: 225°C
- Do not exceed Imax or Vmax when operating module.
- Please consult Melcor for moisture and corrosion protection options

Copyright Laird Technologies. Laird reserves the right to change these specifications without notice. Rev 1.01

Figure H.2: Page 2 of 3 of TEM datasheet used in experiments [4].

Page Intentionally
Left Blank

For additional information please contact Laird:

INTERNET: www.lairdtech.com
N. AMERICA: Laird Technologies, 4707 Detroit Ave, Cleveland, OH 44102
Phone: (216) 939-2300, Fax: (216) 939-2310

Laird and the Laird logo are trademarks of Laird Technologies.

Copyright Laird Technologies. Laird reserves the right to change these specifications without notice. Rev 1.01

Figure H.3: Page 3 of 3 of TEM datasheet used in experiments [4].

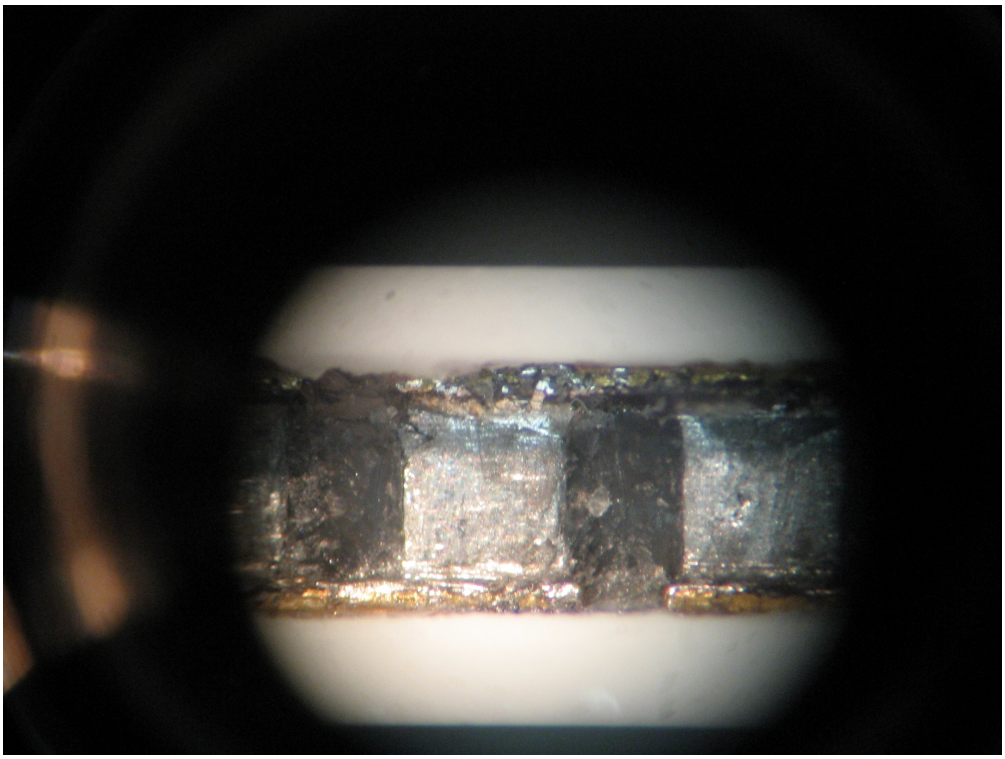

Figure H.4: Microscope photograph of pellets of TEM used in experiments.

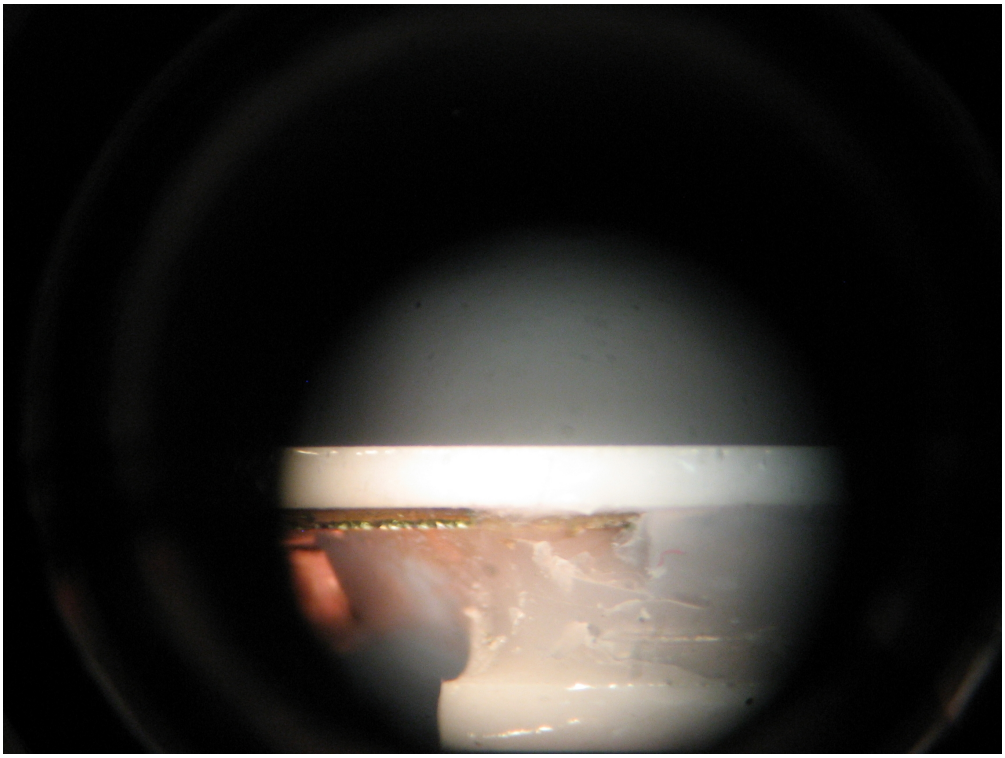

Figure H.5: Microscope photograph of lead attachment of TEM used in experiments.

APPENDIX I

Omega® PX209, PX219, PXM209, PXM219 Pressure Transducer Calibration Data and Instruction Sheet

Table I.1: Calibration data for Omega® pressure transducer used at the condenser (Serial Number: 82975).

p [psia]	V [VDC]
0	-0.0430
15	2.4620
30	4.9510

Table I.2: Calibration data for Omega® pressure transducer used at the reservoir (Serial Number: 87291).

p [psia]	V [VDC]
0	-0.0014
15	2.5077
30	5.0057

omega.com®
OMEGA®

PX209, PX219, PXM209, PXM219

Pressure Transducers

M4085-0407

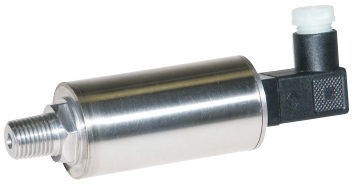

INSTRUCTION SHEET

Shop online at: omega.com e-mail: info@omega.com
For latest product manuals: omegamanual.info

COMMON SPECIFICATIONS FOR ALL UNITS

ACCURACY: (Linearity, Hysteresis, and Repeatability)	0.25%
ZERO BALANCE:	2% FS
COMPENSATED TEMP:	-20 to 80°C (-4 to 176°F)
THERMAL EFFECTS:	0.04% FS over (-20 to 80°C) (-4 to 176°F)
VIBRATION:	Withstands 20 g peak, 10 to 2000 Hz
PRESSURE PORT:	1/4-18 NPT (G1/4 on PXM)
BURST PRESSURE:	300% (250% > 200 PSI)
PROOF PRESSURE:	150%
RESPONSE TIME:	2 msec typ
GAGE TYPE:	Diffused silicon strain gages
ELECTRICAL CONNECTION:	Miniature DIN connection screw terminals or 36" pigtail
WETTED PARTS:	316 SSTL, borosilicate glass, silicon nitrite, aerospace epoxy
CASE:	Stainless steel
FATIGUE:	100 million cycles FS
WEIGHT:	4.5 oz (128 g) max

VOLTAGE OUTPUT

EXCITATION:	5 Vdc Output - 7 to 35 Vdc 10 Vdc Output - 12 to 35 Vdc @ 15mA (reverse polarity protected)
OUTPUT:	0 to 5 Vdc or 0 to 10 Vdc, ±1.5% FSO, 3-wire
ZERO BALANCE:	0 Vdc ±2% FSO
OPERATING TEMPERATURE:	-65 to 250°F
OUTPUT RESISTANCE:	100
WIRING:	+EXC Red/Pin 1; COMMON Black/Pin 2; +OUT White/Pin 3

CURRENT OUTPUT

EXCITATION:	24 Vdc (7 to 35 Vdc) reverse polarity protected
OUTPUT:	4 to 20 mA (2-wire) ±1% FSO
ZERO BALANCE:	4 mA ±2% FSO
OPERATING TEMPERATURE:	-54 to 121°C (-65 to 250°F)
MAX LOOP RESISTANCE:	50 x (supply voltage - 10)
WIRING:	+Red/Pin 1; Black/Pin 2

WIRING PIN CONNECTOR

To access the terminals inside the DIN connector proceed as follows:

1. Remove the screw at the top of the connector.
2. Separate the DIN connector from the transducer.
3. Insert a small blade screwdriver into the slot provided and pry the DIN connector apart.
4. After wiring the terminals, snap the DIN connector back together.
5. Mount the DIN connector to the transducer (using the rubber gasket in between), observing the blade orientations.
6. Insert the screw at the top of the DIN connector and tighten.

WARNING! READ BEFORE INSTALLATION!

Fluid hammer and surges can destroy any pressure transducer and must always be avoided. A pressure snubber should be installed to eliminate the damaging hammer affects. Fluid hammer occurs when a liquid flow is suddenly stopped, as with quick closing solenoid valves. Surges occur when flow is suddenly begun, as when a pump is turned on at full power or a valve is quicky opened.

Liquid surges are particularly damaging to pressure transducers if the pipe is originally empty. To avoid damaging surges, fluid lines should remain full (if possible), pumps should be brought up to power slowly, and valves opened slowly. To avoid damage from both fluid hammer and surges, a surge chamber should be installed, and a pressure snubber should be installed on every transducer.

Symptoms of fluid hammer and surge's damaging effects:

1. Pressure transducer exhibits an output at zero pressure (large zero offset). If zero offset is less than 10% FS, user can usually re-zero meter, install proper snubber and continue monitoring pressures.
2. Pressure transducer output remains constant regardless of pressure.
3. In severe cases, there will be no output.

Figure I.1: Page 1 of 2 of Omega® pressure transducer instruction sheet [5].

DIMENSIONS

219

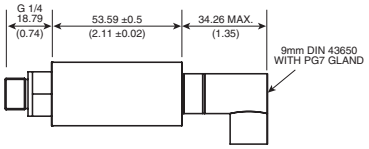

209

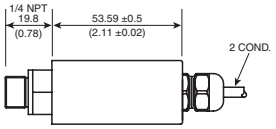

DIMENSIONS mm (in)

WIRING

209/219 VOLTAGE

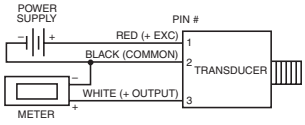

209/219 CURRENT

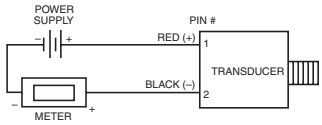

Cable shielding must be terminated at the meter to earth ground to comply with CE.

WARRANTY/DISCLAIMER

OMEGA ENGINEERING, INC. warrants this unit to be free of defects in materials and workmanship for a period of **37 months** from date of purchase. OMEGA's WARRANTY adds an additional one (1) month grace period to the normal **three (3) year product warranty** to cover handling and shipping time. This ensures that OMEGA's customers receive maximum coverage on each product.

If the unit malfunctions, it must be returned to the factory for evaluation. OMEGA's Customer Service Department will issue an Authorized Return (AR) number immediately upon phone or written request. Upon examination by OMEGA, if the unit is found to be defective, it will be repaired or replaced at no charge. OMEGA's WARRANTY does not apply to defects resulting from any action of the purchaser, including but not limited to mishandling, improper interfacing, operation outside of design limits, improper repair, or unauthorized modification. This WARRANTY is VOID if the unit shows evidence of having been tampered with or shows evidence of having been damaged as a result of excessive corrosion; or current, heat, moisture or vibration; improper specification; misapplication; misuse or other operating conditions outside of OMEGA's control. Components in which wear is not warranted, include but are not limited to contact points, fuses, and triacs.

OMEGA is pleased to offer suggestions on the use of its various products. However, OMEGA neither assumes responsibility for any omissions or errors nor assumes liability for any damages that result from the use of its products in accordance with information provided by OMEGA, either verbal or written. OMEGA warrants only that the parts manufactured by the company will be as specified and free of defects. OMEGA MAKES NO OTHER WARRANTIES OR REPRESENTATIONS OF ANY KIND WHATSOEVER, EXPRESSED OR IMPLIED, EXCEPT THAT OF TITLE, AND ALL IMPLIED WARRANTIES INCLUDING ANY WARRANTY OF MERCHANTABILITY AND FITNESS FOR A PARTICULAR PURPOSE ARE HEREBY DISCLAIMED. LIMITATION OF LIABILITY: The remedies of purchaser set forth herein are exclusive, and the total liability of OMEGA with respect to this order, whether based on contract, warranty, negligence, indemnification, strict liability or otherwise, shall not exceed the purchase price of the component upon which liability is based. In no event shall OMEGA be liable for consequential, incidental or special damages.

CONDITIONS: Equipment sold by OMEGA is not intended to be used, nor shall it be used: (1) as a "Basic Component" under 10 CFR 21 (NRC), used in or with any nuclear installation or activity; or (2) in medical applications or used on humans. Should any Product(s) be used in or with any nuclear installation or activity, medical application, used on humans, or misused in any way, OMEGA assumes no responsibility as set forth in our basic WARRANTY/DISCLAIMER language, and, additionally, purchaser will indemnify OMEGA and hold OMEGA harmless from any liability or damage whatsoever arising out of the use of the Product(s) in such a manner.

RETURN REQUESTS/INQUIRIES

Direct all warranty and repair requests/inquiries to the OMEGA Customer Service Department. BEFORE RETURNING ANY PRODUCT(S) TO OMEGA, PURCHASER MUST OBTAIN AN AUTHORIZED RETURN (AR) NUMBER FROM OMEGA'S CUSTOMER SERVICE DEPARTMENT (IN ORDER TO AVOID PROCESSING DELAYS). The assigned AR number should then be marked on the outside of the return package and on any correspondence.

The purchaser is responsible for shipping charges, freight, insurance and proper packaging to prevent breakage in transit.

FOR **WARRANTY** RETURNS, please have the following information available BEFORE contacting OMEGA:

1. Purchase Order number under which the product was PURCHASED,
2. Model and serial number of the product under warranty, and
3. Repair instructions and/or specific problems relative to the product.

FOR **NON-WARRANTY** REPAIRS, consult OMEGA for current repair charges. Have the following information available BEFORE contacting OMEGA:

1. Purchase Order number to cover the COST of the repair,
2. Model and serial number of the product, and
3. Repair instructions and/or specific problems relative to the product.

OMEGA's policy is to make running changes, not model changes, whenever an improvement is possible. This affords our customers the latest in technology and engineering.

OMEGA is a registered trademark of OMEGA ENGINEERING, INC.

© Copyright 2007 OMEGA ENGINEERING, INC. All rights reserved. This document may not be copied, photocopied, reproduced, translated, or reduced to any electronic medium or machine-readable form, in whole or in part, without the prior written consent of OMEGA ENGINEERING, INC.

omega.com®
OMEGA®

OMEGAnet® Online Service omega.com	Internet e-mail info@omega.com

Servicing North America:

U.S.A.:
ISO 9001 Certified
One Omega Drive, Box 4047
Stamford, CT 06907-0047
Tel: (203) 359-1660
FAX: (203) 359-7700
e-mail: info@omega.com

Canada:
976 Bergar
Laval (Quebec) H7L 5A1, Canada
Tel: (514) 856-6928
FAX: (514) 856-6886
e-mail: info@omega.ca

For immediate technical or application assistance:

U.S.A. and Canada:
Sales Service: 1-800-826-6342/1-800-TC-OMEGA
Customer Service: 1-800-622-2378/1-800-622-BEST
Engineering Service: 1-800-872-9436/1-800-USA-WHEN

Mexico:
En Español: (001) 203-359-7803
FAX: (001) 203-359-7807
e-mail: espanol@omega.com
info@omega.com.mx

Servicing Europe:

Czech Republic:
Frystatska 184, 733 01 Karviná, Czech Republic
Tel: +420 (0)59 6311899
FAX: +420 (0)59 6311114
Toll Free: 0800-1-66342
e-mail: info@omegashop.cz

Germany/Austria:
Daimlerstrasse 26, D-75392 Deckenpfronn, Germany
Tel:+ 49 (0)7056 9398-0
FAX: +49 (0)7056 9398-29
Toll Free in Germany: 0800 639 7678
e-mail: info@omega.de

United Kingdom:
ISO 9002 Certified
One Omega Drive, River Bend Technology Centre
Northbank, Irlam, Manchester
M44 5BD United Kingdom
Tel: +44 (0)161 777 6611
FAX: +44 (0)161 777 6622
Toll Free in United Kingdom: 0800-488-488
e-mail: sales@omega.co.uk

It is the policy of OMEGA Engineering, Inc. to comply with all worldwide safety and EMC/EMI regulations that apply. OMEGA is constantly pursuing certification of its products to the European New Approach Directives. OMEGA will add the CE mark to every appropriate device upon certification.

The information contained in this document is believed to be correct, but OMEGA accepts no liability for any errors it contains, and reserves the right to alter specifications without notice.
WARNING: These products are not designed for use in, and should not be used for, human applications.

Figure I.2: Page 2 of 22 of Omega® pressure transducer instruction sheet [5].

APPENDIX J

MKS® 925 Micro Pirani Pressure Transducer Calibration Data

Table J.1: Calibration data for MKS® 925 Micro Pirani pressure transducer.

Reference [torr]	PR1 [torr]	PR1
5.88E-4	5.60E-4	-4.76%
2.34E-3	2.33E-3	-0.43%
2.00E-2	1.99E-2	-0.50%
2.00E-1	2.00E-1	0.00%
2.00E+0	2.01E+0	0.50%
1.36E+1	1.31E+1	-3.68%
1.00E+2	9.47E+1	-5.30%
3.50E+2	3.45E+2	-1.43%
7.00E+2	7.34E+2	4.86%
7.63E+2	8.13E+2	6.55%

APPENDIX K

Laird Technologies® Tgrease™ 2500 Thermal Grease Datasheet

Laird TECHNOLOGIES

Innovative **Technology** for a **Connected** World

Tgrease™ 2500 Series
Thermal Grease

ENVIRONMENTALLY FRIENDLY THERMALLY CONDUCTIVE GREASE

Tgrease™ 2500 is a silicone-free thermal grease for use in high performance CPU's and GPU's. With a high thermal conductivity of 3.8 W/mK, Tgrease™ 2500 thoroughly wets out thermal surfaces to create very low thermal resistance.

Tgrease™ 2500 eliminates the migration issues of siliconebased grease to create superior reliability. Tgrease™ 2500 is ideal for situations where automatic dispensing and screen-printing are required.

Tgrease™ 2500 is non-toxic and environmentally safe. Tgrease™ 2500 is available in 1kg (pint container), 3kg (quart container), and 10kg (gallon container) or custom packaged in syringes for automated applications.

APPLICATIONS

- High performance CPU's and GPU's
- Chipsets
- Graphic processing chips
- Custom ASICS

PROPERTIES	
Color	White
Density	3.42 g/cc
Viscosity Brookfield Viscometer	2,500,000cP TF spindle at 2rpm (helipath) and 23°C
Temperature Range	-55°C to 150°C
Outgassing (TML)	0.91%
Outgassing (CVCM)	0.15%
UL Flammability Rating	94 V0
Thermal Conductivity	3.8 W/mK
Thermal Resistance @ 10 psi @ 50 psi	 0.023°C-in²/W (0.15 C-cm2/W) 0.020°C-in²/W (0.13 C-cm2/W)
Volume Resistivity	3.5 x 1012 Ohm-cm
Dielectric Constant @ 1KHz/1MHz	5.7 / 5.6

global solutions: **local** support™

Americas: +1.800.843.4556
Europe: +49.8031.2460.0
Asia: +86.755.2714.1166

CLV-customerservice@lairdtech.com
www.lairdtech.com/thermal

Figure K.1: Page 1 of 2 of Laird® Tgrease™ 2500 instruction sheet datasheet [6].

Laird TECHNOLOGIES

Innovative **Technology** for a **Connected** World

Tgrease™ 2500 Series
Thermal Grease

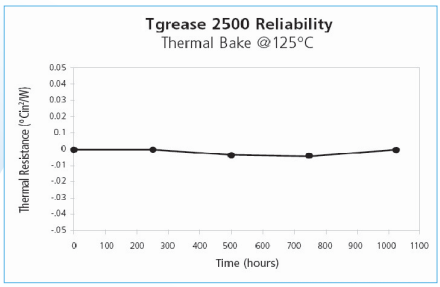

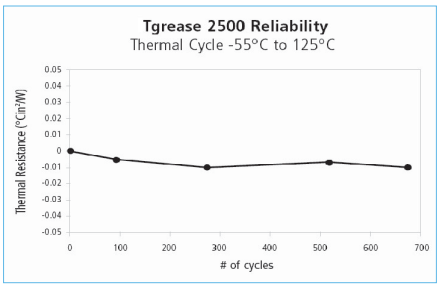

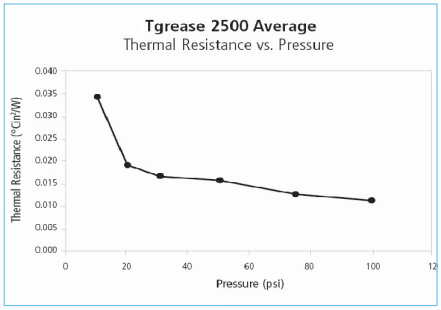

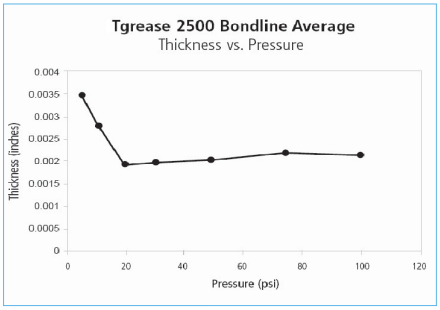

THR-DS-Tgrease-1500 0710

Any information furnished by Laird Technologies, Inc. and its agents is believed to be accurate and reliable. All specifications are subject to change without notice. Responsibility for the use and application of Laird Technologies materials rests with the end user, since Laird Technologies and its agents cannot be aware of all potential uses. Laird Technologies makes no warranties as to the fitness, merchantability or suitability of any Laird Technologies materials or products for any specific or general uses. Laird Technologies shall not be liable for incidental or consequential damages of any kind. All Laird Technologies products are sold pursuant to the Laird Technologies' Terms and Conditions of sale in effect from time to time, a copy of which will be furnished upon request. © Copyright 2010 Laird Technologies, Inc. All Rights Reserved. Laird, Laird Technologies, the Laird Technologies Logo, and other marks are trade marks or registered trade marks of Laird Technologies, Inc. or an affiliate company thereof. Other product or service names may be the property of third parties. Nothing herein provides a license under any Laird Technologies or any third party intellectual property rights. A14265-00 Rev.E 03/29/07.

Figure K.2: Page 2 of 2 of Laird® Tgrease™ 2500 instruction sheet datasheet [6].